

University of Alberta

Development of a 3D Equivalent Continuum Model for Deformation
Analysis of Systematically Jointed Rock Masses

by

Alireza Agharazi

A thesis submitted to the Faculty of Graduate Studies and Research
in partial fulfillment of the requirements for the degree of

Doctor of Philosophy
in
Geotechnical Engineering

Department of Civil and Environmental Engineering

©Alireza Agharazi
Fall 2013
Edmonton, Alberta

Permission is hereby granted to the University of Alberta Libraries to reproduce single copies of this thesis and to lend or sell such copies for private, scholarly or scientific research purposes only. Where the thesis is converted to, or otherwise made available in digital form, the University of Alberta will advise potential users of the thesis of these terms.

The author reserves all other publication and other rights in association with the copyright in the thesis and, except as herein before provided, neither the thesis nor any substantial portion thereof may be printed or otherwise reproduced in any material form whatsoever without the author's prior written permission.

To my late brother

Anoushiravan,

whose memory is always with me....

Abstract

The analysis of deformations in rock masses includes two main steps: a) choosing a proper mechanical model that best describes the rock mass behaviour, and b) determining the rock mass mechanical parameters corresponding to the selected model. Deformability of a rock mass with persistent joint sets is potentially anisotropic and is mainly governed by the mechanical and geometrical characteristics of the joints.

The available models for the deformation analysis of rock masses can be divided into two general categories: continuum models and discontinuum models. In discontinuum models, the joints are simulated explicitly. However, when the number of joints in a model increases, the explicit definition of all joints becomes difficult and, in some cases, impractical. Besides, due to the dependency of numerical discretization on joint spacing and orientation, the size of a discontinuum model increases considerably as the number of joints increases within the model. Equivalent continuum models can be used as an alternative to discontinuum models for the deformation analysis of jointed rocks. In these models, the behaviour of a jointed rock mass is approximated by the analysis of its equivalent continuum. The discontinuities are taken into account implicitly, either by implementing proper constitutive relations or by adopting appropriate mechanical parameters.

In this thesis, the principal deformation mechanisms for a jointed rock mass are defined and characterized through the analysis of the results of 26 plate loading tests conducted on a jointed rock mass at the Bakhtiary dam and hydro electric power plant project in Iran. A new three dimensional equivalent continuum model, the *JointedRock* model, is developed for jointed rock masses that contain up to three persistent joint sets. The geometrical and mechanical parameters of the joint sets are directly incorporated in the

constitutive equations of the model. The constitutive equations are represented in a tensor form so the model can be used for any arbitrary joint set configurations. Non-linearity of the rock mass deformation, caused by the stress-dependency of joint stiffness, can also be modeled by choosing a stress-dependent stiffness model for the rock joints. A Mohr-Coulomb failure criterion is used to check failure of intact rock blocks and slip along the rock joints. The model is implemented in *FLAC^{3D}* and is verified against the distinct element method (*3DEC*) and, where available, analytical solutions.

Plate loading tests are often conducted to determine the large scale deformability parameters of a rock mass. The ISRM suggested equation is routinely used to calculate the rock mass deformation modulus. The method uses the Boussinesq relationships for loading a semi-infinite isotropic linear elastic medium. Inconsistency of the real test gallery geometry with the semi-infinite model assumption leads to overestimation of the rock mass deformation modulus. In jointed rock masses, dependency of the test results on the orientation and spacing of discontinuities also causes a considerable scatter in the test results and consequently in the moduli calculated using the ISRM suggested method.

A method is proposed for interpreting the plate loading test results conducted on jointed rock masses. The *JointedRock* model is used to back calculate the average stiffness of rock joints, from the test results. The rock mass deformability is related to the orientation, spacing and stiffness of the joints and the deformation modulus of intact rock. The equivalent deformation modulus of the rock mass is then determined numerically for any desired direction, relative to the orientation of discontinuities.

Acknowledgments

I would like to take this opportunity to express my sincere gratitude to Dr. Derek C. Martin for his supervision, technical advice and continued support over the course of my PhD program. His insight and guidance had a significant impact on this work.

I would also like to especially thank Dr. D. Dwayne Tannant, who provided me with the opportunity to pursue my PhD studies at the University of Alberta. His support, careful review and critique of this work are deeply appreciated.

I owe thanks to the managers of the Bakhtiary Dam Project and the Stucky Pars Company for providing me with experimental data that added significant value to this thesis.

Finally, I would like to express my warmest appreciation to my family: my parents and sister. I am so thankful for their unconditional support and love over all these years.

Table of Content

Chapter 1: Introduction	1
1.1. Overview	1
1.2. Research scope and focus	4
1.3. Practical implication and outcome	5
Chapter 2: Background and literature review	7
2.1. Hooke's law and material symmetry	7
2.1.1. Isotropic material	9
2.1.2. Transversely isotropic material	9
2.1.3. Orthotropic material	9
2.2. Deformation of jointed rock masses	10
2.3. Deformation analysis of jointed rock masses	15
2.3.1. Discontinuum based methods	15
2.3.2. Equivalent continuum methods	17
2.3.3. Equivalent continuum methods versus discontinuum methods	22
2.4. Determination of rock mass deformability by plate loading test	25
2.5. References.....	29
Chapter 3: Characterizing rock mass deformation mechanisms during plate loading tests at the Bakhtiary dam project	35
3.1. Introduction	35
3.2. Plate loading test - Theory and interpretation	36
3.3. Parameters influencing test results and data interpretation	38
3.4. Deformation of rock discontinuities and rock mass	40
3.5. Bakhtiary dam site	43
3.5.1. Geological description of the dam site	43
3.5.2. Rock mass properties	44
3.5.3. Discontinuities	45
3.6. Interpretation of plate loading test results	47
3.7. Conclusion	58
3.8. References	59

Chapter 4: A three-dimensional equivalent continuum constitutive model for jointed rock masses containing up to three random joint sets	62
4.1. Introduction	62
4.2. <i>JointedRock</i> model: Theory and assumptions	64
4.3. Implementation of the <i>JointedRock</i> model in <i>FLAC^{3D}</i>	69
4.4. Verification examples	71
4.4.1. Elastic deformation	71
4.4.2. Uniaxial compressive strength	74
4.5. <i>JointedRock</i> model application	75
4.5.1. Deformation and stress distribution in a semi-infinite body of jointed rock	75
4.5.2. Stress-dependent joint stiffness and non-linear deformation	78
4.6. Discussion on model applicability and limitations	79
4.7. Conclusion	82
4.8. References	83
Chapter 5: Numerical analysis of plate loading test results using an equivalent continuum model “<i>JointedRock</i>” – Case study: Bakhtiary dam site	85
5.1. Introduction	85
5.2. <i>JointedRock</i> model	87
5.3. Case study: Bakhtiary dam and hydroelectric project	90
5.3.1. Site geology	90
5.3.2. Plate loading test results	91
5.4. Numerical interpretation of the plate loading test results using the <i>JointedRock</i> model	98
5.4.1. Rock mass deformation parameters	98
5.4.2. Back calculation of joint stiffness from the test results	100
5.4.3. Determination of the anisotropic deformation modulus of the rock mass	101
5.5. Conclusion	103
5.6. Reference	104
Chapter 6: Conclusion	106
Appendix 1: <i>JointedRock</i> model - <i>FLAC^{3D}</i> keywords	110
Appendix 2: Effect of boundary conditions and the bending stiffness of intact rock layers on simulations using the <i>JointedRock</i> model	113
Appendix 3: Closed form relationships for loading of a semi-infinite body	124

Appendix 4: Bakhtiary dam site plate loading test data 127

List of Tables

Chapter 2

Table 2.1:	Characteristics of stress-deformation patterns corresponding to three modes of deformation in jointed rocks (after Barton 2007).....	14
------------	--	----

Chapter 3

Table 3.1:	Stress–strain response of a jointed rock mass for three modes of behavior (Barton, 2007).....	42
Table 3.2:	Rock mass classes and engineering ratings (SPEC 2009).....	45
Table 3.3:	Bedding and joint set characteristics (SPEC 2009).....	46
Table 3.4:	Average discontinuity strength parameters based on shear box tests (SPEC 2008).....	46
Table 3.5:	Bedding k_n (MPa/mm) from normal loading–unloading tests.....	47
Table 3.6:	Total surface deformation at each loading–unloading cycle.....	53
Table 3.7:	Deformation moduli calculated using the ISRM method for the tests shown in Figure 3.10.....	57
Table 3.8:	Deformation mechanisms and characteristics for PLTs at Bakhtiary dam site.....	58

Chapter 4

Table 4.1:	Mechanical and strength parameters for uniaxial test.....	71
------------	---	----

Chapter 5

Table 5.1:	Mechanical properties of joints and intact rock for the uniaxial test model.....	88
Table 5.2:	RMR and GSI and modulus of deformation for PLTs.....	95
Table 5.3:	Maximum, minimum and average deformation moduli calculated using different methods.....	97
Table 5.4:	Average normal and shear stiffness values back-calculated from PLT results using <i>FLAC^{3D}-JointedRock</i> model.....	101

Appendix 2

Table 1:	Mechanical parameters of intact rock and rock joints in simulations.....	114
----------	--	-----

List of Figures

Chapter 2

Figure 2.1:	Common physical symmetries for rock masses. (a) Isotropic: every arbitrary plane is a plane of symmetry, (b) Transversely isotropic: κ is axis of symmetry, (c)(d) Orthotropic: two and three planes of symmetry as shown	10
Figure 2.2:	Effect of boundary condition on deformation mechanism of a jointed rock cylinder. (a) Lateral movement is prevented, deformation is a result of intact rock compression and normal closure of joint, (b) dominant deformation mechanism is shear sliding through the joint	11
Figure 2.3:	Idealized model of a discontinuous rock mass with primary and secondary joints	12
Figure 2.4:	Normal stress (σ_n) versus closure (ΔV_j) for a fresh Limestone bedding plane subjected to repeated loading - unloading cycles (after Bandis et al. 1983)	12
Figure 2.5:	Shear stress versus shear displacement models: (a) constant stiffness model, (b) constant displacement model (after Goodman 1976).....	13
Figure 2.6:	Conceptual stress-deformation curves for jointed rocks (after Barton 1986).	14
Figure 2.7:	Available methods for stress-strain analysis of jointed rock masses	15
Figure 2.8:	Sensitivity of discontinuous models to applied boundary conditions. A slight shift in the applied load would potentially result in different displacements	23
Figure 2.9:	Discontinuity patterns and applicability of analysis techniques.....	24
Figure 2.10:	Schematic view of a plate loading test in a test gallery.....	25
Figure 2.11:	Increasing trend of deformation modulus calculated using ISRM suggested relationship based on numerical modelling of plate loading test (after Agharazi et al. (2008)).....	26
Figure 2.12:	Loading plate size relative to spacing of discontinuities. (a) Joint spacing several times of plate diameter. Test results are representative of intact rock deformation (b) Joint spacing is about the loading plate diameter. Test results depend highly on the relative position of the loading plate and the discontinuities. Deformability is highly anisotropic (c) Joint spacing is less than half plate diameter. Test results depend on the direction of loading relative to the direction of discontinuities. (d) Intensely jointed rock mass. Test results are representative of jointed rock mass deformation	28

Chapter 3

Figure 3.1:	Plate loading test set-up (Bakhtiary dam site).....	37
-------------	---	----

Figure 3.2:	Increasing trend of modulus with depth in a PLT at the Bakhtiary dam site	39
Figure 3.3:	Primary and secondary discontinuities in (a) jointed rock mass and (b) idealized model.....	40
Figure 3.4:	Non-linear joint closure curve under normal stress, and hyperbolic function that represent this behavior mathematically (k_{ni} : initial normal stiffness of joint).....	41
Figure 3.5:	Geological section of dam axis and geological units of the Sarvak formation	43
Figure 3.6:	Axial plane of Siah Kuh anticline on abutments, (a) left abutment and (b) right abutment. Red lines show the axial plane outcrop, yellow lines show typical bedding and the green line shows extension joints observed on the left bank. (For interpretation of the references to color in this figure legend, the reader is referred to the web version of this article.)	44
Figure 3.7:	Projection of test galleries on dam axis cross section and plan. Number of PLTs in each gallery, maximum vertical stress, and estimated horizontal stresses at the location of each gallery is also presented.....	48
Figure 3.8:	Loading–unloading cycles used for the Bakhtiary dam site PLTs.....	48
Figure 3.9:	Test groups based on the relative direction of loading to orientation of discontinuities.....	49
Figure 3.10:	Stress-deformation curves of PLTs representing each group. Schematic figures on the right show the relative direction of loading to the orientation of discontinuities for each test. The orientation of the discontinuities and test load along with RQD distribution and GSI value are also presented. Data have been extracted from gallery and test surface mapping, borehole logs, and core photos.....	52
Figure 3.11:	Deformation–time and rate of deformation–time (logarithmic scale) graphs. Time axis shows the elapsed time under constant load of 20 MPa at the peak of 4th loading cycle.....	54
Figure 3.12:	Distribution of total and permanent deformation for each group after five loading–unloading cycles.....	55
Figure 3.13:	Variation of the average ratio of permanent to total deformations for each group.....	56
Figure 3.14:	Idealized load–displacement curves for the deformation of a jointed rock mass. These curves characterize the type of behavior observed during one loading–unloading cycle of PLTs at the Bakhtiary dam site, where deformations are governed by shear and normal displacements along discontinuities	57

Chapter 4

Figure 4.1:	Stress – deformation graphs of plate loading tests on a jointed limestone at the Bakhtiary dam site (loading plate diameter: 971 mm). The graphs show the
-------------	---

	surface deflection for three different test configurations that differ in the relative direction of loading to orientation of discontinuities: normal to bedding (NB), normal to joint set 2 (NJ2) and inclined to all three joint sets, SB12.....	64
Figure 4.2:	Conceptual rock block with three persistent joint sets and its simplified physical model	65
Figure 4.3:	Representative Elementary Volume (REV) for the JointedRock model	66
Figure 4.4:	Joint plane and local coordinate system.....	68
Figure 4.5:	Calculation steps followed for the implementation of the JointedRock model in <i>FLAC^{3D}</i>	70
Figure 4.6:	Geometry and boundary conditions for the uniaxial test model. The first series of tests are run with one joint set with joint spacing of $S = 0.25\text{m}$. The second series of tests used two joint sets with spacings of $S_1 = 0.4\text{m}$ and $S_2 = 0.25\text{m}$	72
Figure 4.7:	Rock deformation in uniaxial test model with one joint set.....	73
Figure 4.8:	Difference between calculated axial deformation by the <i>JointedRock</i> model (d_{JR}) and <i>3DEC</i> model (d_{3DEC}) for different joint set inclinations and three intact rock shear moduli (G)	73
Figure 4.9:	Rock deformation in uniaxial test model with two joint sets	73
Figure 4.10:	Uniaxial compressive strength of a rock sample with weakness plane.....	74
Figure 4.11:	Semi-infinite body of rock loaded on the top in <i>FLAC^{3D}</i>	75
Figure 4.12:	Vertical displacements versus joint set orientation for a semi-infinite body of rock intersected by one and two joint sets. A circular stress of 10 MPa is applied on the top centre of the model and displacements are measured at the centre of the loaded area.	76
Figure 4.13:	Stress distribution beneath the loaded area in the semi-infinite model with one joint set.....	77
Figure 4.14:	Assumed joint closure and tangent normal stiffness curves for the model ($\delta_m = 3.7\text{ mm}$ and $k_m = 1\text{ MPa/mm}$)	78
Figure 4.15:	Axial deformation of a cylindrical rock specimen having a fictitious joint with stress-dependent normal stiffness. a) The total non-linear deformation is the sum of the linear deformation of the intact rock and non-linear closure of the fictitious joint. b) As the angle between fictitious joint and loading direction approaches zero, the deformation of the specimen converges to that of the intact rock	79
Figure 4.16:	Cantilever plate loaded by a line load, F_z	80
Figure 4.17:	Deflection of cantilever plate tip versus discontinuity shear stiffness (K_s) for two intact rock shear moduli (G)	80
Figure 4.18:	Impact of relative spacing of joints on applicability of <i>JointedRock</i> model.	81
Figure 4.19:	A persistent joint set becomes non-persistent as a result of large plastic displacement along another joint set.....	82

Chapter 5

Figure 5.1:	Jointed rock cylinder of the 3D uniaxial test model (left), cross section of the cylinder and boundary condition (right).	87
Figure 5.2:	Deformation versus joint angle plots for uniaxial test with one joint set (left) and two joint sets (right).	88
Figure 5.3:	Maximum principal stress and axial displacement contours for the uniaxial test with one joint set at $\alpha = 30^\circ$ (upper) and $\alpha = 60^\circ$ (lower).	89
Figure 5.4:	Geological section at the dam axis with projection of the test galleries, GL1, GL2 and GL3 on the left abutment and GR1, GR2 and GR2 on the right abutment.	90
Figure 5.5:	Stress-deformation plot of a PLT at the Bakhtiary dam site. The slope of the loading segment of the curves increases over the first three loading cycles.	92
Figure 5.6:	Numerical model of PLT (<i>FLAC^{3D}</i>). The model was cut in half by a vertical plane crossing the centre of the loading plate. Just upper part of the model is shown. Vertical displacements were fixed at the top of the model (excluding the inside of the gallery) to simulate the confining effect of the gallery.	94
Figure 5.7:	Displacement versus deformation moduli plots calculated by the numerical models of the tests.	96
Figure 5.8:	Comparison of moduli calculated using the analytical and numerical methods with the empirical relationships.	97
Figure 5.9:	Correlation of the moduli calculated using the numerical method with those by the analytical relation.	97
Figure 5.10:	Loading direction and the orientation of discontinuities in two test groups	100
Figure 5.11:	Deformation versus joint angle determined by the hypothetical PLT models, for plate diameters of $d = 915$ mm and $d = 971$ mm. The <i>JointedRock</i> model was used as the constitutive model. The estimated average normal and shear stiffness from PLT results were used in the model. The measured PLT deformations are depicted by solid circles.	101
Figure 5.12:	Anisotropic equivalent deformation modulus for the rock mass based on the calculated deformations using the hypothetical <i>FLAC^{3D}</i> - <i>JointedRock</i> models. The back-calculated moduli from the PLT results are depicted by solid circles.	102

Appendix 2

Figure 1:	Geometry and boundary conditions for the uni-axial test on a jointed rock cylinder	113
Figure 2:	Axial deformation versus joint angle plots for confined uni-axial loading of the rock cylinder. Left: one joint set; right: two perpendicular joint sets.	114

Figure 3:	Axial deformation versus joint angle plots for unconfined uni-axial loading of the rock cylinder. Left: one joint set; right: two perpendicular joint sets.....	114
Figure 4:	Bending of intact rock layers during an unconfined uni-axial loading test with joint set angle $\alpha = 30^\circ$. (Grid deformation has been magnified by a factor of 20.) Maximum principal stress distribution in the rock layers (right) follows the typical stress distribution for a bending beam.....	116
Figure 5:	Variation of axial deformation versus joint spacing for a confined uni-axial test with one joint set ($\alpha = 30^\circ$).....	116
Figure 6:	Distribution of the vertical displacement and maximum principal stress in a confined test with one joint set ($\alpha = 30^\circ$).....	117
Figure 7:	Distribution of the vertical displacement and maximum principal stress in a confined test with two joint sets ($\alpha = 30^\circ$).....	117
Figure 8:	Stress tensors for a confined test with two joint sets ($\alpha = 45^\circ$). (Stress indicator bars for the two models are not on the same scale. Positive compressive stress convention applies.).....	118
Figure 9:	Vertical stress and vertical displacement contours for the confined tests with a single joint set ($s = 0.1$ m); left: <i>JointedRock</i> model, right: discontinuum (<i>3DEC</i>) model.....	119
Figure 10:	Vertical stress and vertical displacement contours for the confined tests with double joint sets ($s = 0.1$ m); left: <i>JointedRock</i> model, right: discontinuum (<i>3DEC</i>) model.....	122

Appendix 3

Figure 1:	Geometry Point load on a semi-infinite body (right). Circular and square distributed loads (left).....	124
-----------	--	-----

Chapter 1

Introduction

1.1. Overview

Discontinuities of various scales, ranging from few millimeters to a few kilometers, are common components of a rock mass. Large-scale discontinuities are formed during geological or tectonic activities and are frequently observed in clusters, such as bedding planes and tectonic or release joints. Small-scale discontinuities form following stress changes and disturbances caused by either tectonic or engineering activities, and are usually seen as randomly distributed and isolated fractures that follow the locally-induced major principal stresses. The fractures developed around a tunnel are examples of such discontinuities.

The large-scale discontinuities have a remarkable influence on the mechanical properties of rock masses such as deformability, permeability and strength. Jointed rock masses generally exhibit lower stiffness, higher permeability and lower strength compared to an intact rock.

The rock joints and their influence on the behaviour of rock masses have been an active research area in geomechanics for many years. With advancements in computing capacity, more sophisticated numerical modeling techniques have emerged over recent years. This has made it possible to incorporate more aspects of rock mass behaviour using advanced mechanical models. Researchers have suggested various analytical, numerical and empirical methods, all aimed at taking into account the influence of discontinuities on the mechanical behaviour of rock masses. Considerable attention has been given to the study of the mechanical behaviour of rock joints and to the techniques by which the joint models can be incorporated into the fundamental relationship governing the rock mass behaviour. These techniques can be divided into two general categories: discontinuum-based methods and continuum-based methods. In discontinuum-based methods, the discontinuities are explicitly incorporated into analysis using the principles of discontinuum mechanics, so the discrete nature of jointed rock

masses is directly acknowledged. In continuum-based methods, the jointed rock mass is replaced by an idealized equivalent continuum whose mechanical characteristics are established based on the properties of its constituents, i.e., rock matrix and discontinuities. The techniques used for this purpose can be divided in two general groups: direct methods and reverse methods. In direct methods, the equivalent properties/constitutive model are derived directly from that of the rock matrix and the discontinuities. In reverse methods, equivalent properties are estimated based on the back calculation of the rock mass behaviour observed in experiments or numerical simulations.

Given the discontinuous nature of jointed rock masses, the discontinuum-based methods more accurately represent the physical behaviour of the jointed rock masses. Rotation, dislocation and separation of rock blocks that are common deformation mechanisms for jointed rock masses can be modeled by these methods. However, when the number of discontinuities increases, the explicit definition of discontinuities becomes impractical and, in some cases, even unnecessary. Discontinuum-based models are also very sensitive to the applied boundary conditions, especially when the size of the structure to be modeled is rather small relative to the spacing of discontinuities. For these cases, continuum-based models provide a practical and more computationally efficient tool for analysis of jointed rocks.

The deformational properties of rocks are routinely determined by conducting laboratory and in-situ tests. The most common in-situ tests used for this purpose are plate loading test, dilatometer test, Goodman jack test and large flat-jack test. All of these tests basically involve loading a rock mass and measuring the resultant displacements. The measured displacements are then used to calculate the rock mass deformation modulus using the stress-strain relations developed based on the principles of continuum mechanics.

The plate-loading test has several advantages over the other tests. The test induces deformations in a relatively large volume of rock mass, which makes it better able to address the scale effect on the rock mass deformability. In addition, unlike other tests, no tensile stress component develops during the plate-loading test. The resulting compressive stress regime beneath the loading plate is similar to the stresses at the foundation of large structures such as gravity or arch dams. Hence the plate-loading test

is frequently used to assess the rock mass deformability at the foundation of structures founded on rocks.

The plate-loading test is normally performed in small test galleries. The test simply involves loading two opposite rock surfaces, by means of hydraulic jacks or flat jacks, and measuring the resultant deformations at the surface or within the rock mass. The Boussinesq's equation for a semi-infinite elastic body subjected to a distributed load, as suggested by the International Society for Rock Mechanics (ISRM), is regularly used to interpret the test results and calculate the deformation modulus. The test appears simple in principle but the interpretation of the results is associated with some practical and theoretical complications and uncertainties. The semi-infinite boundary condition assumption embedded in the ISRM suggested equation is not compatible with the real geometry of the test gallery (semi-square cross section). The confinement imposed by the surrounding rocks causes the ISRM suggested equation to overestimate the deformation modulus. The ISRM suggested method assumes the rock mass is a continuous, homogeneous, isotropic, linear elastic material. But in nature, rock masses rarely meet these assumptions, mainly because of discontinuities. In a jointed rock mass, the mechanical and geometrical characteristics of discontinuities have a dominant influence on the test results. Depending on the direction of loading relative to the orientation of discontinuities, different deformation mechanisms can get mobilized during the test. Ignoring the influence of discontinuities on the test results is the main factor that leads to scattered deformation moduli when the ISRM suggested equation is used. The main drawbacks of the ISRM suggested method are:

- Inconsistency of the theoretical assumptions with the real test site geometry, which results in a systematic error in the calculated moduli.
- The Poisson's ratio of the rock mass should be known beforehand.
- No meaningful relation can be established between the calculated deformation moduli and the discontinuities parameters,
- Too many tests are required to determine the deformability of a rock mass with varying discontinuity configurations

Alternatively, the numerical modelling techniques can be used to interpret the plate loading test results. Using this approach, the influence of discontinuities can be taken

into account and the rock mass deformability can be determined as a function of intact rock properties and joint properties. The discontinuities can be incorporated explicitly using discontinuum methods or implicitly using equivalent continuum models. For the discontinuum analysis, the exact geometrical configuration of all discontinuities affecting the test results should be known. These data can be collected by a thorough joint survey of the test site. When such detailed data are not available or when the spacing of joints is small compared to the size of loading plate, equivalent continuum models can be used. The advantages of numerical modeling techniques for interpretation of plate loading test results are:

- The real boundary condition and the test site geometry can be taken into account.
- It is possible to investigate the influence of the mechanical and geometrical properties of the discontinuities on the rock mass deformability.
- Fewer tests are required to determine the rock mass deformability for a jointed rock mass with various joint spacing and orientation.

1.2. Research Scope and Focus

The main focus of this research is to develop a practical continuum equivalent model for the deformation analysis of jointed rock masses. The results of a series of plate loading tests conducted at the Bakhtiary dam site in southwest Iran form the experimental basis of this research. By analyzing the test results, the rock mass deformation mechanisms mobilized during the tests are first investigated and characterized. A new equivalent continuum constitutive model is formulated and implemented in *FLAC^{3D}* for the stress-strain analysis of jointed rock masses. A methodology is proposed for interpretation of plate loading test results using the developed model. The thesis is structured as follows:

In Chapter 2, a brief introduction is provided on the principles of the stress-deformation analysis of continua, the deformation mechanisms of jointed rocks, the available methods for analyzing jointed rocks and, finally, the plate-loading test.

In Chapter 3 the results of 26 large-scale plate-loading tests conducted at the Bakhtiary dam site are studied to investigate the influence of pre-existing small spacing discontinuities on rock mass deformability and the test results. The tests are classified into several groups based on the rock structure and the loading direction relative to the

orientation of major discontinuities. For each group, the dominant deformation mechanism is identified and characterized by detailed analysis of the stress-deformation behaviour of the rock mass during the tests.

Chapter 4 deals with the formulation and implementation of a three-dimensional equivalent continuum constitutive model, namely *JointedRock*. The model is formulated for a Representative Elementary Volume (REV) containing one to three persistent discontinuity planes. The constitutive equations are established in tensor form, using the principles of the conservation of energy for the work done on the REV. A Mohr-Coulomb plasticity model is adopted for both the rock matrix and discontinuities. A C++ code is written for the *JointedRock* model and the model is implemented in *FLAC^{3D}* as a constitutive model. The model is verified against the discontinuum methods, and also closed form solutions, where available.

In Chapter 5, the rock mass deformation modulus is calculated using the ISRM-suggested equation, numerical modelling, and empirical relationships for the Bakhtiary dam foundation. The limitations of all methods are discussed. A new approach is then proposed for interpretation of the PLT results using the *JointedRock* model.

Appendix 1 provides the guidelines for loading the *JointedRock* model by *FLAC^{3D}* and presents the keywords associated with the model.

Appendix 2 includes the results of a detailed study on the boundary condition effect on the simulations done using the *JointedRock* model. The model is compared with distinct element code 3DEC and its limitations are discussed.

In Appendix 3 analytical relationships are derived for loading of a semi-infinite elastic body. Two cases of circular and square loads are considered. These relationships can be used for comparison with numerical simulation of a semi-infinite body.

Appendix 4 provides detailed data on the plate loading tests studied in Chapter 5.

1.3. Practical Implication and Outcome

The *JointedRock* model provides an efficient and practical tool for stress-deformation analysis of systematically jointed rock masses. The model is specifically advantageous in the following situations:

- problems with small spacing joint sets, where discontinuum methods cannot be applied,
- in combination with discontinuum models (hybrid model) for simulating the far-field jointed rock mass,
- bearing capacity analysis of jointed rock foundations in which the rock strength is directional due to the existence of joint sets.

The proposed method for interpretation of PLT results addresses the problems associated with the ISRM suggested method and the empirical relationships. The method potentially reduces the number of tests required to determine the deformability of a jointed rock mass.

Chapter 2

Background and Literature Review

Similar to other materials, rocks deform upon loading until an elastic or plastic equilibrium is reached. Under a given load, the amount by which a rock deforms depends on its elastic deformability and strength characteristics. The deformability of rocks is usually represented by two elastic constants: Deformation modulus (E) and Poisson's ratio (ν), or their reciprocal Lamé's constants. These parameters correspond to Hooke's law for an isotropic linear elastic material.

At the rock mass scale, when the intact rock is intersected by persistent discontinuities, the rock mass deformability becomes anisotropic and in many instances stress-dependent. For a general anisotropic rock mass, 21 elastic constants are required to describe the rock mass deformability by Hooke's law (Jaeger et al. 2007). The natural symmetries existing in some rock masses reduce this number. A review of the common symmetries observed in jointed rocks are provided in this chapter.

The deformation of jointed rocks might also be accompanied by displacement along the joints or the rigid body motion of rock blocks or layers. For such cases deformation of the rock mass cannot be calculated using Hooke's law but require more sophisticated models such as equivalent continuum or discontinuum models. The next sections include a brief review of the models available for deformation analysis of jointed rock masses.

2.1. Hooke's Law and Material Symmetry

Hooke's law establishes a linear relationship between the stress and strain in an elastic material. The material is assumed to be linear and homogeneous. In a general three-dimensional coordinate system, Hooke's law can be written in tensorial form as follows (Jaeger et al. 2007; Timoshenko and Goodier 1970):

$$\boldsymbol{\tau} = \mathbf{D}\boldsymbol{\epsilon} \tag{2.1}$$

Where $\boldsymbol{\tau}$ is the stress tensor, $\boldsymbol{\epsilon}$ is the strain tensor and \mathbf{D} is a fourth order tensor whose 81 components are known as the elastic stiffness constants (Jaeger et al. 2007). The stress

and strain tensors are second-order tensors with six independent components. This limits the number of independent elastic stiffness constants to 36.

It is a common practice to write the equation (2.1) in a matrix form to take advantage of the matrix algebra. Since there is no straightforward way to represent a fourth-order tensor in the matrix form, Voigt's method is usually invoked for this purpose. In this method, the stress and strain tensors are represented by 6×1 matrices and the elastic stiffness tensor is represented by a 6×6 matrix, as follows (Mase and Mase 1999):

$$\begin{bmatrix} \sigma_1 \\ \sigma_2 \\ \sigma_3 \\ \sigma_4 \\ \sigma_5 \\ \sigma_6 \end{bmatrix} = \begin{bmatrix} D_{11} & D_{12} & D_{13} & D_{14} & D_{15} & D_{16} \\ D_{21} & D_{22} & D_{23} & D_{24} & D_{25} & D_{26} \\ D_{31} & D_{32} & D_{33} & D_{34} & D_{35} & D_{36} \\ D_{41} & D_{42} & D_{43} & D_{44} & D_{45} & D_{46} \\ D_{51} & D_{52} & D_{53} & D_{54} & D_{55} & D_{56} \\ D_{61} & D_{62} & D_{63} & D_{64} & D_{65} & D_{66} \end{bmatrix} \begin{bmatrix} \epsilon_1 \\ \epsilon_2 \\ \epsilon_3 \\ \epsilon_4 \\ \epsilon_5 \\ \epsilon_6 \end{bmatrix} \quad (2.2)$$

where the constants D_{ij} are the components of the elasticity matrix. The components of the stress matrix are $\sigma_1 = \sigma_{11}$, $\sigma_2 = \sigma_{22}$, $\sigma_3 = \sigma_{33}$, $\sigma_4 = \sigma_{23}$, $\sigma_5 = \sigma_{13}$ and $\sigma_6 = \sigma_{12}$. The components of the strain matrix are $\epsilon_1 = \epsilon_{11}$, $\epsilon_2 = \epsilon_{22}$, $\epsilon_3 = \epsilon_{33}$, $\epsilon_4 = 2\epsilon_{23}$, $\epsilon_5 = 2\epsilon_{13}$ and $\epsilon_6 = 2\epsilon_{12}$. The factor "2" appears in the strain components in accordance with the original Voigt's work on engineering shear strains (Jaeger et al. 2007). Equation (2.1) can be written briefly as:

$$\boldsymbol{\tau} = \mathbf{D}\boldsymbol{\epsilon} \quad (2.3)$$

where $\boldsymbol{\tau}$, $\boldsymbol{\epsilon}$ and \mathbf{D} are matrix quantities. The inverse of Equation (2.3), which relates the stresses to the strains, can be written as

$$\boldsymbol{\epsilon} = \mathbf{C}\boldsymbol{\tau} \quad (2.4)$$

where \mathbf{C} is the elastic compliance matrix (Mase and Mase 1999).

For a general case of an anisotropic material with no physical symmetry, 36 elastic constants are required to establish the compliance matrix. Due to the symmetry of the strain and stress tensors in equation (2.1), only 21 constants are independent. For materials having some sort of physical symmetry, such as isotropic, transversely isotropic, orthotropic and monoclinic materials, the number of independent elastic constants decreases, depending on the number of symmetry directions.

2.1.1. Isotropic Material

An isotropic material refers to a material for which any arbitrary plane is a plane of symmetry. The compliance matrix of an isotropic material can be established provided two elastic constants, i.e. Young's modulus, E , and Poisson's ratio, ν , or their reciprocal Lamé constants, λ and G , are known (Goodman 1989). Equation (2.4) can be written in the matrix form as follows:

$$\begin{bmatrix} \epsilon_1 \\ \epsilon_2 \\ \epsilon_3 \\ \epsilon_4 \\ \epsilon_5 \\ \epsilon_6 \end{bmatrix} = \begin{bmatrix} 1/E & -\nu/E & -\nu/E & 0 & 0 & 0 \\ -\nu/E & 1/E & -\nu/E & 0 & 0 & 0 \\ -\nu/E & -\nu/E & 1/E & 0 & 0 & 0 \\ 0 & 0 & 0 & 1/G & 0 & 0 \\ 0 & 0 & 0 & 0 & 1/G & 0 \\ 0 & 0 & 0 & 0 & 0 & 1/G \end{bmatrix} \begin{bmatrix} \sigma_1 \\ \sigma_2 \\ \sigma_3 \\ \sigma_4 \\ \sigma_5 \\ \sigma_6 \end{bmatrix} \quad (2.5)$$

where G is the shear modulus. Intact rocks, and massive and densely jointed rock masses usually exhibit isotropic behaviour.

2.1.2. Transversely Isotropic Material

A transversely isotropic material has similar properties in all directions perpendicular to a rotational symmetry axis, κ , which is normal to a plane of isotropy (Jaeger et al. 2007). In other words, in a transversely isotropic material, there is a plane with the normal vector κ such that every plane perpendicular to it is a plane of symmetry. A transversely isotropic material has five independent elastic constants. For a case in which the rotational symmetry axis, κ , is aligned with the coordinate axis, e_3 (Figure 2.1), the stress-strain relationship can be written as follows (Lai et al. 2010):

$$\begin{bmatrix} \epsilon_1 \\ \epsilon_2 \\ \epsilon_3 \\ \epsilon_4 \\ \epsilon_5 \\ \epsilon_6 \end{bmatrix} = \begin{bmatrix} 1/E_1 & -\nu_{12}/E_1 & -\nu_{13}/E_3 & 0 & 0 & 0 \\ -\nu_{12}/E_1 & 1/E_1 & -\nu_{13}/E_3 & 0 & 0 & 0 \\ -\nu_{13}/E_1 & -\nu_{13}/E_1 & 1/E_3 & 0 & 0 & 0 \\ 0 & 0 & 0 & 1/G_{13} & 0 & 0 \\ 0 & 0 & 0 & 0 & 1/G_{13} & 0 \\ 0 & 0 & 0 & 0 & 0 & 1/G_{12} \end{bmatrix} \begin{bmatrix} \sigma_1 \\ \sigma_2 \\ \sigma_3 \\ \sigma_4 \\ \sigma_5 \\ \sigma_6 \end{bmatrix} \quad (2.6)$$

where indices 1, 2 and 3 refer to principal axes e_1 , e_2 and e_3 respectively. Sedimentary rocks with evenly spaced bedding planes and metamorphic rocks with foliations are examples of transversely isotropic rocks.

2.1.3. Orthotropic Material

A material with two or three mutually perpendicular planes of symmetry is called orthotropic. An orthotropic material has nine independent elastic constants. Provided the

coordinate axes are aligned with the normals to the three symmetry planes, the stress-strain relationship can be written as follows (Lai et al. 2010):

$$\begin{bmatrix} \epsilon_1 \\ \epsilon_2 \\ \epsilon_3 \\ \epsilon_4 \\ \epsilon_5 \\ \epsilon_6 \end{bmatrix} = \begin{bmatrix} 1/E_1 & -\nu_{12}/E_2 & -\nu_{13}/E_3 & 0 & 0 & 0 \\ -\nu_{12}/E_1 & 1/E_2 & -\nu_{23}/E_3 & 0 & 0 & 0 \\ -\nu_{13}/E_1 & -\nu_{23}/E_1 & 1/E_3 & 0 & 0 & 0 \\ 0 & 0 & 0 & 1/G_{23} & 0 & 0 \\ 0 & 0 & 0 & 0 & 1/G_{13} & 0 \\ 0 & 0 & 0 & 0 & 0 & 1/G_{12} \end{bmatrix} \begin{bmatrix} \sigma_1 \\ \sigma_2 \\ \sigma_3 \\ \sigma_4 \\ \sigma_5 \\ \sigma_6 \end{bmatrix} \quad (2.7)$$

Layered sedimentary rocks intersected with orthogonal tension joints are examples of orthotropic rock masses.

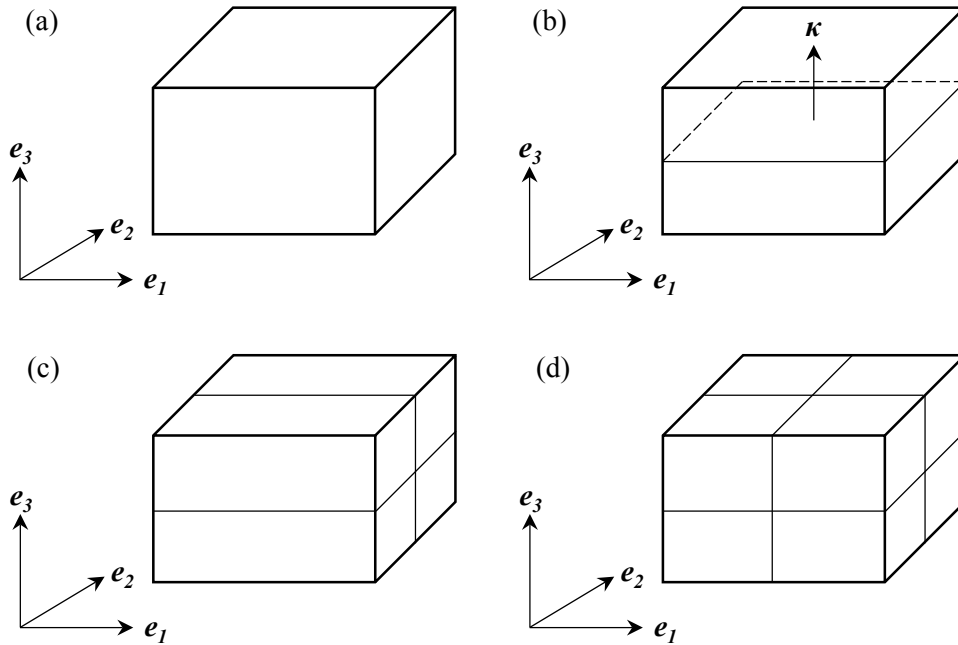


Figure 2.1: Common physical symmetries for rock masses. (a) Isotropic: every arbitrary plane is a plane of symmetry, (b) Transversely isotropic: κ is axis of symmetry, (c)(d) Orthotropic: two and three planes of symmetry as shown

Other forms of material symmetry, such as monoclinic symmetry, are rarely observed in rocks. One can refer to (Cowin and Mehrabadi 1987) for further discussion on the physical symmetry in anisotropic materials.

2.2. Deformation of Jointed Rock Masses

In nature, rocks are frequently intersected by discontinuities of random orientations. The intersection of these discontinuities results in a layered or blocky structure whose

mechanical characteristics are a function of the properties of the intact rock blocks and the discontinuities.

Deformation of a jointed rock mass consists of two components: deformation of intact rocks, and displacement along the joints. Depending on the boundary conditions and orientation of discontinuities, the translation and rotation of rock blocks might also occur. Therefore, the deformability of a jointed rock mass depends not only on the mechanical properties of the intact rock and the joints, but also on the geometrical factors. Figure 2.2 shows the effect of the boundary condition on the deformation of a jointed rock cylinder. When the lateral movement is prevented by the applied roller boundary condition, the axial deformation of the cylinder will be composed of the joint closure and the intact rock compression. If the roller boundary is removed, the dominant deformation mechanism switches to sliding and rigid translation of the upper rock block. The resultant axial deformation (δ_1 or δ_2) will depend on the mobilized deformation mechanism.

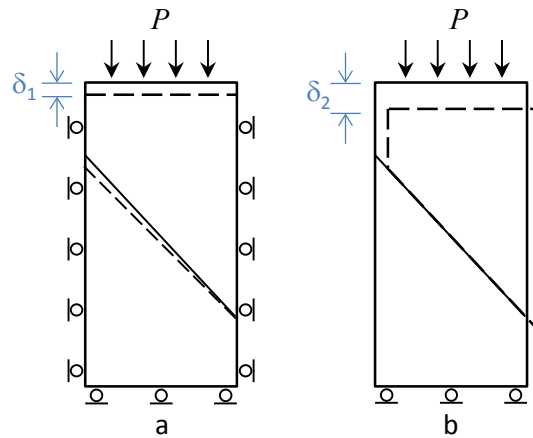


Figure 2.2: Effect of boundary condition on deformation mechanism of a jointed rock cylinder. (a) Lateral movement is prevented, deformation is a result of intact rock compression and normal closure of joint, (b) dominant deformation mechanism is shear sliding through the joint.

In a jointed rock mass, discontinuities can be divided into primary and secondary discontinuities. The primary discontinuities are those with high persistency that appear either in sets, such as bedding planes, or as a single plane, such as faults. The primary discontinuities have a dominant influence on the mechanical behaviour of the rock mass. The secondary joints include small-scale, randomly oriented single joints that are usually limited in size and have minimal influence on the large scale behaviour of the rock mass. A jointed rock mass, containing primary and secondary joints, can be considered as an assemblage of intact rock blocks, with downgraded mechanical properties, that are attached at the primary discontinuities, as shown in Figure 2.3.

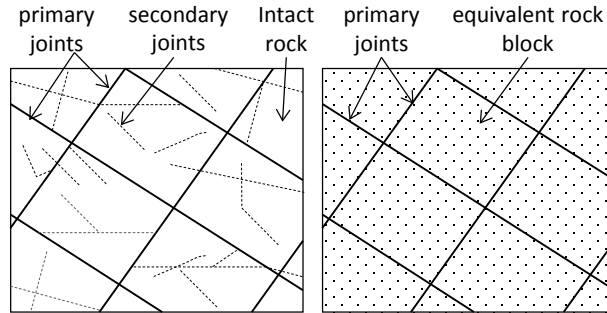


Figure 2.3: idealized model of a discontinuous rock mass with primary and secondary joints

Deformability of such idealized rock mass is a function of the following parameters:

- Deformability of rock blocks
- Normal and shear stiffness of primary discontinuities.
- Spatial configuration of primary discontinuities.
- Boundary conditions.

Due to the stochastic distribution of secondary joints, deformability of the rock blocks can be assumed to be isotropic and be represented by Hooke's law for the isotropic materials (Jaeger et al. 2007). The elastic constants for the rock blocks can be determined directly through laboratory testing, or indirectly through empirical relationships such as the one suggested by Hoek and Diederichs (2006). Alternatively, more advanced techniques such as the Synthetic Rock Mass (SRM) approach can be used (Ivars et al. 2007).

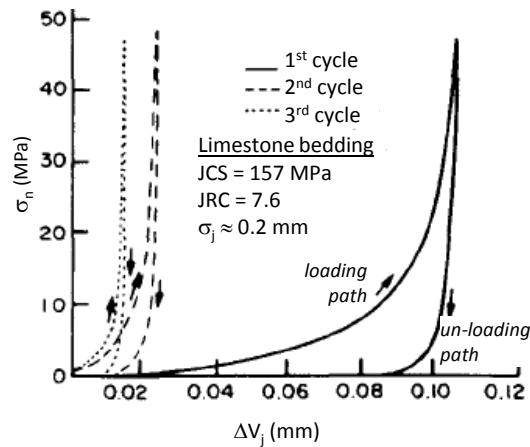


Figure 2.4: Normal stress (σ_n) versus closure (ΔV_j) for a fresh Limestone bedding plane subjected to repeated loading - unloading cycles (after Bandis et al. 1983)

Deformability of the discontinuities is usually represented by normal and shear stiffness. The experiments by Goodman (1976) and Bandis et al. (1983) showed that the normal

displacement of joints follows a non-linear relationship with the applied normal stress and can be represented by a hyperbolic function (Figure 2.4). Bandis et al. (1983) also observed a considerable hysteresis in the normal stress-normal displacement curves obtained from their experiments on mated and unmated joints of various rock types. They proposed a semi-logarithmic function for normal displacement of unmated joints (Bandis et al. 1983).

Misra (1999) and Misra and Marangos (2011) developed a joint deformation model using the principles of contact theory. In this method the intact rock is assumed to be linear elastic. The stiffness of joint asperities is defined using the Hertz or Mindlin contact model. The non-linearity of joint deformation is related to variations in total contact area during the loading and unloading process (Cook 1992).

Goodman (1976) proposed two models for the shear displacement of rock joints under various normal stresses, as shown in Figure 2.5. The first model represents a constant shear stiffness behaviour, whose peak elastic shear displacement is a function of the applied normal stress (constant stiffness model). In the second model the peak shear displacement is constant, and the shear stiffness varies as a function of the applied normal stress level (constant displacement model). The experimental studies by Bandis et al. (1983) demonstrate that the constant displacement model matches better the behaviour of the studied rock joints. Barton (2007; 1986) and Bandis et al. (1983) suggested that rock joints' shear stiffness is generally lower than their normal stiffness, which results in an anisotropic deformability for the rock joints.

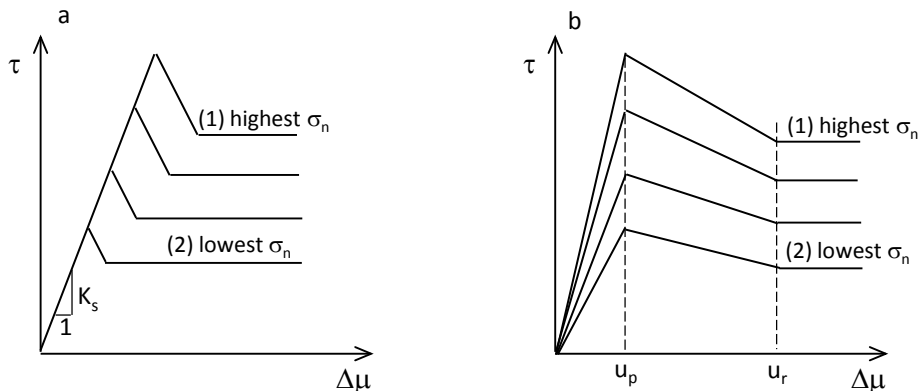


Figure 2.5: Shear stress versus shear displacement models: (a) constant stiffness model, (b) constant displacement model (after Goodman 1976)

Saeb and Amadei (1992) developed an incremental joint model that accounts for the coupling effect of normal stress-shear displacement and shear stress-normal displacement

for dilatant joints. They showed that for a dilatant joint, the normal stiffness decreases as the joint undergoes shear displacement.

Barton (1986; 2007) analyzed the results of several flat jack and plate loading tests conducted on jointed rock masses. He concluded that the rock mass deformability depends on the configuration of primary joints and is dominated by one of the following deformation modes:

- Normal closure or opening of discontinuities (Type A),
- Combination of normal and shear displacement along discontinuities (Type B),
- Shear displacement along discontinuities (Type C)

Figure 2.6 schematically shows the stress-deformation pattern and corresponding joint configuration for each deformation type as defined by Barton (1986). The main features of the rock mass deformation for each type are provided in Table 2.1.

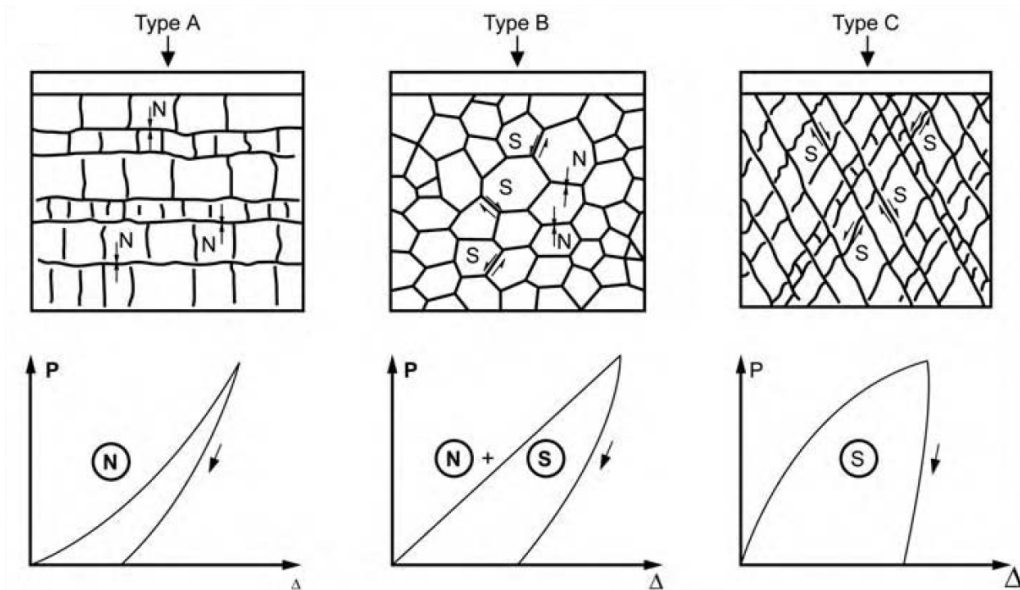


Figure 2.6: Conceptual stress-deformation curves for jointed rocks (after Barton 1986).

Table 2.1: Characteristics of stress-deformation patterns corresponding to three modes of deformation in jointed rocks (after Barton 2007).

Type	Dominant mode	Shape	Hysteresis	Lateral expansion	Poisson's ratio
A	normal	concave	small	small	low
B	normal+shear	linear	moderate	moderate	medium
C	shear	convex	large	large	high

2.3. Deformation Analysis of Jointed Rock Masses

Available methods for the analysis of jointed rock masses can be divided into two general categories: discontinuum-based methods, and continuum-based methods. Both methods depend extensively on numerical modelling techniques. Discontinuum-based methods acknowledge the discrete nature of a jointed rock mass. The rock mass is considered as an assemblage of rigid or deformable particles or blocks connecting along discontinuities. Equations of motion and contact models are used to calculate the dynamic equilibrium of the system and to update the position of the blocks in the model at each calculation step.

In continuum-based methods, on the other hand, the discontinuities are taken into account implicitly either by adopting proper equivalent continuum parameters or by using equivalent continuum models that incorporate the parameters of discontinuities into the constitutive equations of the model. Either methods are based on the principles of continuum mechanics. Figure 2.7 shows a classification of the most common methods available for the stress-strain analysis of jointed rock masses.

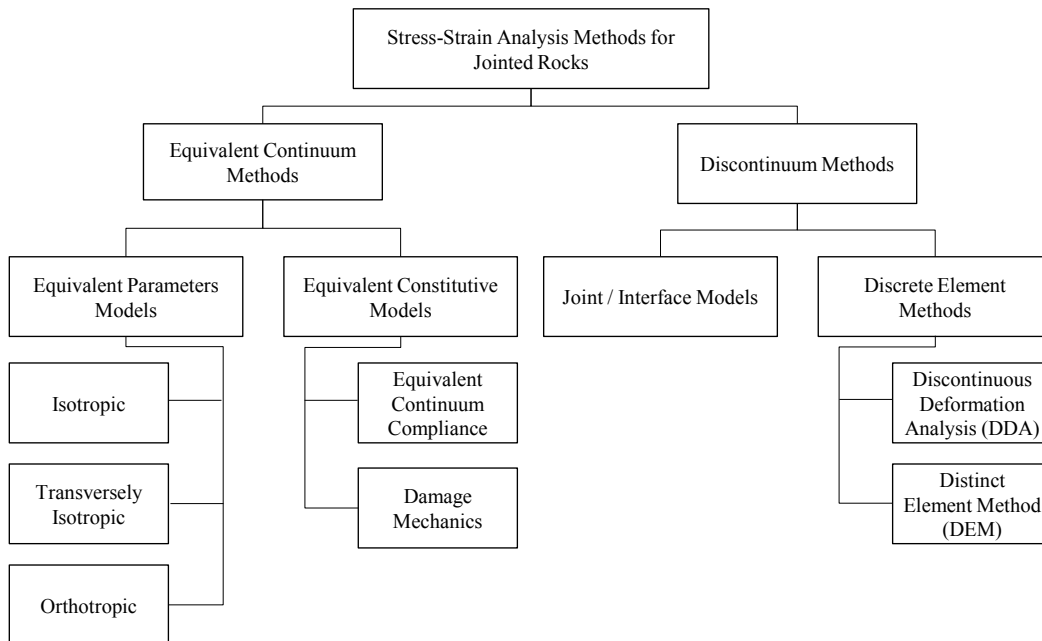


Figure 2.7: Available methods for stress-strain analysis of jointed rock masses

2.3.1. Discontinuum-Based Methods

The most common discontinuum-based methods for analysis of jointed rock masses are Distinct Element Method (DEM), Discontinuous Deformation Analysis (DDA) and Finite Element Method with interface model (FEM).

The Distinct Element Method (DEM), also called the explicit Discrete Element Method, was introduced by Cundall (1988, 1979). The method was originally created as a two-dimensional representation of a jointed rock mass, but it has been extended to applications in particle flow research, studies on microscopic mechanisms in granular material, and crack development in rocks and concrete (Itasca 2007). The model has developed over years and now can be used to analyze two- and three-dimensional problems with complex block geometries. In this method, the equations of motion are solved for the blocky system by an explicit finite difference method. The intact rock blocks can be rigid or deformable. Finite difference zones or finite volume elements are used for internal discretization of deformable blocks. The interaction between two contacting blocks is characterized by a stiffness (spring) in the normal direction and a stiffness and friction angle (spring-slip surface series) in the tangential directions with respect to the contact plane. Further discussion on the theoretical basis of the method can be found in the publications by Cundall (1988), Jing and Stephansson (2007) and Itasca (2007).

The DDA method, also referred to as the implicit Discrete Element Method, was originated by Goodman and Shi (1985) and further developed by Shi (1988). This method is formulated as a work-energy method and is based on the principle of minimum total potential energy for a mechanical system under loading. Similar to the explicit DEM, the DDA method also treats the rock mass as an assemblage of independent blocks separated by joints. Since the method accounts for the inertial forces of the blocks mass, it can be used to solve the full dynamic problem of block motion (Jing 2003). The original DDA formulation had embedded a first-order polynomial displacement function so the stress and strain were constant within the intact rock blocks. More recent versions of the DDA account for variations in stress (or strain) by adopting higher order elements (Grayeli and Hatami 2008). Jing (2003) lists the advantages of DDA over the explicit DEM, mainly from a numerical efficiency perspective, as follows:

- It is easy to convert an existing FEM code into a DDA code and benefit from many well-established techniques of the FEM without being restricted to the limitations of the ordinary FEM, such as deformation continuity and reduced efficiency for dynamic analysis.
- The equilibrium condition is automatically satisfied for quasi-static problems without using excessive iteration cycles.

- The length of the time step can be larger, and without causing numerical instability.
- Closed-form integrations for the element and block stiffness matrices can be performed without the need for Gaussian quadrature techniques.

Discontinuities can also be added explicitly to a finite element model using specially formulated continuum solid elements known as joint or interface elements. The four-node one-dimensional joint element introduced by Goodman et al. (1968) (Pande et al. 1990) has been used extensively in finite element modelling of problems in rock mechanics. Examples of such elements include the joint elements developed by Zienkiewicz et al. (1970), Ghabousi et al. (1973), and Desai et al. (1984) (Jing, 2003) (Pande et al. 1990) , and the interface elements developed by Katona (1983) and Wang and Yuan (1997).

A main disadvantage of the joint/interface models is their inability to address properly the large-scale opening or sliding of the joints, due to the continuum nature of FEM. In this method, once the interconnectivity between solid and joint elements is established upon meshing, it remains unchanged throughout the solution process. Therefore, large displacements of discrete rock blocks can be accommodated as long as the contact of node couples remains unchanged. DEM and DDA methods have no such restrictions: old contacts can be broken and new ones can be established and contact modes can change (Riahi and Hammah 2010).

The Discrete Fracture Network (DFN) model, in which a stochastic system of interconnected fractures is considered, has also received considerable attention for seepage analysis through fractured rocks. Min and Jing (2003) provide an example application of DFN for numerical determination of the equivalent continuum compliance tensor for a fractured rock.

2.3.2. Equivalent Continuum Methods

The continuum-based methods can be divided into two general categories: equivalent continuum parameters methods, and equivalent continuum constitutive methods. A review of these methods follows.

Equivalent Continuum Parameters Method:

In this method, the mechanical behaviour of a jointed rock mass is represented using a classical continuum constitutive model, and the influence of discontinuities is addressed by adopting proper equivalent continuum elastic constants. The Hooke's law for the isotropic, transversely isotropic or orthotropic rocks, discussed earlier in this chapter, are frequently used for this purpose. The main challenge of this method is determining the equivalent elastic parameters, i.e., the deformation modulus and Poisson's ratio, for the jointed rock mass.

A rough estimate of the equivalent deformation modulus can be obtained by using empirical equations developed based on the engineering rock mass classification systems. The relationships suggested by Hoek and Diederichs (2006), based on GSI, by Bieniawski (1978) and Serafim and Pereira (1983) based on the rock mass rating system (RMR); and by Barton (2002), based on the Q-system are the most common empirical equations used for this purpose. However, a fundamental assumption embedded in all empirical equations is that the rock mass deformability is isotropic (Hoek and Diederichs 2006), which is not usually the case in jointed rock masses. Such assumption limits the application of these equations to massive rocks or intensely jointed rocks whose deformability is mainly isotropic. Also, because the empirical equations have been established based on limited experimental data from in-situ tests, they are mainly valid for rock masses with comparable structure and stress field.

More reliable estimates of the modulus of deformation for a jointed rock mass can be obtained from in-situ tests conducted on a representative volume of the rock mass. Plate loading, flat jack, dilatometer and Goodman jack tests are the most common in-situ tests used for this purpose. The reliability of the deformation modulus determined by in-situ tests depends on factors such as test scale, frequency of test results, and the method used to interpret the test results. The number of tests required to determine the deformation modulus of a jointed rock mass depends on factors such as orientation and spacing of major discontinuities and variation of these parameters within a given rock mass. For transversely isotropic and orthotropic rocks, more tests, oriented properly with respect to major discontinuities, are required to determine the equivalent continuum elastic constants. Given the practical limitations associated with the size of the test apparatus, testing a representative volume of the rock mass might not be feasible when spacing of discontinuities are relatively large. The plate loading test is considered to provide the

most reliable results, in that a relatively large volume of rock mass is loaded by compressive stresses during the test (Bieniawski 1978). A detailed discussion on the plate loading test will follow in the next section and in the subsequent chapters.

Analytical solutions have also been suggested to derive the equivalent mechanical properties for a jointed rock mass. Gerard (1982) developed analytical relations to calculate the nine equivalent elastic constants for an orthotropic rock mass, based on the mechanical properties of intact rock and spacing of discontinuities. His method takes no account of joint mechanical parameters. Sitharam et al. (2007), Yoshinaka and Yamabe (1986) and Haung et al. (1995) also established closed-form solutions to determine the equivalent elastic constants for jointed rock masses.

The equivalent properties of a fractured rock can also be determined numerically, using the Synthetic Rock Mass (SRM) concept introduced by Ivars et al. (2007, 2011). In this method, a Discrete Fracture Network (DFN) is used to represent the discontinuities in a discrete model of the rock mass. The equivalent continuum mechanical properties of the rock mass is determined through running virtual tests on the numerical model. The examples of this method have been provided by Min and Jing (2003) and Pierce et al. (2007).

The main advantage of the equivalent continuum parameters method is its simplicity. There is no need to develop new sophisticated constitutive models or codes. The well-established models and codes available for analysis of continua can be readily used, provided that the elastic constants are known. The main drawbacks of this approach, excluding the SRM method, can be listed as follows:

- Its application is limited to some specific cases where rock mass is either isotropic, such as intensely fractured rocks; or features one of the elastic symmetries, such as transversely isotropic rocks.
- It is not compatible with real deformation mechanisms mobilized during deformation of jointed rock masses,
- It cannot be easily used to study the influence of the variation of discontinuities parameters on rock mass behaviour.
- It is mainly limited to elastic analysis.

Equivalent Continuum Constitutive Method

In this method, discontinuities parameters are directly incorporated into the constitutive equations of the equivalent continuum. Principles of continuum mechanics are used to establish an equivalent continuum constitutive model for the jointed rock mass. Depending on the assumed stress condition for the representative elementary volume (REV), two groups of these models can be distinguished, i.e., equivalent continuum compliance models and damage mechanics models.

Equivalent continuum compliance models assume a uniform stress within the REV. The total strain of the REV is related to the intact rock strains and the displacement along discontinuities. Governing equations for the equivalent continuum are established between the total strain and the assumed uniform stress for the REV. In damage mechanics models, the fundamental assumption is that the joints transmit no stress, and rock matrix is the solely load carrying element. The effective stresses on rock matrix are calculated using a so-called damage tensor. The constitutive relations are established between the effective stresses and the REV strain.

In damage mechanics models, joints are considered as the defect (damage) of intact rock (matrix) that transmit no stress. All stresses is carried by the intact rock. A so-called damage tensor is established, using the geometrical parameters of the joints, to determine the net or effective stresses on the intact rock. The constitutive laws are established between the net stresses and the total strain of the REV. A fundamental assumption embedded in this method is the non-persistence of rock joints. An evolution law is adopted to model the propagation of joints within the rock. Kawamoto et al. (1988) and Swoboda et al. (1998) provide more details on the method. While the method can be used for deformation analysis of jointed rock masses, it seems more suitable for failure analysis of rocks with non-persistent joints.

Singh (1973) used the concept of average strain energy density for an inhomogeneous elastic body, and established the constitutive equations for a rock mass containing three orthogonal joint sets. Using the same concept, Cai and Horii (1992) developed an equivalent continuum model by defining an REV and adopting a non-linear elasto-plastic model for joints. In both models, a so-called stress concentration tensor is used to calculate the stresses on joints. The joints can be non-persistent in both models. Interaction of the joints is taken into account by reducing the stiffness of surrounding

material using homogenization techniques. The main drawback to this method is that by assuming non-persistent joints of various dimensions, it becomes very difficult to find a proper REV for the rock mass.

Huang et al. (1995) suggested that the equivalent compliance tensor of a rock mass can be defined using the principle of conservation of energy for the work done by an external force on an elastic body. In this thesis this idea is used to establish a three-dimensional equivalent continuum constitutive model for rock masses containing up to three randomly oriented joint sets. In this model, joint sets are assumed to be planar and persistent throughout the REV. The model adopts an elasto-plastic model for both intact rock and rock joints. In Chapter 4, the theoretical details of this model and its formulation are presented, along with some example applications on the analysis of jointed rock masses.

Amadei and Goodman (1981) established closed-form relations to calculate compliance coefficients for a jointed rock mass containing three orthogonal persistent joint sets. Oda et al. (1993) introduced a crack tensor representing the geometry of discontinuities, and developed an elastic stress-strain relationship for rocks with random joints.

None of the abovementioned models account for the bending stiffness of rock layers in the equivalent continua. Rihai (2008) used the Cosserat theory for mechanics of micropolar continua and formulated a three-dimensional equivalent continuum model for finite element analysis of jointed rocks. The model takes into account the influence of micromoments on behaviour of the equivalent continuum. So, the model can account for the bending stiffness of intact rock layers, such as in stratified rock masses. The model potentially extends the application of the equivalent continuum modelling concept to analysis of problems in which the toppling or buckling of rock layers are likely instability/deformation mechanisms.

In the models developed based on the damage mechanics theory, joints are represented by a second-order symmetric tensor, known as the damage tensor. The concept is that if a rock mass involves a number of joints (or cracks) which are sufficiently small compared to the overall dimensions of the problem, the joints can be regarded as defects (or damages) of the rock mass. Joints are considered to transmit no stresses. The damage tensor is actually a measure used to calculate the effective load-bearing surface of intact (or undamaged) rock. So, effective stresses are calculated accordingly from the average stresses in an REV. The constitutive laws are established between the effective stresses

and actual strains in the REV. Joints are considered non-persistent within the REV. An evolution law is adopted to address the propagation of joints within the rock. Kawamoto et al. (1988), Swoboda et al. (1998) and Homan-Etienne et al. (1998) provide more details on the method. While the method can be used for deformation analysis of jointed rock masses, it seems more suitable for failure analysis of rocks with non-persistent joints.

2.3.3. Equivalent Continuum Methods versus Discontinuum Methods

Given the discontinuous nature of jointed rock masses, discontinuum-based models provide a more accurate description of the rock mass behaviour. However, these techniques are associated with some disadvantages, as follows:

- From a numerical modelling perspective, having the mesh size depend on the spacing and orientation of discontinuities significantly reduces the technique's efficiency for models with small spacing discontinuities relative to the model's overall size.
- Detailed geometry of all major joints needs to be known for a discontinuum model to be constructed. Such data is not usually available and not easy to collect. Besides, in many cases such detailed analysis of discontinuities is not required.
- Discontinuum models are more sensitive to applied boundary conditions, compared to equivalent continuum models. Figure 2.8 shows schematically two possible scenarios for a discontinuum model involving stiff loading of a jointed rock (displacement boundary condition). A slight shift in the applied load can potentially result in a different displacement beneath the rigid loading plate.

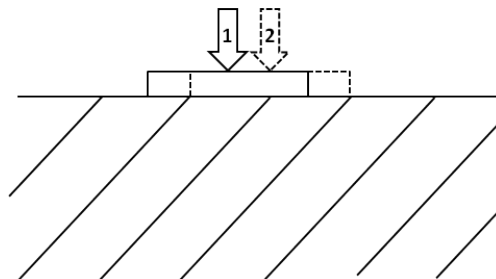


Figure 2.8: Sensitivity of discontinuous models to applied boundary conditions. A slight shift in the applied load would potentially result in different displacements

Equivalent continuum models, on the other hand, provide an average solution to the problem of jointed rock masses. The main advantages of this method are:

- The numerical discretization is independent of the spacing and orientation of discontinuities. This significantly reduces the model size and increases modelling efficiency,
- The method can be used even if the available data on the geometry and properties of discontinuities is limited.
- It can be readily used in combination with well-established continuum-based analysis methods, such as the finite element method and boundary element method.

The choice of continuum or discontinuum methods depends on many problem-specific factors, but mainly on the problem scale and the geometry of discontinuities. Figure 2.9 illustrates the alternative model choices for five common rock structures encountered in rock mechanics problems. Generally, continuum models can be applied to problems with no major joints (Figure 2.9a), with an intensely jointed structure (Figure 2.9b) and with joint sets of medium spacing (Figure 2.9c). The continuum methods should not be used when the spacing of joint sets is large with respect to the overall size of the problem (Figure 2.9d) or when discontinuities pattern and boundary conditions provoke rigid body motion of rock blocks (Figure 2.9d, 2.9e), and also when the behaviour of rock mass is potentially governed by few individual discontinuities (Figure 2.9e).

Continuum equivalent models can also be used in combination with discontinuum models (hybrid models), to model far-field discontinuities, while near-field discontinuities are represented explicitly using discontinuum models (Jing 2003).

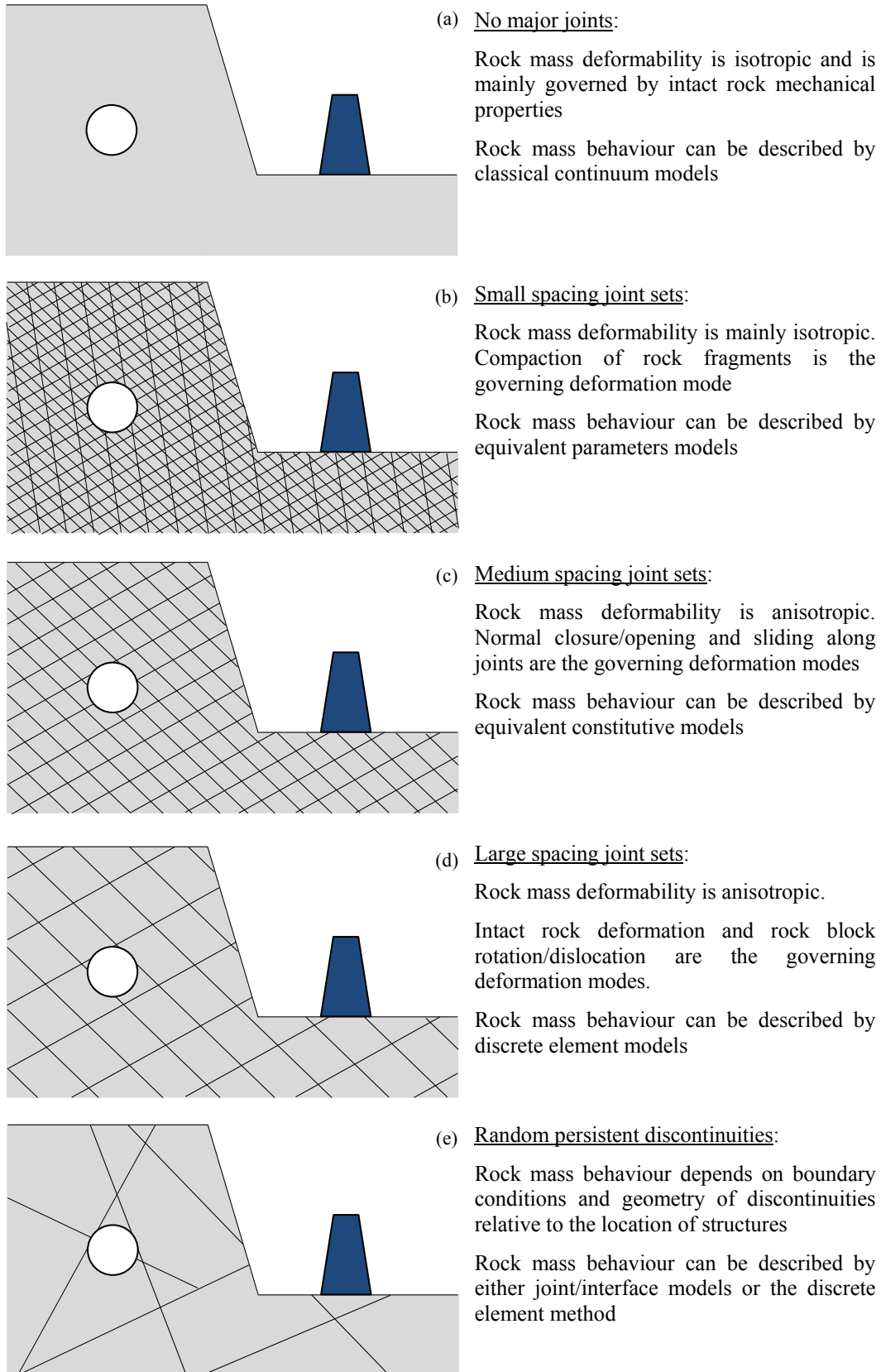


Figure 2.9: Discontinuity patterns and applicability of analysis techniques

2.4. Determination of Rock Mass Deformability by Plate Loading Test

The plate loading test is a common in-situ test for determination of the large scale deformability characteristics of rock masses. The test involves loading two opposite surfaces in a test gallery and measuring the induced deformations beneath loading plates and through the rock mass (Figure 2.10). Compared to borehole tests, i.e., dilatometer and Goodman jack tests, the plate loading test engages a considerably larger volume of rock mass, making it possible to obtain more accurate estimates of the deformability parameters.

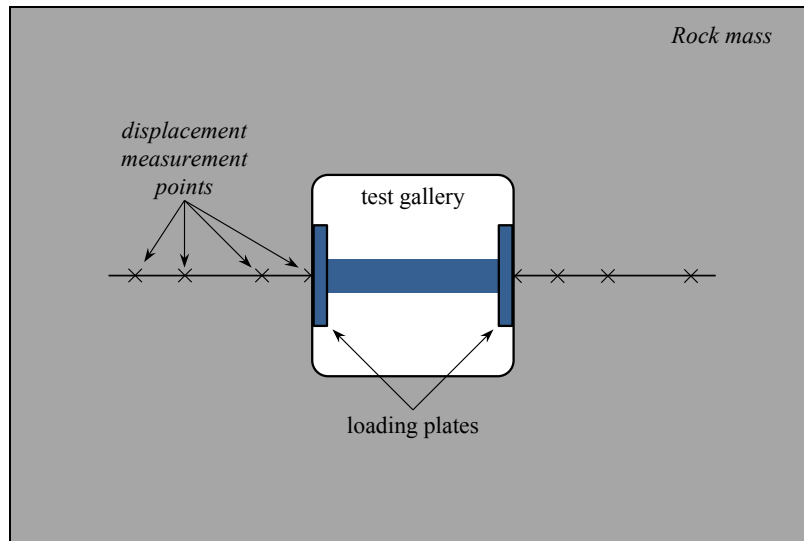


Figure 2.10: schematic view of a plate loading test in a test gallery

The accuracy and reliability of test results depend on factors such as the quality of testing operations, size of the loading plates relative to the spacing of discontinuities (scale effect), and consistency of the interpretation method with real rock mass conditions. Agharazi et al. (2008) divided the factors affecting the test results into two categories: operational factors and theoretical factors. Rock disturbance caused by blasting or stress release around the test gallery is an operational factor affecting the displacements measured during the test. The study of some plate loading test results by Palmstrom and Singh (2001) indicated that a correction factor as high as $f = 3$ is required to compensate for the effect of blasting damages on plate loading test results.

The ISRM (1979) suggested relationship is commonly used for interpretation plate loading test results. The relationship follows the Boussinesq's solution (Timoshenko & Goodier 1970) for loading a semi-infinite elastic homogeneous isotropic medium. Rock

masses rarely meet these assumptions. ISRM (1979) and Boyle (1992) recommend that a minimum ratio of $w/d = 2$ should be kept between the width (or height) of the test gallery (w) and the loading plate diameter (d) in order to avoid the influence of test gallery geometry on the test results. However, the numerical analysis of the test by Agharazi et al. (2008) showed that when displacement measurements are taken through depth, even for ratios as high as $w/d = 10$, the influence of test gallery geometry is not negligible on the deformation moduli calculated using the ISRM suggested relationship (Figure 2.11).

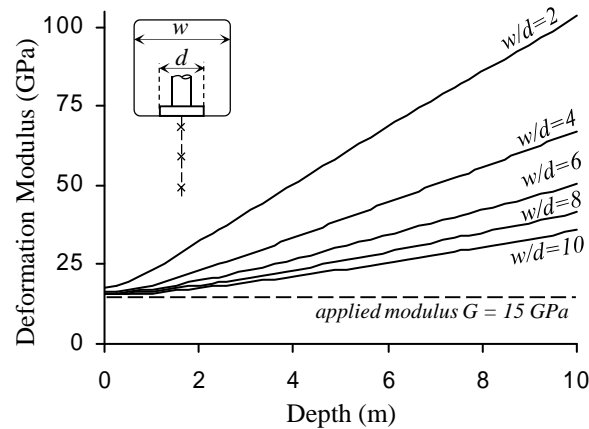


Figure 2.11: Increasing trend of deformation modulus calculated using ISRM suggested relationship based on numerical modelling of plate loading test (after Agharazi et al. (2008))

The inconsistency of the gallery geometry with the semi-infinite geometry assumption, leads to the overestimation of moduli by the ISRM suggested relationship. This error increases with depth as shown in Figure 2.12. To address this problem, Boyle (1992) proposed a statistical approach that finds a pair of deformation modulus and Poisson's ratio that fits best the results of a given test. However, this approach does not address the main problem associated with the ISRM suggested method. The influence of test gallery geometry on deformation moduli calculated from the plate loading test results will be discussed in more details in Chapter 5.

The plate loading test usually results in higher deformation moduli than do borehole tests, such as the Dilatometer test and Goodman jack test. Various researchers have reported a ratio of $D_p / D_b = 2-3$ for the moduli calculated from plate loading test results (D_p) and those from borehole tests (D_b) (Bieniawski 1978; Palmstrom and Singh 2001; Singh 2011; Agharazi and Moradi 2004). This difference can be attributed, to some extent, to the difference between the stress regime of the tests. In the Plate loading test, a completely compressive stress regime develops within the rock mass, while the borehole tests generate a tangential tensile stress at the borehole periphery. Another reason for this

issue is that the plate loading test overestimates the rock mass stiffness because of the test gallery's confining effect.

When the plate loading test is conducted on jointed rock masses, the size of the loading plate relative to the spacing of discontinuities is an important factor affecting the test results. Plate size should be large enough to load a representative volume of rock mass, or the results will not be valid. The size of the loading plate, on the other hand, is limited by some practical factors, such as mobility, minimum required plate stiffness and the dimension of test gallery. Plates with diameters of up to $d \approx 1$ m are common for tests on fair to competent rocks.

The deformation mechanisms mobilized during a plate loading test depend on the discontinuities pattern and the size of the loading plate. The test results interpretation method should be consistent with the mobilized deformation mechanism. Figure 2.12 illustrates schematically possible joint patterns for a plate loading test. When the spacing of discontinuities is several times that of the plate diameter (Figure 2.12a), test results are mainly representative of intact rock deformation, provided individual discontinuities do not intersect the test influence zone. For this case, the ISRM suggested method or, alternatively, the back calculation techniques using an elastic isotropic model, can be applied. If the ISRM suggested relationship is used, corrections for the test gallery geometry effect should be made. The discontinuities intersecting the test influence zone and affecting the test results should be explicitly taken into account by adopting a proper model, such as joint or interface models.

When the spacing of discontinuities is about the size of the loading plate (Figure 2.12b), the test influence zone will not be representative of the rock mass. The test results will depend on the position of the loading plate relative to the discontinuities and on the loading direction relative to the orientation of the discontinuities. The ISRM suggested relationship or any continuum model will potentially produce scattered and non-representative moduli. In such cases, a discontinuum-based model should be used for interpretation of the test results.

When the spacing of discontinuities is less than half a plate size (diameter) (Figure 2.12c), test results depend highly on the direction of loading relative to the orientation of discontinuities. For such cases, the influence of the discontinuities should be taken into account by a proper interpretation method. In these cases, the ISRM suggested

relationship will potentially produce scattered and non-representative moduli. An equivalent continuum constitutive model, which incorporates the mechanical and geometrical parameters of discontinuities, can be efficiently applied for this case.

For intensely jointed rock masses, where the spacing of joint sets is a fraction of the loading plate diameter (Figure 2.12d), the test influence zone can be assumed to be a representative volume of rock mass. The ISRM suggested relationship, or an equivalent continuum parameters model, can be used to determine the equivalent deformability parameters of the rock mass. Extra care should be used in selecting the Poisson's ratio in this case.

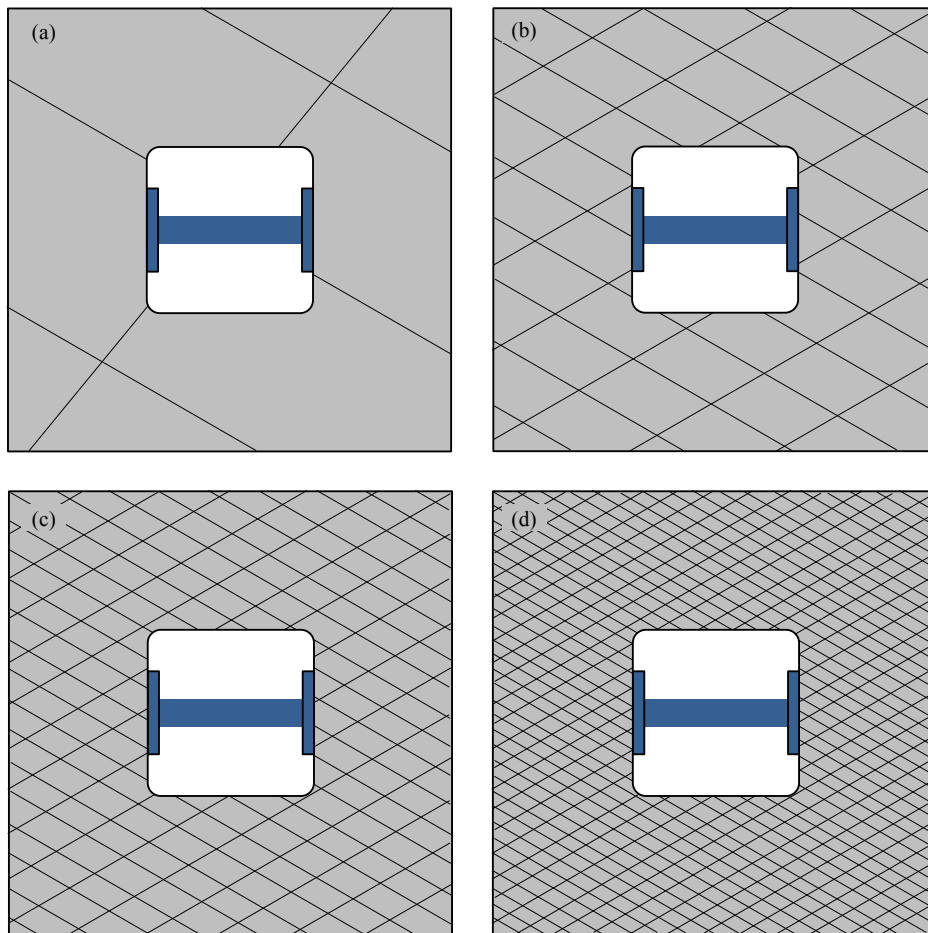


Figure 2.12: Loading plate size relative to spacing of discontinuities. (a) Joint spacing several times of plate diameter. Test results are representative of intact rock deformation (b) Joint spacing is about the loading plate diameter. Test results depend highly on the relative position of the loading plate and the discontinuities. Deformability is highly anisotropic (c) Joint spacing is less than half plate diameter. Test results depend on the direction of loading relative to the direction of discontinuities. (d) Intensely jointed rock mass. Test results are representative of jointed rock mass deformation.

In Chapter 5, the *JointedRock* model is used to interpret the results of the plate loading tests conducted at the Bakhtiary dam and hydro-electric power plant site. The tests were conducted on a rock mass with two sets of regular persistent discontinuities. The spacing of discontinuities ranges from 150 mm to 600 mm, while the diameter of the loading plates used for the tests ranges from 650 mm to 975 mm. This resembles the configuration illustrated in Figure 2.12c. This study indicates that deformation of the rock mass is highly anisotropic and highly dependent on the geometry and mechanical properties of the discontinuities.

2.5. References

- Agharazi, A., Moradi, M. (2004). Comparison between plate load test results and dilatometer test results - Case study, Seymareh dam and Sazbon dam projects. Proceedings International Conference on Geotechnical and Geophysical Site Characterization ISC-2, Porto, Volume 1, pages 265-270, Millpress, Rotterdam
- Agharazi, A., Tannant, D., Jafari, A. (2008). Stress and tunnel geometry effects on deformation modulus derived from plate load tests. Proceedings of 61st Canadian Geotechnical Conference & 9th Joint CGS/IAH-CNC Groundwater, Edmonton, volume 1, pages 601-608. Bi-Tech Publishers Ltd., Richmond.
- Amadei, B., Goodman, R. E. (1981). A 3-D constitutive relation for fractured rock masses. Proceedings of the International Symposium on the Mechanical Behaviour of Structured Media, Ottawa Part B, pages 249-268
- Bandis, S., Lumsden, A., Barton, N. (1983). Fundamentals of rock joint deformation. International Journal of Rock Mechanics and Mining Sciences & Geomechanics Abstracts, 20(6), 249-268.
- Barton, N. (2002). Some new Q value correlations to assist in site characterization and tunnel design. International Journal of Rock Mechanics and Mining Sciences, 39, 185-216.
- Barton, N. (2007). Rock Quality, Seismic Velocity, Attenuation and Anisotropy. Leiden: Taylor & Francis.

- Barton, N. R. (1986). Deformation phenomena in jointed rock. *Geotechnique*, 36(2), 147-167.
- Barton, N., Bandis, S., Bakhtar, K. (1985). Strength, deformability and conductivity coupling effect of rock joints. *International Journal of Rock Mechanics and Mining Sciences & Geomechanics Abstracts*, 22(3), 121-140.
- Bieniawski, Z. T. (1978). Determining rock mass deformability - experience from case histories. *International Journal of Rock Mechanics and Mining Sciences & Geomechanics Abstracts*, 15(5), 237-247.
- Boyle, W. (1992). Interpretation of plate load test data. *International Journal of Rock Mechanics and Mining Sciences*, 29, 133-141.
- Cai, M., Horii, H. (1992). A constitutive model of highly jointed rock masses. *Mechanics of Materials*, 13, 217-246.
- Cook, N. G. (1992). Natural joints in rock: mechanical, hydraulic and seismic behaviour and properties under normal stress. *International Journal of Rock Mechanics and Mining Sciences & Geomechanics Abstracts*, 29, 198-223.
- Cowin, S. C., Mehrabadi, M. M. (1987). On the identification of material symmetry for anisotropic elastic materials. *Quarterly Journal of Mechanics and Applied Mathematics*, 40, 451-476.
- Cundall, P. (1988). Formulation of a three-dimensional distinct element model - Part I: a scheme detect and represent contacts in a system composed of many polyhedral blocks. *International Journal of Rock Mechanics and Mining Sciences & Geomechanics Abstracts*, 25(3), 107-16.
- Cundall, P., Strack, O. (1979). A discrete numerical model for granular assemblies. *Geotechnique*, 29(1), 47-65.
- Gerrard, C. M. (1982). Elastic models of rock masses having one, two and three sets of joints. *International Journal of Rock Mechanics and Mining Sciences & Geomechanics Abstracts*, 19(1), 15-23.
- Goodman, R. E. (1976). *Methods of Geological Engineering in Discontinuous Rocks*. St Paul: West Publication.

- Goodman, R. E. (1989). Introduction to Rock Mechanics (2nd edition). John Wiley & Sons.
- Goodman, R. E., Shi, G. (1985). Block Theory and Its Application to Rock Engineering. Prentice-Hall.
- Grayeli, R., Hatami, K. (2008). Implementation of the finite element method in the three-dimensional discontinuous deformation analysis (3D-DDA). International Journal for Numerical and Analytical Methods in Geomechanics, 32, 1883-1902.
- Hoek, E., Diederichs, M. (2006). Empirical estimation of rock mass modulus. International Journal of Rock Mechanics and Mining Sciences, 43, 203-215.
- Homand-Etienne, F., Hoxha, D., Shao, J. F. (1998). A continuum damage constitutive law for brittle rocks. Computers and Geotechnics, 22(2), 135-151.
- Huang, T. H., Chang, C. S., Yang, Z. Y. (1995). Elastic moduli for fractured rock mass. Rock Mechanics and Rock Engineering, 28(3), 135-144.
- ISRM. (1979). Suggested method for determination of insitu deformability of rock. International Journal of Rock Mechanics and Mining Sciences(16), 143-146.
- Itasca Consulting Group, Inc. (2007). 3DEC, 3 Dimensional Distinct Element Code, User's Guide. Minneapolis.
- Ivars, D. M., Deisman, N., Pierce, M., Fairhurst, C. (2007). The Synthetic rock mass approach - A step forward in the characterization of jointed rock masses. 11th Congress of the International Society for Rock Mechanics. Lisbon.
- Ivars, D. M., Pierce, M. E., Darcel, C., Reyes-Montes, J., Potyondy, D. O., Young, R. P., Cundall, P. A. (2011). The synthetic rock mass approach for jointed rock mass modelling. International Journal of Rock Mechanics & Mining Sciences, 48, 219-244.
- Jaeger, J., Cook, N., Zimmerman, R. (2007). Fundamentals of Rock Mechanics (Fourth ed.). Blackwell Publishing Ltd.

- Jing, L. (2003). A review of techniques, advances and outstanding issues in numerical modelling for rock mechanics and rock engineering. *International Journal of Rock Mechanics and Mining Sciences*, 40, 283-353.
- Jing, L., Stephenson, O. (2007). *Fundamentals of Discrete Element Methods for Rock Engineering, Theory and Applications*. Elsevier.
- Jing, L., Nordlund, E., Stephenson, O. (1992). An experimental study on the anisotropy and stress dependency of the strength and deformability of rock joints. *International Journal of Rock Mechanics and Mining Sciences & Geomechanics Abstracts*, 29, 535-542.
- Katona, M. G. (1983). A simple contact-friction interface element with applications to buried culverts. *International Journal for Numerical and Analytical Methods in Geomechanics*, 7, 371-384.
- Kawamoto, T., Ichikawa, Y., Kyoya, T. (1988). Deformation and fracturing behaviour of discontinuous rock mass and damage mechanics theory. *International Journal for Numerical and Analytical Methods in Geomechanics*, 12, 1-30.
- Lai, W. M., Rubin, D., Krempl, E. (2010). *Introduction to Continuum Mechanics* (4th ed.). Elsevier.
- Mase, G.T., Mase, G.E. (1999). *Continuum Mechanics for Engineers*. CRC Press LLC.
- Min, K. B., Jing, L. (2003). Numerical determination of the equivalent elastic compliance tensor for fractured rock masses using distinct element method. *International Journal of Rock Mechanics and Mining Sciences*, 40, 795-816.
- Misra, A. (1999). Micromechanical model for anisotropic rock joints. *Journal of Geophysical Research: Solid Earth*, 104, 23175-23187.
- Misra, A., Marangos, O. (2011). Rock-joint micromechanics: Relationship of roughness to closure and wave propagation. *International Journal of Geomechanics*, 11, 431-439.
- Oda, M., Yamabe, T., Ishizuka, Y., Kumasaka, H., Tada, H., Kimura, K. (1993). Elastic stress and strain in jointed rock masses by means crack tensor analysis. *Rock Mechanics and Rock Engineering*, 26(2), 89-112.

- Palmstrom, A., Singh, R. (2001). The deformation modulus of rock masses - comparisons between in situ tests and indirect estimates. *Tunnelling and Underground Space Technology*, 16, 115-131.
- Pande, G. N., Beer, G., Williams, J. R. (1990). *Numerical methods in rock mechanics*. Chichester: John Wiley & Sons.
- Pierce, M., Cundall, P., Potyondy, D., Mas Ivars, D. (2007). A synthetic rock mass model for jointed rock. *Rock Mechanics: Meeting Society's Challenges and Demands*.
- Riahi, A. (2008). *3D Finite Element Cosserat Continuum Simulation of Layered Geomaterials*. PhD Thesis. Toronto: University of Toronto.
- Riahi, A., Hammah, E. R. (2010). Limits of applicability of the finite element explicit joint model in the analysis of jointed rock problems. *Proceeding of 44th US Rock Mechanics Symposium and 5th US-Canada Rock Mechanics Symposium*. Salt Lake City, ARMA.
- Saeb, S., Amadei, B. (1992). Modelling rock joints under shear and normal loading. *International Journal of Rock Mechanics and Mining Sciences & Geomechanics Abstracts*, 29(3), 267-278.
- Serafim, J. L., Pereira, J. P. (1983). Consideration of the geomechanical classification of Bieniawski. *Proceedings of International Symposium on Engineering Geology and Underground Construction*. Lisbon , Portugal, LNEC, volum 1 (I), pages 33–44.
- Shi, G. H. (1988). *Discontinuous deformation analysis: A new numerical model for the statics and dynamics of block systems*. PhD Thesis. University of California, Berkeley.
- Singh, B. (1973). Continuum characterization of jointed rock masses. *International Journal of Rock Mechanics and Mining Sciences & Geomechanics Abstracts*, 10, 311-335.
- Singh, R. (2011). Deformability of rock mass and a comparison between plate jacking and Goodman jack tests. *International Journal of Rock Mechanics and Mining Sciences*, 48, 1208-1214.

- Sitharam, T. G., Maji, V. B., Verma, A. K. (2007). Practical equivalent continuum model for simulation of jointed rock mass using FLAC3D. *International Journal of Geomechanics*, 7, 389-395.
- Swoboda, G., Shen, X. P., Rosas, L. (1998). Damage Model for Jointed Rock Mass and Its Application to Tunnelling. *Computers and Geomechanics*, 22(3/4), 183-203.
- Timoshenko, S., Goodier, J. (1970). *Theory of Elasticity* (3rd ed.). McGraw-Hill.
- Yoshinaka, R., Yamabe, T. (1986). Joint stiffness and the deformation behaviour of discontinuous rocks. *International Journal of Rock Mechanics and Mining Sciences & Geomechanics Abstracts*, 23(1), 19-28.
- Zienkiewicz, O. C., Best, B., Dullage, C., Stagg, K. (1970). Analysis of non-linear problems in rock mechanics with particular reference to jointed rock systems. *Proceedings of the Second International Conference on Rock Mechanics*. Belgrade, Yugoslavia, 3 pp. 501–509

Chapter 3

Characterizing Rock Mass Deformation Mechanisms During Plate Loading Tests at the Bakhtiary Dam Site¹

3.1 Introduction

The deformation modulus of a rock mass is an important parameter in the design of large concrete dams. Due to scale dependency and influence of discontinuities, results from laboratory tests on samples of intact rock cannot be relied on for the determination of the rock mass deformability characteristics. The empirical relationships, such those established by Bieniawski (1978) that relates the rock mass modulus E_{rm} to the Rock Mass Rating RMR and Hoek and Diederichs (2006) and Hoek et al. (2002) that relates E_{rm} to the Geological Strength Index GSI, unconfined compressive strength UCS, and disturbance factor, can be used to estimate rock mass modulus in the preliminary stages of design. However for final design purposes, in situ testing remains the most reliable means for establishing the rock mass deformation modulus. The plate loading test (PLT), dilatometer and large flat jack test are common tests for this purpose (Bieniawski 1978; Palmstrom and Singh 2001; Boyle 1992).

In the plate loading test, a distributed load is applied on rock mass surface and the induced displacement below the loaded plate and through the rock is measured. A mathematical model is then used to relate the applied stress to measured deformations in order to calculate the deformation modulus. Therefore, compatibility of the assumptions in the model with the actual rock mass response is an important factor in the interpretation of the test results and for obtaining an accurate assessment of the rock mass deformability characteristics.

The ISRM suggested method (ISRM 1979) is commonly used for the interpretation of plate loading test results. In this method, the rock mass is assumed to deform as a

¹ A version of this chapter has been published as a paper by International Journal of Rock Mechanics & Mining Sciences:

Agharazi, A., Tannant, D. D. and Martin, C. D. (2012). "Characterizing rock mass deformation mechanisms during plate load tests at the Bakhtiary dam project". International Journal of Rock Mechanics & Mining Sciences, 49,1-11

Continuous Homogeneous Isotropic Linear Elastic (CHILE) material with a semi-infinite geometry.

These conditions are typically not met when the test is carried out in small test galleries on a jointed rock mass. Deformation of a jointed rock mass involves two components: 1) deformation of intact rock, which usually exhibits a linear elastic behaviour, and 2) deformation of the joints, which may behave in an anisotropic, nonlinear and plastic manner. Depending on which component prevails, different deformation mechanisms may be mobilized and govern the total response of the rock mass. In this paper, the analysis of 26 plate loading tests from the Bakhtiary dam site in Iran is presented to demonstrate the influence of different deformation mechanisms on the interpretation of the plate loading tests.

3.2 Plate Loading Test - Theory and Interpretation

“Plate loading” covers a range of similar tests that are performed on rock and soil, in small exploratory galleries or at surface, to measure the deformational characteristics of the in situ rock or soil. The plate loading test, which has wide application in rock engineering practice, involves loading two opposite sides of a test gallery, by stiff or flexible plates, and measuring the corresponding deflections at the surface and at depth below the plate (Figure 3.1).

Depending on the method of transferring the test load to the rock mass, two types of plate loading tests are distinguished: “rigid loading” and “flexible loading”. In the first type, a rigid plate transfers the load generated by the hydraulic jack(s) to the rock and theoretically produces a uniform displacement boundary condition on the rock surface. In the second type, a flat jack transfers the load to the rock mass and produces a uniform stress boundary condition. In the former case, the minimum required stiffness of the loading plate limits the application of this test to soils and soft rocks, where the stiffness of the loading plate is at least twice that of the stiffness of the rock mass, as proposed by Lama and Vutukuri (1978). In hard rocks, loading plates of one metre in diameter and larger rarely have enough stiffness and rigidity to resist distortion under the high test loads and therefore they cannot maintain a uniform displacement boundary condition (Van Heerden and Maschek 1979).

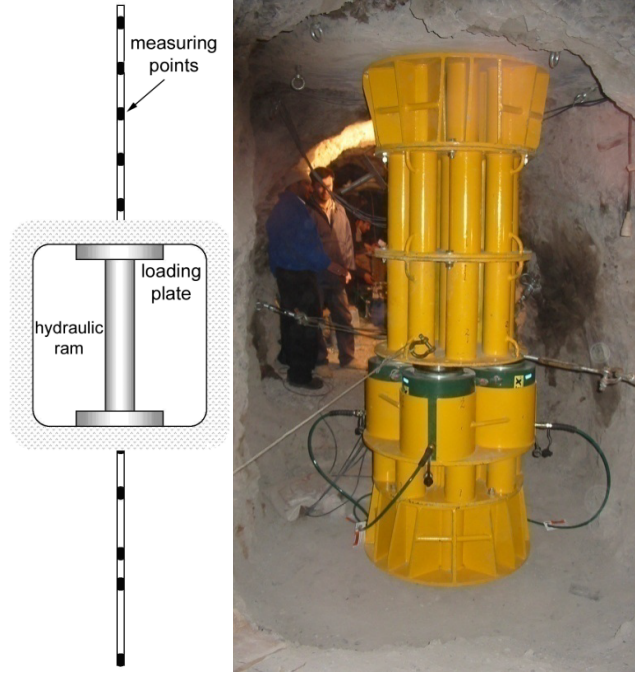


Figure 3.1: Plate loading test set-up (Bakhtiary dam site).

The main objective of a plate loading test is to determine the deformation modulus of the rock mass. This is usually done by interpretation of the measured displacements using the ISRM suggested method for “determination of the deformation modulus of the rock mass” (ISRM 1979). The theoretical basis of this method is the theory of linear elasticity and the relations presented by Boussinesq for a semi-infinite medium loaded on the boundary.

The equation for the calculation of the modulus is obtained by the integration of the deformations caused by individual elements of the load, distributed over a given area on the boundary of the semi-infinite medium. Depending on the boundary condition at the loading surface, i.e. rigid or flexible loading, the following equations are used, respectively (Timoshenko and Goodier 1970):

$$w = \frac{a q(1+\nu)}{2E} \left[2(1-\nu) \text{Cot}^{-1} \left(\frac{z}{a} \right) + \frac{a z}{z^2+a^2} \right] \quad (3.1)$$

$$w = \frac{zq(1+\nu)}{E} \left[1 - z(a^2 + z^2)^{-1/2} \right] + \frac{2q(1-\nu^2)}{E} \left[(a^2 + z^2)^{1/2} - z \right] \quad (3.2)$$

where:

w = vertical displacement

a = radius of loading plate

q = applied stress

E = modulus of elasticity

ν = Poisson's ratio

z = depth of deformation measurement along loading plate axis.

The component of stress perpendicular to the loaded surface ' σ_z ' developed in the semi-infinite body because of the circular distributed load q on the boundary is:

$$\sigma_z = q \left[-1 + \frac{z^3}{(a^2+z^2)^{3/2}} \right] \quad (3.3)$$

3.3 Parameters Influencing Test Results and Data Interpretation

The main factors influencing the PLT results can be classified into two categories. First are "operational factors" directly related to the quality of the test such as the resolution of measurement instruments, quality of the site preparation and its effect on the in situ condition of the rock mass, and proper installation of the test apparatus. Blast damage and rock disturbance around the test gallery are the important examples of this category. In the field experiment described by Palmstrom and Singh (2001), a blast damage factor of three was applied to the calculated moduli to compensate for the damages to the rock caused by blasting.

The second category includes "theoretical factors" that give rise to inconsistency between the theoretical basis and test assumptions and the actual condition and behaviour of the rock mass during the test. These factors cause misinterpretation of the test results and generation of invalid moduli. The main factors in this category are:

- geometry of the test gallery,
- influence of discontinuities on stress distribution and deformations,
- different deformation mechanisms that might be mobilized during the test, depending on the relative direction of loading to the orientation of major discontinuities, and
- stress dependency and non-linearity of deformational parameters of discontinuities (or intact rock) and influence of the in situ stress field.

A common problem in the interpretation of PLT results, using the ISRM suggested method, is the apparent trend of increasing moduli with depth of deformation measurement for a given test (Figure 3.2). In some cases, this trend results in calculated rock mass moduli that are greater than that of the intact rock. This problem mainly occurs due to the special configuration of the test in small test galleries, which differs from the semi-infinite geometry assumption taken in the ISRM suggested method (Boyle 1992; Agharazi et al. 2008).

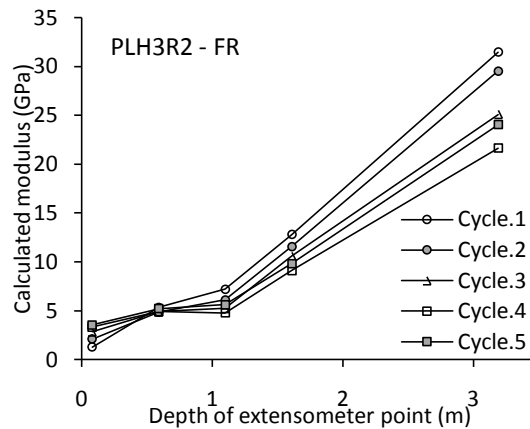


Figure 3.2: Increasing trend of modulus with depth in a PLT at the Bakhtiary dam site

ISRM (1979) and Boyle (1992) recommend a ratio of two between test gallery width (or height) and loading plate diameter to avoid the influence of test gallery geometry on the test results. However, the study by (Van Heerden and Maschek 1979) and Agharazi et al. (2008), show that this influence is considerable for commonly used test gallery dimensions of 2 to 3 m.

In situ stresses are not routinely taken into account in the interpretation of the plate loading test results, which may be acceptable for the rocks with stress-independent deformation parameters. However, in many cases, especially for jointed rock masses at shallow depths, deformation is non-linear and deformational characteristics of the rock mass depend on the existing confining stress level. Some authors (Bieniawski 1978; Afrouz 1990; Asefand & Reddish 2002; Sitharam et al. 2007) have reported that plate loading test results and calculated modulus are dependent on the stress field (or depth). Others (Brown et al. 1989; Nawrocki and Dusseault 1995) have applied an increasing modulus with distance from tunnel wall, where a high stress gradient occurs due to the geometry of the excavation.

In jointed and fractured rock masses, the confining stress influences the deformations in two ways: first it affects the magnitude of non-linear deformational parameters (such as joint stiffness) and second it mobilizes different deformation modes. An example is shearing along persistent joints at low normal stress versus compacting the rock blocks under high confining stress. The mobilized deformation mechanisms are also very dependent on the geometry and deformational characteristics of the rock discontinuities and may include plastic deformation along joints at stress levels much lower than the overall strength of the rock mass. Existence of discontinuities may also cause stress distributions different from what is predicted by equation 3.3.

3.4 Deformation of Rock Discontinuities and Rock Mass

In a jointed rock mass, usually two types of joints can be distinguished: primary joints and secondary joints (Ku et al. 2004). Primary joints are those with high persistency that control the general response of the rock mass. These joints can be mapped in the form of systematic joint sets with similar properties. Secondary joints are randomly oriented non-persistent joints that do not follow any systematic pattern (Figure 3.3).

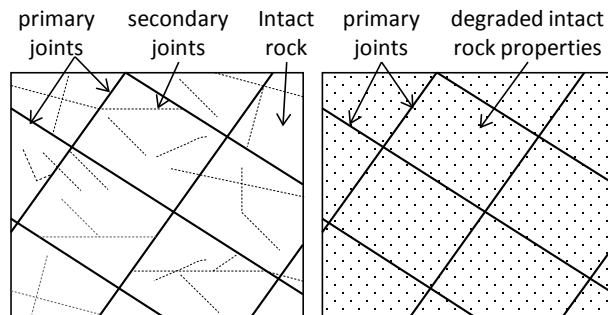


Figure 3.3: Primary and secondary discontinuities in (a) jointed rock mass and (b) idealized model.

For practical purposes, a jointed rock mass can be represented by an idealized model including just the primary joints and the blocks of rock. In this model, the blocks of rock surrounded by primary joints have equivalent characteristics determined by degrading the mechanical properties of intact rock to take into account the influence of the secondary joints. The deformation behaviour of this model depends on 1) the deformational properties of the rock block and the primary joints and 2) the deformation mechanism mobilized upon applied stress. Three deformation components of a jointed rock mass can be listed as follow:

- deformation of the rock block; in many cases this can be assumed linear elastic,
- normal closure of primary discontinuities, and
- shear displacement along primary discontinuities; this can be divided into pre-peak and post-peak displacements.

Depending on the imposed stresses, joint deformation can be in the form of 1) closure under increasing normal stress or "loading", 2) opening or dilation under decreasing normal stress or "unloading" or dilation due to shear displacement, 3) shearing or 4) a combination of the previous types of deformations.

Studies on the normal deformation of joints by Goodman et al. (1968) and Bandis et al. (1983) showed that the closure, v , of a mated joint follow a nonlinear relation with applied normal stress σ_n and finally becomes asymptotic to a line corresponding to the maximum joint closure v_m . This response can be best represented by a hyperbolic function as seen in Figure 3.4.

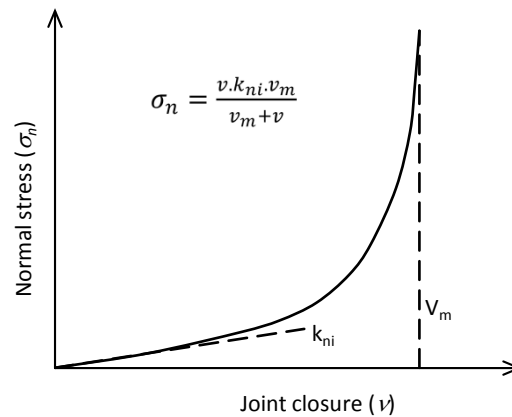


Figure 3.4: Non-linear joint closure curve under normal stress, and hyperbolic function that represent this behavior mathematically (k_{ni} : initial normal stiffness of joint).

Given the initial normal stiffness, k_{ni} , and maximum closure for a given joint, the normal stiffness, k_n , can be calculated at any stress level using the derivative of the joint closure function in Figure 3.4 as follow (Bandis et al. 1983):

$$k_n = \frac{\partial \sigma_n}{\partial v} = k_{ni} \left(\frac{k_{ni} \cdot v_m + \sigma_n}{k_{ni} \cdot v_m} \right)^2 \quad (3.4)$$

The variation of k_n with normal stress depends on some joint characteristics such as roughness, wall stiffness and infilling material thickness and the stress history of the joint. Experiments done by Chappell (1987) on rock joints in limestone, sandstone, shale

and coal showed that joint stiffness increases significantly as the normal stress is raised on joints in limestone and sandstone, while coal and shale samples showed effectively constant stiffness. Other laboratory tests on joint samples also showed stiffening and reduction of maximum closure under consecutive loading-unloading cycles (Bandis et al. 1983).

Souley et al. (1995) proposed a model that takes into account the hysteresis and permanent deformation of the joint upon unloading and incorporates the hardening behaviour of joints under consecutive loading-unloading cycles. Saeb and Amadei (1992) established a model that takes account of normal stiffness reduction with shear displacement.

For a given joint, laboratory tests usually show much higher normal stiffness than the shear stiffness. The difference between normal stiffness and shear stiffness causes joint deformation anisotropy. For a given joint, the ratio between normal and shear stiffness is not constant but depends on normal stress level. The highest anisotropy occurs at low stress levels, and with increase of stress, this ratio decreases (Bandis et al. 1983). This anisotropy in the joint deformation directly influences the rock mass deformational characteristics, by decreasing the shear modulus, G , of the rock mass.

Deformation of systematically jointed rock masses located near the ground surface at low stress levels is governed by the deformational characteristics of the main joints, quantitatively and qualitatively. In this case, deformation of the intact rock blocks has little contribution to the total deformation.

Barton (2007) classifies the deformation of jointed rock masses into three general modes: 1) joint compaction mode, 2) joint shearing mode, and 3) combination of both. Table 3.1 includes the main characteristics of rock mass deformation under these modes. The mobilization of each of these three modes depends on the direction of loading relative to the orientation of the discontinuities.

Table 3.1: Stress–strain response of a jointed rock mass for three modes of behavior (Barton, 2007).

Dominant joint deformation mode	Compaction	Shearing	Compaction+Shearing
stress-strain curve shape	concave	convex	linear
deformation hysteresis	small	large	moderate
lateral expansion of rock mass	small	large	moderate
Poisson's ratio	low	high	medium

In the next section the rock mass encountered at a dam site is examined in the context of the behaviour described in this section.

3.5 Bakhtiary Dam Site

The Bakhtiary dam and hydroelectric power plant project includes the design and construction of a 315 m high, double curvature, concrete dam and an underground powerhouse, with nominal capacity of 1500 MW, in the Zagros mountains in south west Iran (IWPCO).

3.5.1 Geological Description of the Dam Site

Limestone layers of Sarvak formation, which are Mid-Cretaceous marine sediments, form the foundation of the dam, powerhouse and other appurtenant structures. These layers are generally tightly folded. An anticline (Siah Kuh anticline) with a sharp axial plane exists at the location of the planned dam axis (SPEC, 2009). The Sarvak formation is divided into seven geological units, namely Sv1 to Sv7, with Sv1 being the oldest with no outcrop at the dam axis, and Sv7 the youngest. Figure 3.5 shows the geological section of the dam axis with the rock units in direct contact with the dam body.

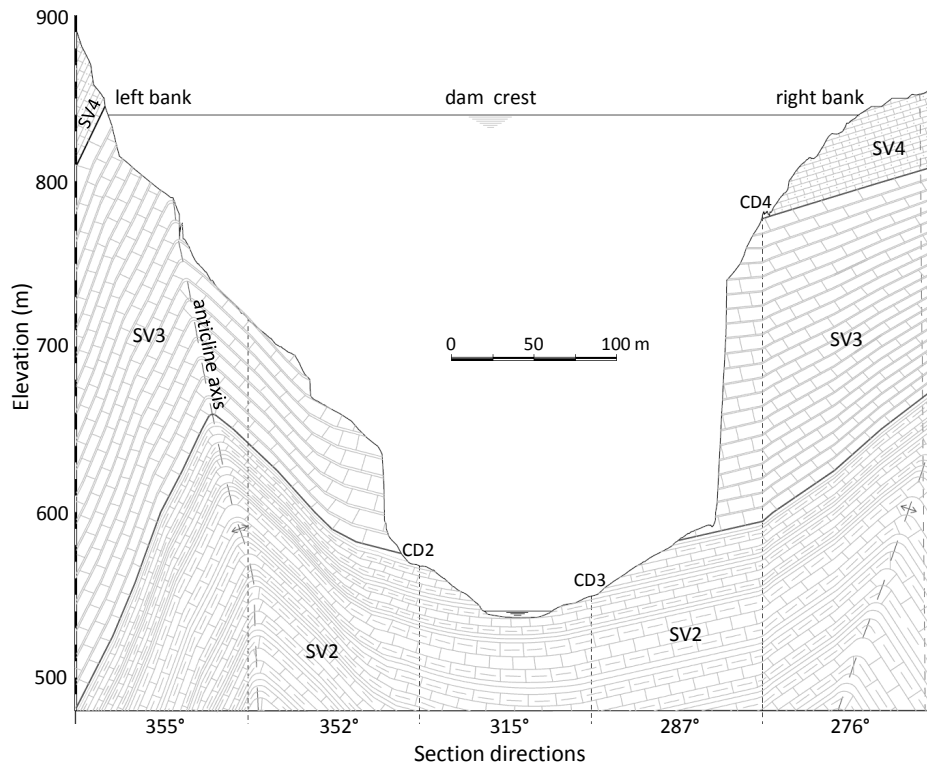


Figure 3.5: Geological section of dam axis and geological units of the Sarvak formation

Rock unit Sv2 is formed by thinly to medium bedded dark grey limestone to marly limestone with thin black laminated marlstone to shale interbeds. This unit forms the central outcrop of the anticline at the valley bottom. Rock unit Sv3 is formed by thinly to medium bedded dark grey marlstone and siliceous limestone and will form the lower abutments of the dam body. At the crest level, the dam will be in contact with the Sv4 rock unit, which is formed by medium to thickly bedded dark grey limestone with small siliceous nodules (SPEC, 2009).

The Siah Kuh anticline has influenced the structural and geomechanical characteristics of the rock mass near the dam axis and has created disturbed zones (zones A and B) in the anticline core. This disturbed zone consists of intensely folded rocks, with weaker geomechanical properties.

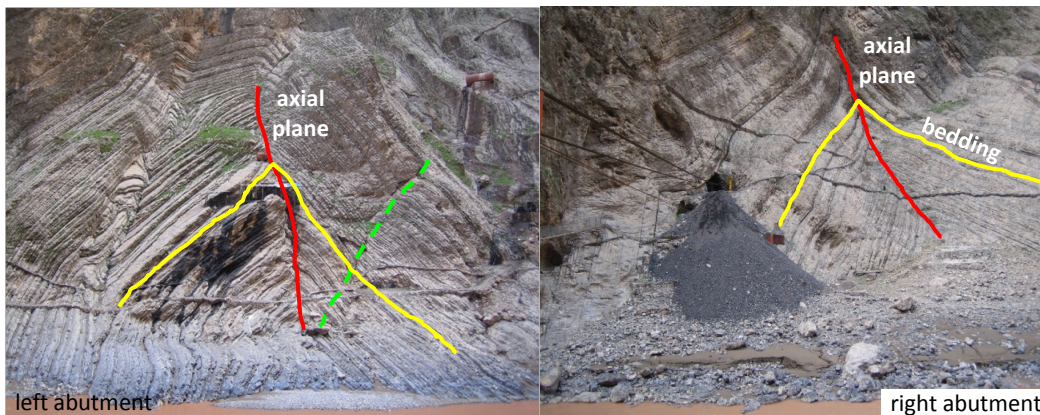


Figure 3.6: Axial plane of Siah Kuh anticline on abutments, (a) left abutment and (b) right abutment. Red lines show the axial plane outcrop, yellow lines show typical bedding and the green line shows extension joints observed on the left bank. (For interpretation of the references to color in this figure legend, the reader is referred to the web version of this article.)

3.5.2 Rock Mass Properties

Based on geophysical surveys of the dam site using the petite seismic method, the rock mass is categorized into three general classes. Slightly deformed limestones of Sv2 unit form the most competent class with $E \approx 14$ GPa and intensely folded rocks of Sv3 form the weakest rock with $E \approx 2.7$ GPa. The middle class are slightly deformed thin layers of Sv3 with estimated $E \approx 7.3$ GPa (SPEC 2009). Table 3.2 shows the rock classes and their ratings based on rock engineering classifications, for the rock units.

Table 3.2: Rock mass classes and engineering ratings (SPEC 2009).

Lithology	RMR ₈₉ *	Q	GSI
Sv2 & Sv3 (dist. A)	30 - 51	0.46	35 - 50
Sv2 & Sv3 (dist. B)	44 - 55	1.00	45 - 50
Sv2 & Sv3 & Sv4	48 - 66	1.25	45 - 60

Laboratory tests on cored samples showed no distinct difference between the mechanical characteristics of the intact rocks taken from different geological units. Uniaxial compressive tests on 162 samples of intact rock gave an average unconfined compressive strength of 125 ± 40 MPa for dry samples and 110 ± 30 MPa for saturated samples, excluding the tests on samples with pre-existing weakness planes. The Young's modulus for intact rock E_i was determined from the linear part of the axial stress-axial strain curves with the average value of $E_i = 69 \pm 10$ GPa for all tests. Axial deformation in these tests exhibits mainly linear response after the micro crack closure phase of the test (up to stress levels of $\approx 5\%$ of the unconfined compressive strength).

3.5.3 Discontinuities

Systematic discontinuities at the dam site consist of bedding surfaces and two joint sets that intersect at almost right angles and form a conjugate perpendicular system. A further joint set is observed at a few locations but its occurrence is not common throughout the site.

Bedding surfaces are characterized as planar and persistent with average spacing of 60 to 600 mm. The bedding has a dip direction/dip of $215^\circ/75^\circ$ on the downstream limb of the anticline and $030^\circ/50^\circ$ on the upstream limb. The main joint set running through the dam site is J1 ($310^\circ/40^\circ$ to 70°). Joints in this set have a persistency of several to tens of metres. A second joint set J2 ($125^\circ/35^\circ$ to 75°) exists with persistency from a few centimetres to a few metres. The joint set characteristics are summarized in Table 3.3.

The deformational and strength characteristics of the discontinuities were assessed from the results of in situ and laboratory shear tests done on natural joints and bedding. Nineteen tests, out of a total of 86 shear box tests were done on bedding samples. The samples were less than 100 mm in diameter. Tests on joint samples were divided into two groups in terms of their joint roughness coefficient (JRC) value with $JRC = 6$ being the cut-off number. In each test, the sample was sheared under three normal stresses,

ranging from 0.5 to 5.5 MPa. By linear regression of shear box test results, the strength characteristics of the discontinuities were determined (Table 3.4).

Table 3.3: Bedding and joint set characteristics (SPEC 2009).

	Value or description	Frequency (%)		
		Bedding	J1	J2
Aperture (mm)	0.1 - 1	90	90	95
	1 - 5	10	10	5
Spacing (cm)	2 - 6	1.5	2.5	3
	6 - 20	47	48.5	52
	20 - 60	44.5	45	43.5
	60 - 200	3.5	4	1.5
	200 - 600	3.5	0	0
Infilling	Clay	42.5	10	2
	Calcite	46	67.5	55
	Bitumen	4.5	1	0
	FeO	2	0	0
	Tight	5	21.5	43
Roughness	undulating-Ss	19	2	0
	planar - Ss	41	2	1
	undulating-Sm	5	1	1
	planar - Sm	18	47	54.5
	undulating-Ro	1	0	0
	planar - Ro	16	48	43.5

Ss: Slickensided, Sm: Smooth, Ro: Rough

Table 3.4: Average discontinuity strength parameters based on shear box tests (SPEC 2008).

	Peak		Residual		JRC	JCS
	c (MPa)	ϕ	c (MPa)	ϕ		
Bedding	0.28	44°	0	33°	7	27
Joints (JRC≤6)	0.25	35°	0	32°	4	27
Joints (JRC>6)	0.45	38°	0	36°	9	24

In six of the laboratory tests on bedding planes, the test specimen was subjected to three normal loading-unloading cycles and the corresponding normal displacements were recorded. The normal stiffness k_n was determined for each loading cycle by fitting a straight line to test results (Table 3.5).

In addition to laboratory shear box tests, three in situ direct shear tests were performed on the Sv3 bedding planes in gallery GR2. These tests were performed on three adjacent 70×70×35 cm blocks in general accordance with the ISRM suggested test method (ISRM 1974). All blocks were subjected to several normal loads and tested to the residual shear strength stage.

Table 3.5: Bedding k_n (MPa/mm) from normal loading–unloading tests.

	Cycle 1	Cycle 2	Cycle 3
Sample 1	2.6	11.7	17.6
Sample 2	3.2	7.9	10.3
Sample 3	3.1	6.0	6.9
Sample 4	6.9	14.6	15.4
Sample 5	7.4	14.6	16.2
Sample 6	4.5	11.3	17.0
Average	4.6	11.0	13.9

From the results of the in situ tests, the average cohesion value of $c = 0.3$ MPa, peak/residual friction angle of $\phi = 33^\circ$ and $JRC = 2$ to 3 were estimated for the bedding surfaces.

Based on the results of unconfined compressive strength tests, deformation of the intact rock can be assumed linear. In comparison, joint normal displacements exhibit slight nonlinearity in the applied normal stress range for the shear tests (1 to 5 MPa) and stiffens under successive loading-unloading cycles.

3.6 Interpretation of Plate Load Test Results

The plate loading tests were run using a rigid loading type apparatus with three plate diameters of 971 mm, 915 mm and 650 mm. The smallest plate was used for three tests with a maximum pressure of 40 MPa and the two larger plates were used for rest of the tests with a maximum pressure of 20 MPa. Induced deformations were measured at the rock surface and four depths beneath the loading plates, distributed up to a depth of about 3m. Measurements were taken at one minute time intervals, using a data logger connected to the measurement devices and a computer.

The plate loading tests were done in eight galleries with a nominal cross-section size of about $2 \text{ m} \times 2 \text{ m}$. These galleries were excavated in the abutments of the planned dam and the underground powerhouse area. Figure 3.7 shows a projection of the galleries onto the dam axis section and plan. Based on the results from hydraulic fracturing tests, the principal horizontal field stresses at the elevation of the test galleries and valley bottom are also presented. The vertical stress is assumed as the weight of the overburden rock at each elevation (vertical stress gradient = 0.026 MPa/m).

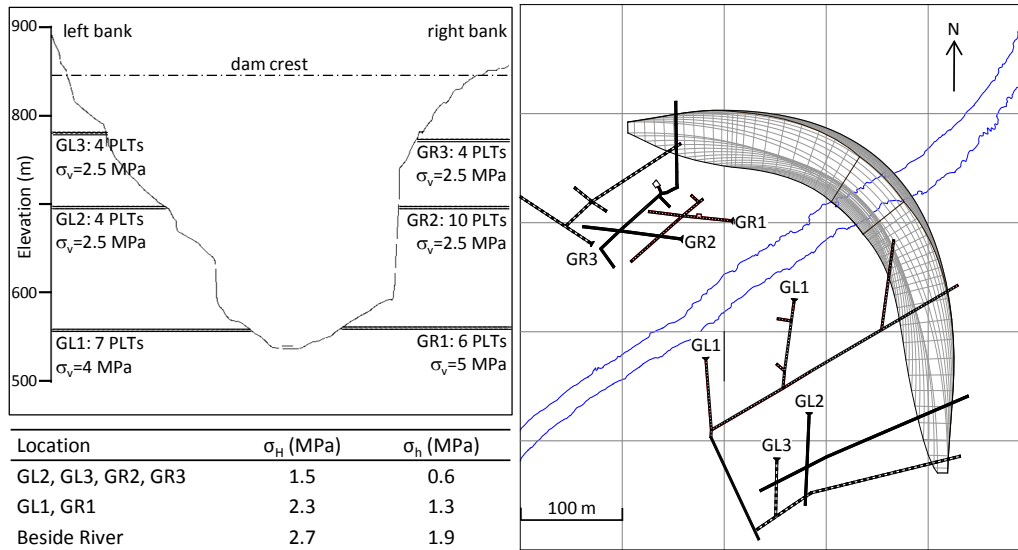


Figure 3.7: Projection of test galleries on dam axis cross section and plan. Number of PLTs in each gallery, maximum vertical stress, and estimated horizontal stresses at the location of each gallery is also presented.

Forty two large scale plate loading tests (including the tests carried out at powerhouse site) were carried out as part of the site investigation program for the dam design. Figure 3.8 shows the common loading pattern applied to all the plate loading tests. At the peak of each loading cycle, stress was kept constant to measure the deformability characteristics of the rock mass under constant load. Each test includes two opposing loading plates, with a five-point borehole extensometer underneath each plate. Each test included five loading-unloading cycles under various loads, with 10 displacement measurements recorded per loading cycle.

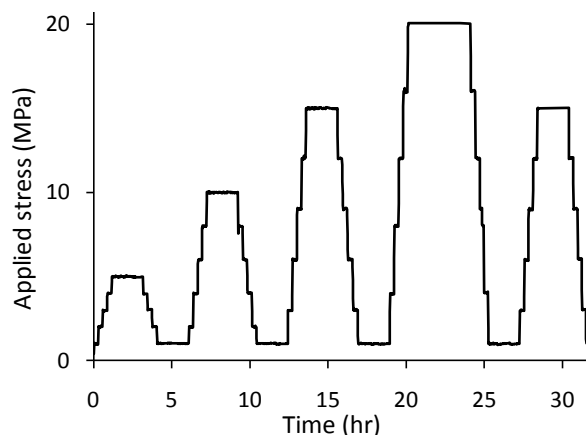


Figure 3.8: Loading-unloading cycles used for the Bakhtiary dam site PLTs.

After filtering out the tests with missing geological or joint data, and the tests with unreliable results according to the site reports, 26 well documented tests were selected for this study.

Based on the test quality and availability of data regarding the geology of the test site, 26 plate loading tests were selected for this study. These tests are analyzed to study the influence of the three main systematic discontinuities on the deformation of the rock mass and to determine the mechanisms controlling the deformations during the tests. Calculation of the deformation modulus was not the focus of this study.

For the interpretation of the test results, PLTs were classified into three configuration groups based on the relative direction of the test loading to the orientation of the three major discontinuity sets (Figure 3.9). The first group include those tests in which the direction of loading is normal to one of the three primary discontinuities, i.e. bedding, J1 or J2 and accordingly are named NB, NJ1 and NJ2, respectively. The second group includes the tests in which direction of loading makes an angle greater than 15° with the normal to the discontinuity planes. The tests fall in this group are named SB12. In addition to these tests, there were some PLTs done on intensively folded and fractured rocks. These tests form the third group and are named Fractured Rock (FR) group. The remaining tests that do not fall within these groups are excluded from these analyses.

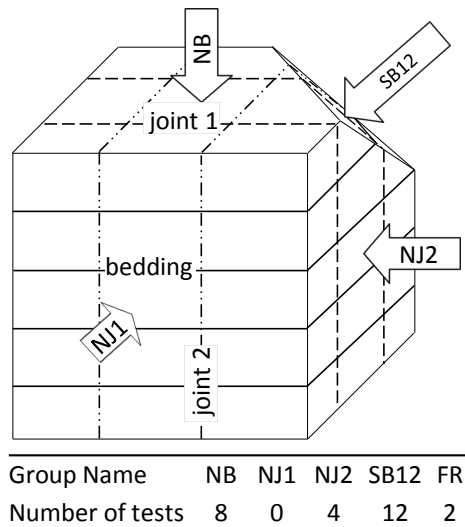
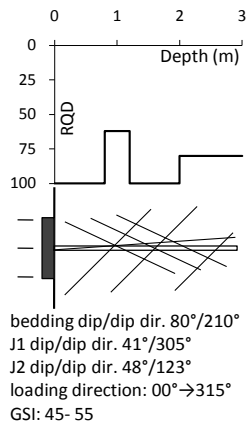
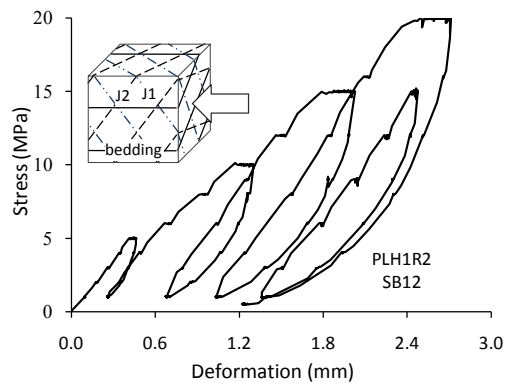
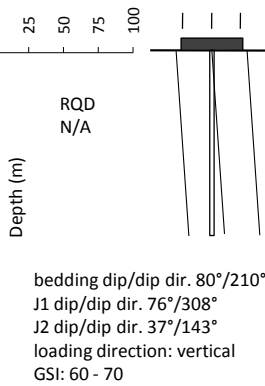
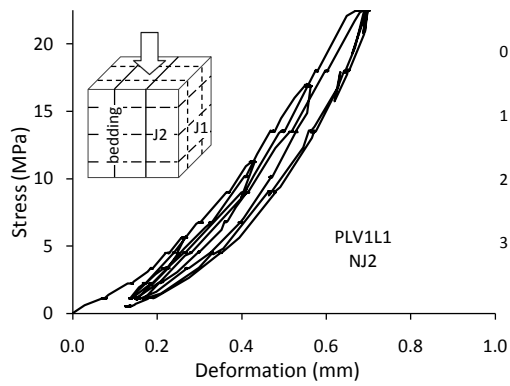
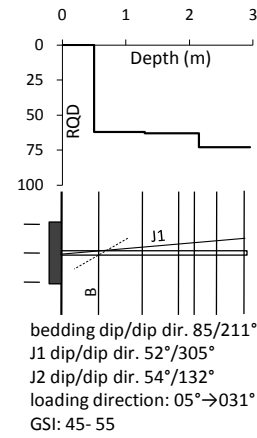
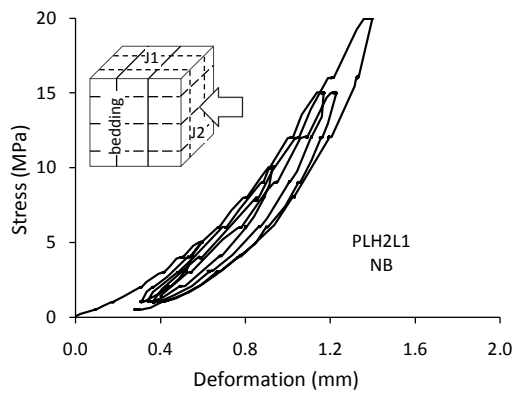
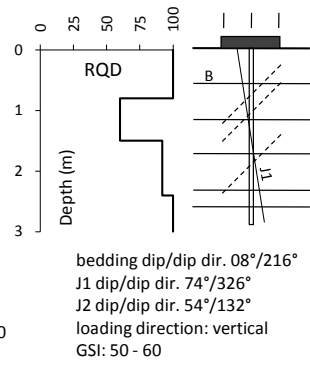
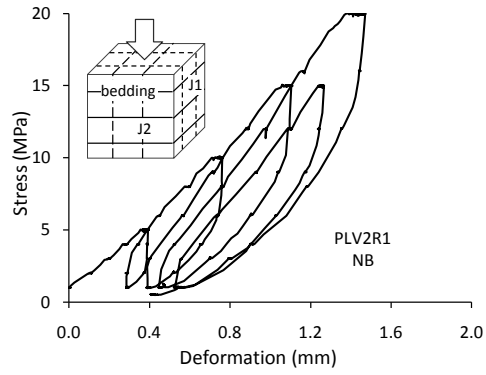


Figure 3.9: Test groups based on the relative direction of loading to orientation of discontinuities.

To assess the influence of primary discontinuities on rock mass deformation and to determine deformation mechanisms mobilized in each configuration, five characteristics of the deformations were studied and compared for the tests in each group, as follows:

- shape of the stress-deformation curve (concave, linear or convex),
- deformation under constant load at the peak of each loading cycle,
- total and permanent deformation of the test (after five loading cycles),
- ratio of permanent to total deformation in each loading-unloading cycle and its variation over successive loading cycles of the test,
- deformation hysteresis.

In all tests, a set-up similar to Figure 3.1 was used with the first measuring point (surface deformation) installed in the first 0.1 m of the borehole and the reference anchor fixed at a depth of about 5 to 6 m in the central borehole. Figure 3.10 shows typical stress-displacement curves for tests from each group. These plots are associated with the surface displacements at one side of the test. The RQD values measured along each extensometer borehole and GSI numbers for the test location are also presented on each plot for comparison.



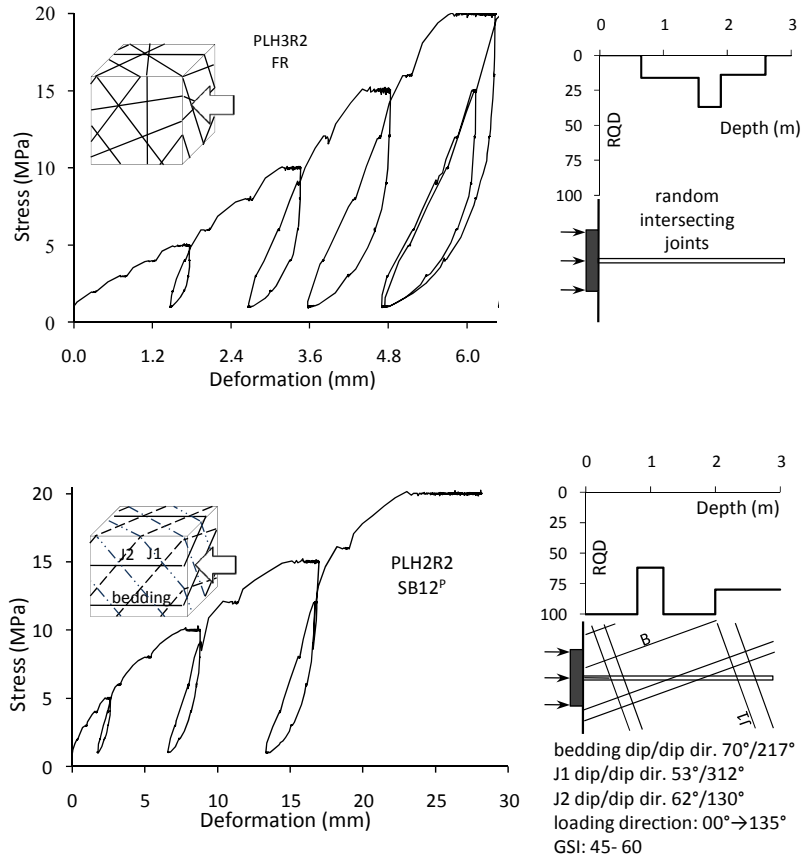


Figure 3.10: Stress-deformation curves of PLTs representing each group. Schematic figures on the right show the relative direction of loading to the orientation of discontinuities for each test. The orientation of the discontinuities and test load along with RQD distribution and GSI value are also presented. Data have been extracted from gallery and test surface mapping, borehole logs, and core photos.

The first three graphs of Figure 3.10 come from tests conducted normal to the dominant discontinuity orientation (bedding or joint). As observed, tests in which loading is normal to bedding (NB) produce two typical curves; one with considerable energy dissipation over a full cycle of loading-unloading, which is usually typical of disturbed open joints, and one with slightly nonlinear response with concave upward shape over the loading and unloading stage. The PLTs conducted normal to the discontinuities result in total deformations that are lower than the tests conducted with other loading configurations. In addition, the permanent deformation is low and deformation hysteresis is not observed.

For tests in which the direction of loading is inclined relative to the orientation of discontinuities (SB12 and SB12^P), much higher total and permanent deformation is observed (Table 3.6) compared to NB and NJ2 tests. In these tests, the loading and

unloading secant moduli for a given cycle are very close, i.e. the immediate deformation that occurs during loading is mostly recovered upon unloading. The results show that the permanent deformations are mainly caused by the constant stress that is applied for a period of time at the peak of the loading-unloading cycles. These deformations can be attributed to creep-like behaviour of the rock mass.

In SB12 tests, the absolute displacement of a given loading cycle is much larger compared to NB and NJ2 tests (Table 3.6). Given that the deformation in SB12 tests is accompanied by shear displacement along the discontinuities, and assuming a similar behaviour for the intact rock blocks in all test configurations, this difference indicates the anisotropy of discontinuity stiffness in shear and normal displacement. This result is consistent with laboratory tests that show lower shear stiffness for the rock joints.

Table 3.6: Total surface deformation at each loading–unloading cycle.

cycle	Stress (MPa)	Total deformation (mm)				
		NB	NJ2	SB12	SB12 ^P	FR
1	5	0.40	0.20	0.39	2.65	1.48
2	10	0.52	0.29	0.98	7.07	2.04
3	15	0.76	0.42	1.24	10.40	2.34
4	20	1.09	0.53	1.52	14.92	2.88
5	15	0.72	0.53	1.09	3.86	1.82

Depending on shear strength of the discontinuities in a SB12 loading configuration, loading of the rock mass can result in non-recoverable slip along discontinuities (Figure 3.10: SB12^P). The displacement plot for the SB12^P test shows high total deformations with negligible recovery upon unloading. Hysteresis is large and the deformational response keeps a ‘memory’ of the previous loading cycle stress. The stress-deformation curves are mainly concave downward in shape, which is similar to shear stress versus shear displacement curves for joints in laboratory and in situ tests.

Deformation of the rock mass with closely spaced randomly orientated fractures (FR) is mainly caused by the compaction of small rock pieces formed by intersection of joints and fractures. Deformation plots for these tests show mainly nonlinear behaviour with high total and permanent deformation. Their characteristics are a combination of the deformation responses seen in all other tests.

The deformation of the rock mass under the constant applied load at the peak of each loading cycle is different for each loading configuration. Figure 3.11 illustrates the

deformation versus time plots (the same tests used for Figure 3.10) under the maximum stress applied at the fourth loading cycle of each test. The rate of deformation is also depicted in Figure 3.11 for each test. Other tests of the same group had a similar behaviour. As can be seen, tests with loading oriented normal to the discontinuities (NB and NJ2) show negligible deformation with the deformation rate approaching zero over a short time span of about 15 minutes, which is equal to the time steps followed during loading and unloading cycles. In other words, practically no deformation occurs under constant load in these tests (≈ 0.1 mm for NB test and 0.05 mm for NJ2 test). On the other hand, the SB12^P test undergoes substantial deformation under constant load (≈ 4.5 mm) with the rate of deformation gradually approaching zero after 3 hours. The FR tests and SB12 tests show moderate deformation under constant load (≈ 0.63 mm and ≈ 0.45 mm, respectively) but the rate of deformation drops fast and becomes zero after about 2 hours of loading.

Deformation of the rock mass under constant load can occur by the following mechanisms or a combination of them:

- consolidation of the joint infilling materials,
- normal and shear displacement along joints, and
- compaction of rock blocks.

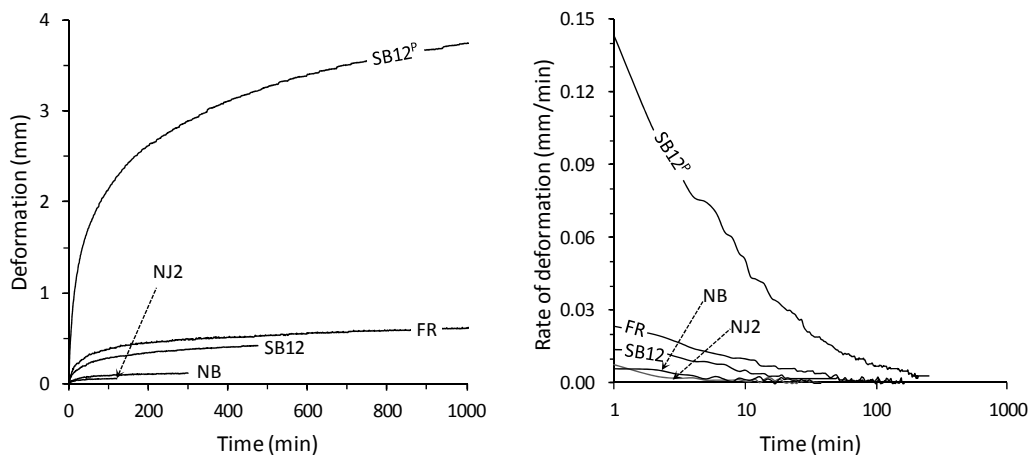


Figure 3.11: Deformation–time and rate of deformation–time (logarithmic scale) graphs. Time axis shows the elapsed time under constant load of 20 MPa at the peak of 4th loading cycle.

By assessment of the deformation-time and rate of deformation-time graphs, it can be concluded that the shear displacement along discontinuities (in SB12 and SB12^P tests) and relative dislocation of the rock blocks (in FR tests) are the main mechanisms

contributing to the deformation of the rock mass under constant load. As observed in the case of NB and NJ2 tests, consolidation has little influence on the deformations because the joints and bedding have no infillings or are filled with a very thin layer of calcite or clayey materials.

Figure 3.12 illustrates the distribution of absolute total and permanent deformations of the tests, after five loading-unloading cycles. The minimum total and permanent deformation belong to NB, NJ1 and NJ2 tests. In contrast, SB12^P tests have the highest total and permanent deformations.

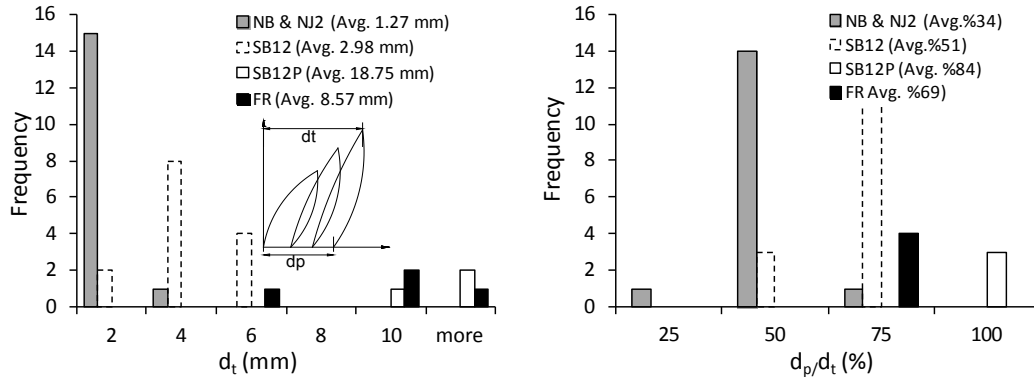


Figure 3.12: Distribution of total and permanent deformation for each group after five loading–unloading cycles.

Analysis of stress-displacement plots shows that for a given test, the secant moduli over successive unloading cycles remain almost unchanged, i.e. the value of the recovered deformation (elastic deformation, d_e) is a linear function of the total stress drop over unloading (Figure 3.13 (a)):

$$d_{ei} = E_e \cdot \Delta\sigma_i \quad (3.5)$$

where:

d_e = recovered part of deformation upon unloading

E_e = secant modulus over unloading

$\Delta\sigma$ = maximum stress change in each loading cycle

i = loading-unloading cycle number

Given a constant E_e for a specific test, the increase of the loading to unloading secant modulus ratio ($k_i = E_{ti}/E_{ei}$) indicates that the rock mass stiffens under successive loading-unloading cycles and with increase of the applied stress level. Assuming a constant E_e

for a given test, this ratio is inversely proportional to the irrecoverable deformation ratio of each cycle defined as $P_i = (d_{ti} - d_{ei})/d_{ti}$. Figure 3.13(b) shows the variation of P_i with number of loading cycles.

The SB12P and FR tests show the highest average irrecoverable deformation ratio during the first cycle ($P_{i1} \approx 80\%$). In the former case, the low rate of the reduction of P_i over successive loading-unloading cycles indicates the development of shear displacements along the failed discontinuities. In comparison, FR tests have the highest stiffening rate which is an indication of the interlocking of the rock pieces under increasing load. The stiffening of rock mass in NB and NJ2 tests follows the type of behaviour observed in tests on bedding samples and the experiment by Bandis et al. (1983) on limestone bedding planes, in which the maximum closure v_m became progressively smaller under repeated normal loading-unloading cycles.

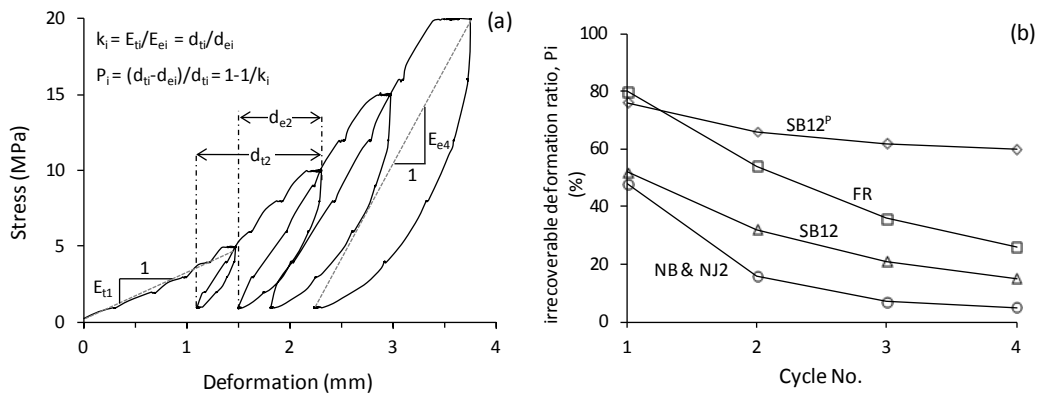


Figure 3.13: Variation of the average ratio of permanent to total deformations for each group

Table 3.7 shows the calculated moduli for the tests, based on the deformations taken at rock surface. As observed, a significant scatter occurs in the calculated moduli for a given rock mass when the real mechanism governing the deformation of the rock mass is ignored and the ISRM suggested method is used to interpret the test data. From this table, when the direction of loading is perpendicular to a joint set (J2), the deformation modulus of the rock mass is twice as high as the case in which loading is perpendicular to beddings, and is up to 25 times higher compared to the case in which plastic deformation occurs along discontinuities.

Table 3.7: Deformation moduli calculated using the ISRM method for the tests shown in Figure 3.10.

Cycle	Stress (MPa)	Deformation modulus (GPa)				
		NB	NJ2	SB12	SB12 ^P	FR
1	5	6.7	14.3	7.6	1.0	1.2
2	10	12.6	22.3	6.0	0.8	2.0
3	15	12.9	23.5	7.3	0.9	2.7
4	20	12.3	25.3	8.1	0.8	3.0
5	15	12.4	25.3	8.2	2.4	3.5

Based on the comparison of the aforementioned five key parameters, four deformation mechanisms can be distinguished as the governing modes of deformation of the rock mass during plate loading tests at the Bakhtiary dam site, as follow:

- joint normal displacement governed mechanism (JND)
- joint shearing displacement governed mechanism (JSD)
- joint shearing displacement governed mechanism with plastic deformation (JSDP)
- complex deformation mechanism, which is a combination of all above modes (CD).

Figure 3.14 shows simplified models for each deformation mechanism and its associated idealized load-deformation curve. The characteristics of each mechanism and the plate loading test category associated with each mechanism are presented in Table 3.8.

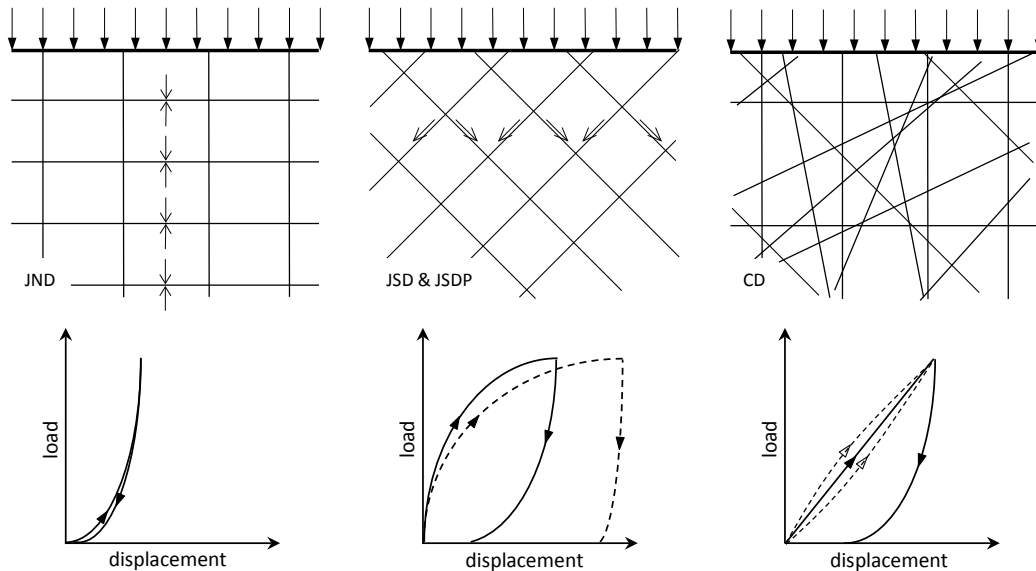


Figure 3.14: Idealized load–displacement curves for the deformation of a jointed rock mass. These curves characterize the type of behavior observed during one loading– unloading cycle of PLTs at the Bakhtiary dam site, where deformations are governed by shear and normal displacements along discontinuities

Table 3.8: Deformation mechanisms and characteristics for PLTs at Bakhtiary dam site

Dominant deformation mechanism	Test configuration	Stress-deformation curve shape	Deformation hysteresis	Total deformation	Permanent deformation	Stiffening under successive loading cycles
JND	NB & NJ2	concave to linear	small	small	small	high
JSD	SB12	linear	small	moderate	small	moderate
JSDP	SB12 ^p	convex	high	high	high	small
CD	FR	linear to convex	moderate	moderate to high	moderate to high	high

3.7 Conclusion

Analysis of the Bakhtiary dam plate loading test results showed the dominant influence of the major discontinuities on deformation of the rock mass. Discontinuities influence the deformation of the rock mass in two ways: 1) by their spatial configuration, which causes mobilization of a specific deformation mechanism and 2) by their contribution to total deformation of the rock mass including anisotropy and stress-dependency.

By analysis of deformations measured with plate loading tests, four deformation mechanisms were identified and their characteristics were presented. Generic load-deformation curves for each deformation mechanism are introduced. These models are in general agreement with the deformation modes suggested by Barton (2007) (Table 3.1), except the model in which plastic deformations develop because of the shear displacements along discontinuities. Mobilization of these mechanisms depends mainly on the relative direction of loading to the orientation of the discontinuities. The main characteristics of the rock mass deformation under these mechanisms are:

- Deformation anisotropy is related to the orientation of the primary discontinuities. This anisotropy should be taken as an important factor in geomechanical zoning of the dam foundation.
- The rock mass exhibits stiffer response during unloading compared to the loading stage. For joint normal or shear displacement governed mechanisms (JND and JSD) this difference becomes smaller as the rock mass undergoes successive loading-unloading cycles. This type of behaviour is important as the same response should be anticipated for the dam foundation during the dam construction, first impounding and successive drawdown-impounding cycles. Assuming a CHILE model for the rock blocks, the minor non-linearity observed

in deformation graphs is caused directly by the non-linear nature of rock discontinuity deformation.

- Test results show the potential for plastic deformations along joints for the JSDP loading configuration. As these local failures might occur at stress levels lower than the overall strength of the rock mass, the potential loading configuration and stress level that cause this type of deformation mechanism should be identified based on the test results.

The study shows that test results should be interpreted taking into account the structural features of the rock mass. Ignoring this factor causes a considerable scatter in results. Given the other sources of error/scatter in test results, a simple closed-form solution may not provide an efficient tool for the interpretation of plate loading test results. For plate loading tests conducted on systematically jointed rock masses, more sophisticated methods, such as numerical modeling along with a proper constitutive model, should provide more consistent results.

3.8 References

- Afrouz, A. (1990). Determination of rock mass modulus nonlinear variation with loading and depth. *Mining Science and Technology* (11), 179-83.
- Agharazi, A. (2003). Effects of rock mass natural features on the in-situ determination of rock mass modulus of deformation. MSc Thesis. Tehran: University of Tehran.
- Agharazi, A., Tannant, D., Jafari, A. (2008). Stress and tunnel geometry effects on deformation modulus derived from plate load tests. *Proceedings of 61st Canadian Geotechnical Conference & 9th Joint CGS/IAH-CNC Groundwater*, Edmonton, volume 1, pages 601-608. Bi-Tech Publishers Ltd., Richmond.
- Asef, M. R., & Reddish, D. J. (2002). The impact of confining stress on the rock mass deformation modulus. *Geotechnique*, 4(52), 235-41.
- Bandis, S., Lumsden, A., Barton, N. (1983). Fundamentals of rock joint deformation. *International Journal of Rock Mechanics and Mining Sciences & Geomechanics Abstracts*, 20(6), 249-268.
- Barton, N. (2007). *Rock Quality, Seismic Velocity, Attenuation and Anisotropy*. Leiden: Taylor & Francis.
- Bieniawski, Z. T. (1978). Determining rock mass deformability - experience from case

- histories. *International Journal of Rock Mechanics and Mining Sciences & Geomechanics Abstracts*, 15(5), 237-247.
- Boyle, W. (1992). Interpretation of plate load test data. *International Journal of Rock Mechanics and Mining Sciences*, 29, 133-141.
- Brown, E. T., Bray, J. W., & Santarelli, F. J. (1989). Influence of stress-dependent elastic moduli on stresses and strains around axi-symmetric boreholes. *Rock Mechanics and Rock Engineering* (22), 189-203.
- Chappel, B. A. (1987). Predicted and measured rock mass moduli. *Mining Science and Technology* (6), 89-104.
- Goodman, R. E., Taylor, R. L., & Brekke, T. (1968). A model for the mechanics of jointed rock. *Journal of the Soil Mechanics and Foundations Division ASCE*, 637-59.
- Hoek, E., & Diederichs, M. (2006). Empirical estimation of rock mass modulus. *International Journal of Rock Mechanics and Mining Sciences* , 43, 203-215.
- Hoek, E., Carranza-Torres, C., Corkum, B. (2002). Hoek - Brown failure criterion: 2002 edition. *Proceedings of the 5th North American Rock Mechanics Symposium and 17th Tunnelling Association of Canada Conference: NARMS-TAC, Toronto, volume 1, pages. 267-273.*
- ISRM. (1974). Suggested method for in situ determination of direct shear strength. *International Journal of Rock Mechanics and Mining Sciences & Geomechanics Abstracts* (32), 101-9.
- ISRM. (1979). Suggested method for determination of insitu deformability of rock. *International Journal of Rock Mechanics and Mining Sciences* (16), 143-146.
- IWPCO. (n.d.). Iran Water and Power Resources Development Co. Retrieved 11 01, 2009, from <http://en.iwpc.ir/Bakhtiari>
- Ku, C. Y., Lin, J. S., Chern, J. C. (2004). Modeling of jointed rock masses using a combined equivalent continuum and discrete approach. *International Journal of Rock Mechanics and Mining Sciences*, 3(41), 434.
- Lama, P., & Vutukuri, V. (1978). *Handbook on mechanical properties of rocks (Vol. III)*. Bay Village: Trans Tec Publications.
- MeSy GmbH. (2008). Bakhtyari Dam & H.E.P.P. Project; Hydraulic fracturing tests at the dam site: results of laboratory tests.
- Nawrocki, P. A., Dusseault, M. B. (1995). Modelling of damaged zones around openings using radius-dependent Young's modulus. *Rock Mechanics and Rock Engineering*

(28), 227-39.

- Palmstrom, A., Singh, R. (2001). The deformation modulus of rock masses - comparisons between in situ tests and indirect estimates. *Tunnelling and Underground Space Technology*, 16, 115-131.
- Saeb, S., Amadei, B. (1992). Modelling rock joints under shear and normal loading. *International Journal of Rock Mechanics and Mining Sciences & Geomechanics Abstracts*, 29(3), 267-278.
- Sitharam, T. G., Maji, V. B., Verma, A. K. (2007). Practical equivalent continuum model for simulation of jointed rock mass using *FLAC^{3D}*. *International Journal of Geomechanics*, 7, 389-395.
- Souley, M., Homand, F., Amadei, B. (1995). An extension to the Saeb and Amadei constitutive model for rock joints to include cyclic loading paths. *International Journal of Rock Mechanics and Mining Sciences & Geomechanics Abstracts* (32), 101-9.
- SPEC. (2008). Engineering geology and rock mechanics report - site investigation phase I & II: Rev 0. Tehran: Stucky Pars Engineering Co.
- SPEC. (2009). Engineering geology and rock mechanics report on completion of site investigations; Phase I & II: Revision 1. Tehran: Stucky Pars Engineering Co.
- Timoshenko, S., Goodier, J. (1970). *Theory of Elasticity* (3rd ed.). McGraw-Hill.

Chapter 4

A three-dimensional equivalent continuum constitutive model for jointed rock masses containing up to three random joint sets²

4.1 Introduction

The deformational response of jointed rock masses is potentially anisotropic, non-linear and stress dependent because of the inherent anisotropy and non-linearity of rock joint displacements. The influence of the discontinuities on the mechanical properties of rock masses has been an active subject of study in geomechanics. Different techniques have been developed, all seeking an approach to take into account, analytically or empirically, the influence of discontinuities on the rock mass mechanical behavior. These techniques can be classified into two general categories: discontinuum-based methods and continuum-based methods. In the discontinuum methods, the rock discontinuities are incorporated into analysis in an explicit fashion, e.g., the distinct element method by Hart et al. (1988). Alternatively, in continuum methods, the effect of discontinuities are taken into account in an implicit way, either by using downgraded mechanical parameters for the equivalent continua or by establishing constitutive relationships based on the principles of continuum mechanics that incorporate effect of discontinuities into analysis. The later models are known as “equivalent continuum models”.

Analytical relationships proposed by Amadei and Goodman (1981), Yoshinaka and Yamabe (1986), and Huang et al. (1995) are examples of such models that can be used for deformation analysis of rocks with simple joint configuration and elastic behavior. For more general cases of non-orthogonal joint sets, non-linear joint deformation and plastic deformation, more advanced equivalent continuum models were proposed by different authors, such as those by Wang and Huang (2009) and Samadhiya et al. (2008) that can be used for numerical analysis of jointed rocks. Non-persistence of the joints can also be considered in the models developed by Singh (1973) and Cai and Horii (1993)

² A version of this chapter has been published as a paper by Geomechanics and Geoengineering: An international journal:

Alireza Agharazi, C. Derek Martin & Dwayne D. Tannant (2012). "A three-dimensional equivalent continuum constitutive model for jointed rock masses containing up to three random joint sets". Geomechanics and Geoengineering: An international journal, 7:4, 227-238

based on the principles of composite mechanics and introduction of the so-called stress concentration tensor. All of the above models share the basic concept of superposition of deformations that occur in the components of the system, i.e. intact rock and rock joints. There are also other models that were developed based on other theoretical concepts such as damage mechanics by Kawamoto et al. (1988), crack tensor theory by Oda et al. (1993) and homogenization techniques by Min and Jing (2003).

Anisotropy in deformability and stress-dependency of stiffness are two important characteristics of the rock mass deformation. These characteristics are frequently observed in results of in-situ deformation tests on layered rocks such as plate loading tests. Figure 4.1 shows load-deformation graphs of three plate loading tests conducted on a jointed limestone rock mass. As observed, for a given stress level and rock, induced deformations can vary to an order of magnitude depending on the relative direction of loading to the joints. Anisotropy is also observed in rock mass strength due to shear failure through an existing discontinuity plane at stress levels well below the overall strength of the rock mass.

In a larger scale, a similar response is anticipated where a jointed rock mass forms the foundation of a dam or where it encompasses an underground space such as a cavern or tunnel. While the available discontinuum based models, such as Distinct Element Code (*UDEC* or *3DEC*) (Itasca 2007) generally provide robust tools that can be used for deformation and stress analysis of such problems, there are some conditions that make the application of these models inefficient or non-beneficiary. One example is where the spacing of discontinuities is very small compared to the size of model or structure to be analyzed. In such cases, the size of numerical elements is controlled by the spacing of the joints. This can considerably increase the computation time of a densely jointed rock model. In addition, in practice the detailed joint data that is required for a discontinuum model is not always available or even a detailed analysis of joint behavior is not necessary but the overall effect of joints on the rock mass response is of interest. In these situations, an equivalent continuum model that takes into account the influence of the joints implicitly provides a desirable alternative to discontinuum based models.

In this paper, a three dimensional equivalent continuum constitutive model, named *JointedRock*, is introduced for a rock mass containing up to three persistent joint sets with arbitrary orientation and spacing. By using the concept of the conservation of energy,

associated with the work done by an external force on an elastic body, the equivalent compliance matrix of the rock mass is established and the constitutive model is implemented in *FLAC^{3D}*. The *JointedRock* model is well suited to deformation analysis of systematically jointed rocks that show anisotropic and nonlinear response to loading. The model also checks the violation of the Mohr-Coulomb failure criterion in the intact rock and along one of the joint sets, as defined by the user. The validity of the approach is checked by comparing the *JointedRock* model results with those obtained from three dimensional discontinuum models and available closed form solutions.

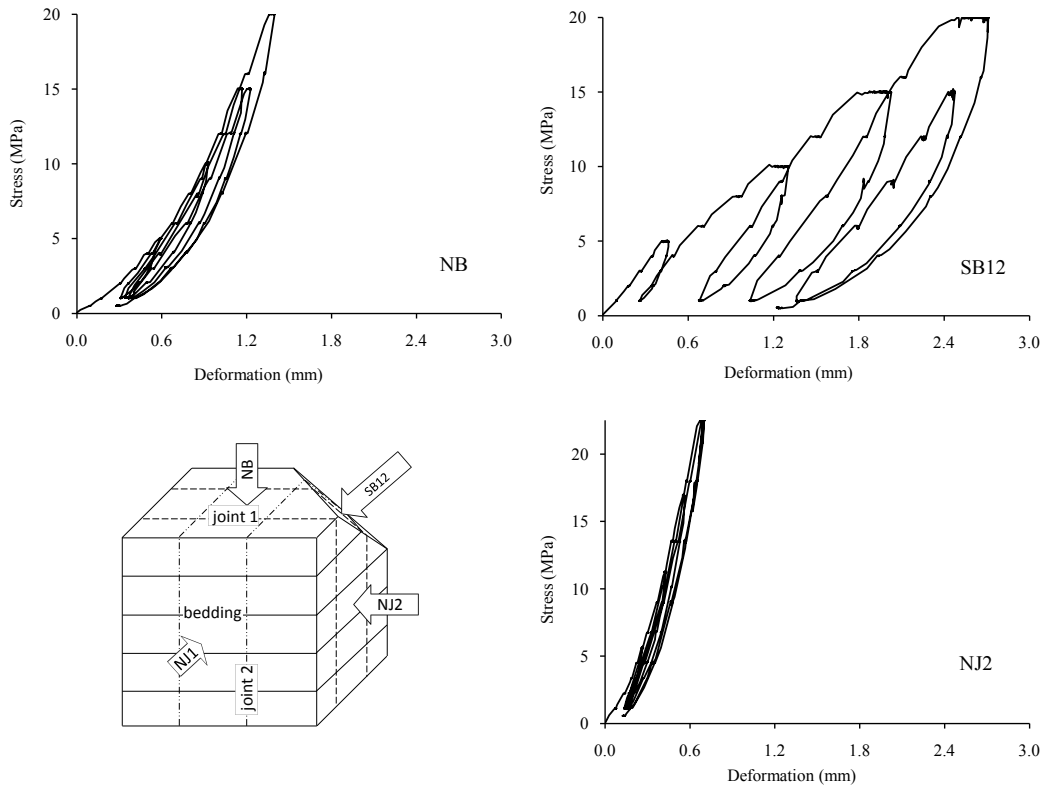


Figure 4.1: Stress – deformation graphs of plate loading tests on a jointed limestone at the Bakhtiary dam site (loading plate diameter: 971 mm). The graphs show the surface deflection for three different test configurations that differ in the relative direction of loading to orientation of discontinuities: normal to bedding (NB), normal to joint set 2 (NJ2) and inclined to all three joint sets, SB12.

4.2 *JointedRock* Model: Theory and Assumptions

A rock mass with persistent joint sets can be mechanically represented by spring-slider-dashpot models interacting in series as depicted in Figure 4.2. Similarly, the equivalent continuum model of this rock can be shown by another spring-slider-dashpot model

where the spring represents the equivalent elastic stiffness and sliders represent elements with potential of failure in the model, i.e. intact rock and the critical joint set.

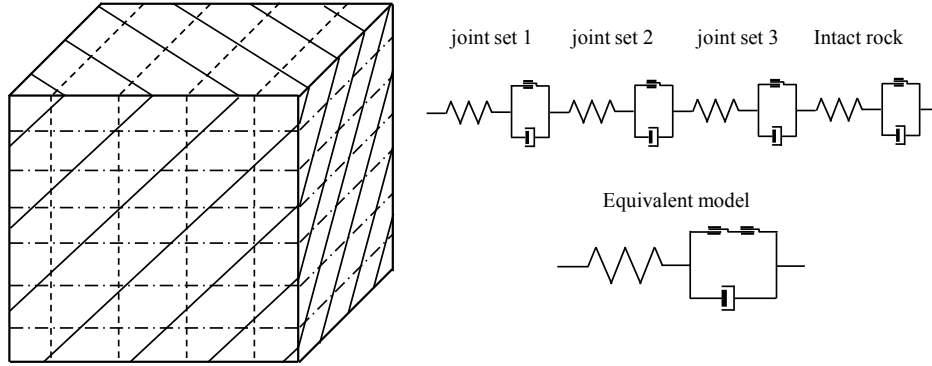


Figure 4.2: Conceptual rock block with three persistent joint sets and its simplified physical model

Given the above physical model under the action of an external force, the total elastic strain increment in the equivalent model are the sum of the elastic strains in each component of the system, i.e. intact rock and three joint sets. In a global coordinate system this can be written as follow:

$$\Delta\epsilon_{ij} = \Delta\epsilon_{ij}^R + \Delta\epsilon_{ij}^{J1} + \Delta\epsilon_{ij}^{J2} + \Delta\epsilon_{ij}^{J3} \quad (4.1)$$

where $\Delta\epsilon_{ij}$ is total strain increment of the equivalent continua and $\Delta\epsilon_{ij}^R$ is the intact rock strain increment and $\Delta\epsilon_{ij}^{J1}$, $\Delta\epsilon_{ij}^{J2}$ and $\Delta\epsilon_{ij}^{J3}$ are the strain increments in the joint sets.

Assuming the intact rock is isotropic, the incremental strain in the rock can be related to the increment of stress in the global coordinate system as follow (Jaeger et al. 2007)

$$\Delta\epsilon_{ij}^R = C_{ijmn}^R \Delta\sigma_{mn} \quad (4.2)$$

where C_{ijmn}^R is the elastic compliance tensor of the intact rock.

For this model, a representative elementary volume (REV) can be defined as a block of rock that encompasses one plane of each joint set with the dimensions being equivalent to the average spacing of the joint sets (Figure 4.3). This REV defines the minimum volume of rock that represents the average characteristics of the domain determined by the model.

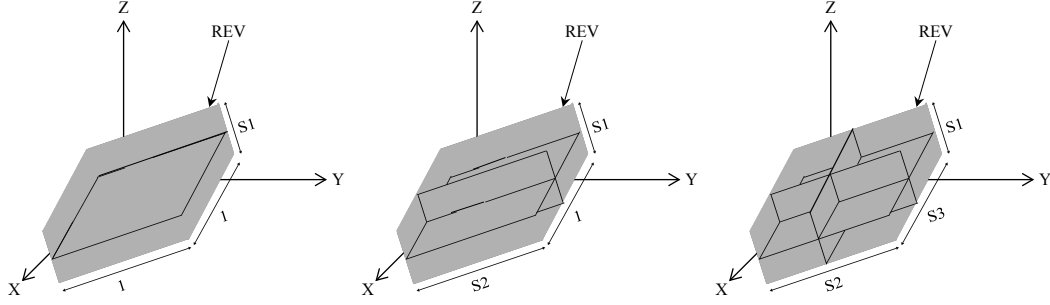


Figure 4.3: Representative Elementary Volume (REV) for the *JointedRock* model

For a representative volume of V subjected to a stress increment of $\Delta\sigma_{ij}$ with corresponding strain increment of $\Delta\varepsilon_{ij}$, the increment of strain energy due to deformation along joint set k , ΔE^{Jk} , can be mathematically written as:

$$\Delta E^{Jk} = \sigma_{ij} \Delta \varepsilon_{ij}^{Jk} V \quad (4.3)$$

where σ_{ij} is the average stress of the REV. Assuming that joints are persistent and planar in the model, the tractions on joint, τ_{ij} , can be calculated from average stress of REV as follow:

$$\tau_j = \sigma_{ij} n_i \quad (4.4)$$

where n_i is normal unit vector of joint. The work done by traction on the k^{th} joint plane can be calculated as:

$$\Delta w^{Jk} = \tau_j^k \Delta \delta_j^k A^k \quad (4.5)$$

where $\Delta \delta_j^k$ is elastic displacement along k^{th} joint plane in REV.

According to the principle of conservation of energy, the part of the elastic strain energy stored in the system due to elastic displacement along a given joint set (equation (4.3)), is equal to the work done by surface traction on the joint plane (Huang et al. 1995) as defined in equation (4.5). By substituting equation (4.4) into (4.5), the strain increment caused by elastic displacement along k^{th} joint plane in REV is given by:

$$\Delta \varepsilon_{ij}^{Jk} = n_i \Delta \delta_j^k \frac{1}{s^k} \quad (4.6)$$

where s^k is the dimension of the REV in the direction normal to the joint plane k^{th} .

In the global coordinate system, the joint displacements can be related to stresses acting on the joint plane by using joint elastic compliance matrix, D_{jm} , as follow:

$$\delta_j = D_{jm} \tau_m \quad (4.7)$$

Substituting equation (4.4) in (4.7) and an incremental form of equation (4.7) into (4.6), yields:

$$\Delta \epsilon_{ij}^{Jk} = n_i^k D_{jm}^k n_n^k \frac{1}{s^k} \Delta \sigma_{mn} \quad (4.8)$$

From equation (4.8) the elastic compliance of joint set k^{th} can be expressed in the form of a fourth-order tensor, C_{ijmn}^{Jk} , as follow:

$$C_{ijmn}^{Jk} = n_i^k D_{jm}^k n_n^k \frac{1}{s^k} \quad (4.9)$$

Following the same steps for all joint sets in the model, the equivalent compliance tensor of the model, C_{ijmn}^{Eq} can be theoretically determined by summation of the compliance tensors of model elements in the global coordinate system:

$$C_{ijmn}^{Eq} = C_{ijmn}^R + C_{ijmn}^{J1} + \dots + C_{ijmn}^{Jk} \quad (4.10)$$

The Mohr-Coulomb failure criterion with a tension cut-off is used to check failure through intact rock and along the joint set. A perfect plastic behavior is assumed for both after yielding. Further details can be found in (Jaeger et al. 2007; Itasca 2006).

To establish the equivalent compliance tensor of the rock mass in the matrix form, equation (4.2) is written in the Voigt notation (Jaeger et al. 2007) as follow:

$$\begin{bmatrix} \epsilon_{11} \\ \epsilon_{22} \\ \epsilon_{33} \\ 2\epsilon_{23} \\ 2\epsilon_{13} \\ 2\epsilon_{12} \end{bmatrix} = \begin{bmatrix} \epsilon_1 \\ \epsilon_2 \\ \epsilon_3 \\ \epsilon_4 \\ \epsilon_5 \\ \epsilon_6 \end{bmatrix} = \begin{bmatrix} \frac{1}{E} & -\frac{\nu}{E} & -\frac{\nu}{E} & 0 & 0 & 0 \\ -\frac{\nu}{E} & \frac{1}{E} & -\frac{\nu}{E} & 0 & 0 & 0 \\ -\frac{\nu}{E} & -\frac{\nu}{E} & \frac{1}{E} & 0 & 0 & 0 \\ 0 & 0 & 0 & \frac{1}{G} & 0 & 0 \\ 0 & 0 & 0 & 0 & \frac{1}{G} & 0 \\ 0 & 0 & 0 & 0 & 0 & \frac{1}{G} \end{bmatrix} \begin{bmatrix} \sigma_1 \\ \sigma_2 \\ \sigma_3 \\ \sigma_4 \\ \sigma_5 \\ \sigma_6 \end{bmatrix} \quad (4.11)$$

where E is Young's modulus, G is shear modulus and ν is the Poisson's ratio of the intact rock. Due to the isotropic assumption for the intact rock, the above relationship is valid in all coordinate systems.

The elastic compliance tensor of a single joint plane (Figure 4.4) can be written in the following general form:

$$D = \begin{bmatrix} D_{11} & D_{12} & D_{13} \\ D_{21} & D_{22} & D_{23} \\ D_{31} & D_{32} & D_{33} \end{bmatrix} = \begin{bmatrix} D_{ss} & D_{st} & D_{sn} \\ D_{ts} & D_{tt} & D_{tn} \\ D_{ns} & D_{nt} & D_{nn} \end{bmatrix} \quad (4.12)$$

where the indices s , t and n denotes the components of the local coordinate system. The local coordinate system of a joint set is oriented such that s -axis points to dip direction, t -axis is aligned with the joint strike direction and n -axis defines the normal to the joint plane, that together form a right-handed coordinate system.

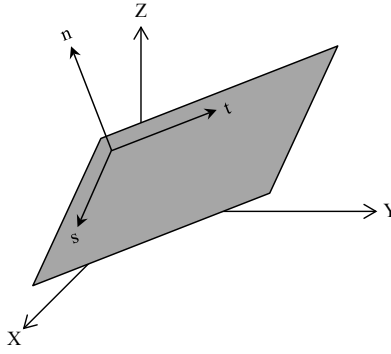


Figure 4.4: Joint plane and local coordinate system

In general, the compliance tensor for a joint is not symmetric due to the normal and shear displacements that develop under shear and normal stresses, respectively. But for the sake of simplicity these components of joint deformation are ignored by setting the off-diagonal terms of (4.12) to zero in the local coordinate system of the joint set.

For the implementation purpose, the compliance tensor of each joint set is first built in the local coordinates of the joint set, according to equation (4.9). Therefore equation (4.8) can be written in the matrix form as follow:

$$\begin{bmatrix} \epsilon_{11} \\ \epsilon_{22} \\ \epsilon_{33} \\ 2\epsilon_{23} \\ 2\epsilon_{13} \\ 2\epsilon_{12} \end{bmatrix} = \begin{bmatrix} \epsilon_1 \\ \epsilon_2 \\ \epsilon_3 \\ \epsilon_4 \\ \epsilon_5 \\ \epsilon_6 \end{bmatrix} = \begin{bmatrix} C_{11} & C_{12} & C_{13} & C_{14} & C_{15} & C_{16} \\ C_{21} & C_{22} & C_{23} & C_{24} & C_{25} & C_{26} \\ C_{31} & C_{32} & C_{33} & C_{34} & C_{35} & C_{36} \\ C_{41} & C_{42} & C_{43} & C_{44} & C_{45} & C_{46} \\ C_{51} & C_{52} & C_{53} & C_{54} & C_{55} & C_{56} \\ C_{61} & C_{62} & C_{63} & C_{64} & C_{65} & C_{66} \end{bmatrix} \begin{bmatrix} \sigma_1 \\ \sigma_2 \\ \sigma_3 \\ \sigma_4 \\ \sigma_5 \\ \sigma_6 \end{bmatrix} \quad (4.13)$$

With zero off-diagonal terms in the joint compliance tensor of equation (4.12), the only non-zero terms of the compliance matrix of the joint set, in local coordinates, are C_{33} , C_{44} and C_{55} . From equation (4.9) the values of these terms can be determined as:

$$C_{33} = \frac{D_{nn}}{S} = \frac{1}{k_n S} \quad (4.14)$$

$$C_{44} = \frac{D_{tt}}{S} = \frac{1}{k_t S} \quad (4.15)$$

$$C_{55} = \frac{D_{ss}}{S} = \frac{1}{k_s S} \quad (4.16)$$

where k_n , k_t and k_s are joint stiffness in directions of local coordinate axes n , t and s , respectively.

The joint set compliance matrix as defined in (4.13) is no longer a tensor quantity and the common tensor transformation rule cannot be used for transformation of this matrix to the global coordinate system. Instead this can be done using the method described by Riahi (Riahi 2008). Once the compliance matrices of all components are formed in the global coordinate system, the equivalent compliance matrix of the rock mass is obtained using equation (4.10). Finally, the equivalent elasticity matrix is determined by inverting the equivalent compliance matrix, in the global coordinate system.

4.3 Implementation of the *JointedRock* Model in *FLAC^{3D}*

FLAC^{3D} is a three-dimensional finite difference program for engineering mechanics computation (Itasca 2006). In this program, materials are represented by polyhedral elements within a three-dimensional grid. Each element behaves according to a prescribed constitutive model and failure criterion in response to applied forces or boundary restraints. The constitutive models in *FLAC^{3D}* follow an incremental numerical algorithm, i.e. given the stress state at time t , and the total strain increment at time step, dt , the purpose is to determine the corresponding stress increment and the new stress state at time $t+dt$.

In the Jointed Rock model, when plastic deformations are allowed, upon each stress increment the failure of intact rock and the first joint set is checked using the Mohr-Coulomb failure criterion with a tension cut-off. No check is made by the code for failure along the second or third joint set, if there is any. The code also does not check for multiple active yield surfaces. After each stress increment, general failure through the intact rock is first checked and if there is any violation of the failure criterion the

corresponding plastic stress correction is applied. Using the most updated stress state, a further check is made for the failure along the joint set.

The number of joint sets to be modeled is controlled by the user and varies from one to three joint sets. It is also possible to ignore the failure check for either intact rock and/or joint set using a built-in option in the model. The mechanical parameters required for the model are the cohesion, friction angle, normal and shear stiffness, spacing, dip and dip direction of joints, and cohesion, friction angle, shear and bulk moduli of intact rock. Figure 4.5 shows the steps that are followed by the model during each time step of calculation in a *FLAC^{3D}* model.

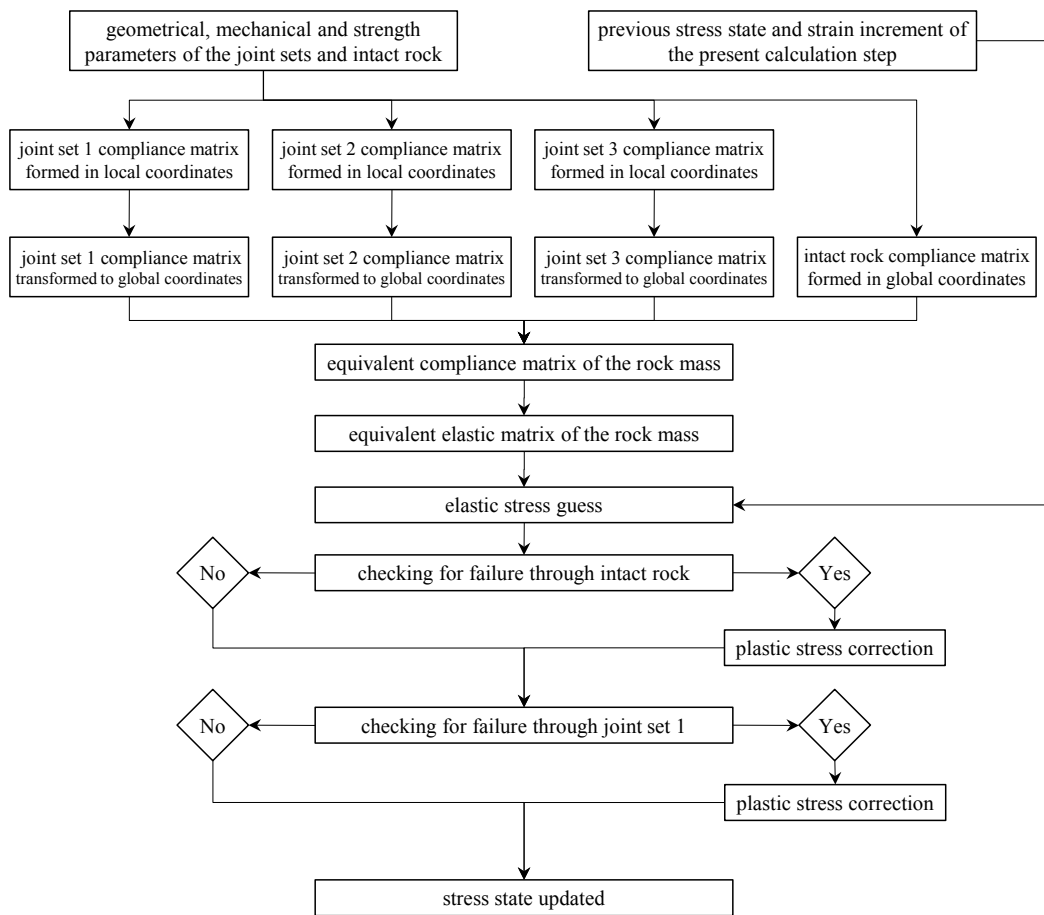


Figure 4.5: Calculation steps followed for the implementation of the *JointedRock* model in *FLAC^{3D}*

4.4 Verification Examples

4.4.1 Elastic Deformation

The deformation of a cube of rock in a uniaxial test is analyzed by three different methods: the *JointedRock* model, the built-in Elastic model in *FLAC^{3D}* (Itasca 2006) and the three-dimensional Distinct Element Code *3DEC* (Itasca 2007). For the Elastic model, the relationships developed by Yoshinaka and Yamabe (1986) are used to calculate the equivalent Young's and shear moduli. For the discrete element analysis, the same rock geometry, as in *FLAC^{3D}*, is used in *3DEC* and the joint sets are explicitly added to the model.

Two series of tests are modeled. The model consists of a 2×2×2 m rock block that is cut through by one joint set (two joint sets for the second series of tests) at different angles ranging $\beta = 0$ to 90° measured from z-plane (Figure 4.6). Joints are spaced at $S = 0.25$ m. Roller boundary conditions are applied to the x-planes (planes normal to x-axis). A pressure of 10 MPa is applied to the top and bottom of the model by assigning z-velocities to the boundary grid points on the z-planes. The two other sides of the model are left unsupported to meet the plane stress assumption as taken in the applied closed form relationships (Yoshinaka and Yamabe 1986). In all models plastic deformations are prevented. In the *3DEC* model, high cohesion and tensile strength are assigned to the joints to prevent plastic deformation and block separation during the test. Table 4.1 shows the mechanical properties that are used for these models.

Table 4.1: Mechanical and strength parameters for uniaxial test

Mechanical Parameter	intact rock	joint set 1	joint set 2
bulk modulus (GPa)	4.28	--	--
shear modulus (GPa)	1.75	--	--
normal stiffness (GPa/m)	--	15	30
shear stiffness (GPa/m)	--	12	25
cohesion (kPa)	50	10	--
friction angle (degree)	40	30	--
tensile strength (kPa)	200	20	--
dilation angle (degree)	0	0	--

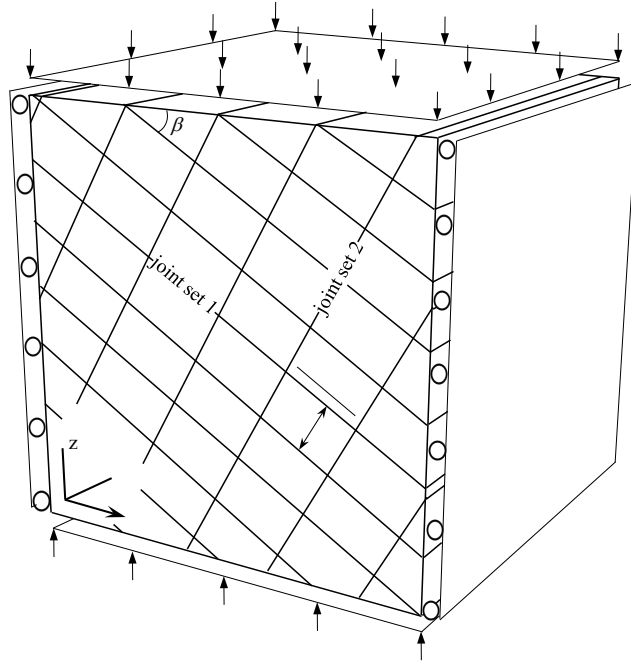


Figure 4.6: Geometry and boundary conditions for the uniaxial test model. The first series of tests are run with one joint set with joint spacing of $S = 0.25\text{m}$. The second series of tests used two joint sets with spacings of $S_1 = 0.4\text{m}$ and $S_2 = 0.25\text{m}$.

Figure 4.7 shows the variation of the axial deformation versus joint inclination. In comparison with the *3DEC* model, the *JointedRock* model tends to slightly overestimate the deformations for β values in the middle of the study range. For the assumed mechanical parameters the difference reaches its maximum of 10% at $\beta = 50^\circ$. This issue can be attributed to bending stiffness of the rock layers in the *3DEC* model. As depicted in Figure 4.8, reducing the shear modulus of the intact rock reduces the bending stiffness of the layers, and the difference between the predicted deformations decreases for the two models. The influence of bending stiffness is discussed in more detail in the next section. The analytical method tends to considerably underestimate the axial deformations over the applied range of joint inclination except for the two cases of $\beta = 0^\circ$ and $\beta = 90^\circ$.

Figure 4.9 shows the results of the same uniaxial test model for a block of rock with two perpendicular joint sets with the joint spacing being $S_1 = 0.4\text{m}$ and $S_2 = 0.25\text{m}$. Again the *JointedRock* model produces slightly higher deformations, compared to the *3DEC* results, for the middle range β angles.

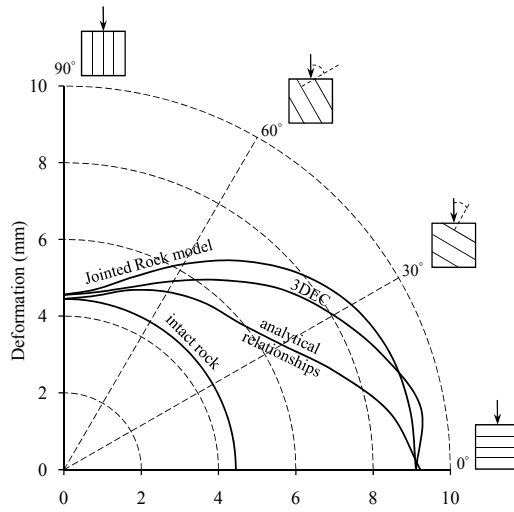


Figure 4.7: Rock deformation in uniaxial test model with one joint set

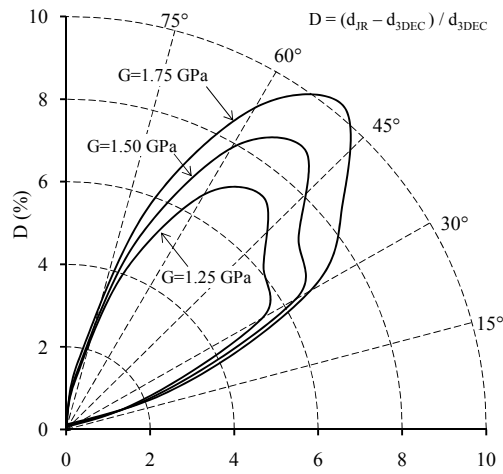


Figure 4.8: Difference between calculated axial deformation by the *JointedRock* model (d_{JR}) and *3DEC* model (d_{3DEC}) for different joint set inclinations and three intact rock shear moduli (G)

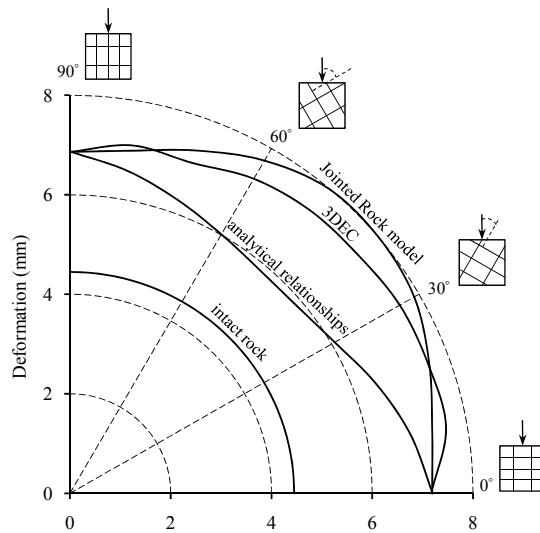


Figure 4.9: Rock deformation in uniaxial test model with two joint sets

4.4.2 Uniaxial Compressive Strength

The uniaxial compressive strength of a cylindrical sample of rock containing a plane of weakness is evaluated using three different methods. The closed form solution proposed by Jaeger et al. (2007) is used to determine the strength of the sample when the angle between the weakness plane and axis of the sample varies from $\beta = 0^\circ$ to 90° . The same problem is solved numerically in *FLAC^{3D}* using two different mechanical models. In one model, the effect of the weakness plane is taken into consideration implicitly by the *JointedRock* model. In the second model, the built-in Interface model in *FLAC^{3D}* is used to define the weakness plane explicitly in the model. For the weakness plane, the properties of joint set 1 are adopted from Table 4.1. The intact rock properties are also those listed in Table 4.1.

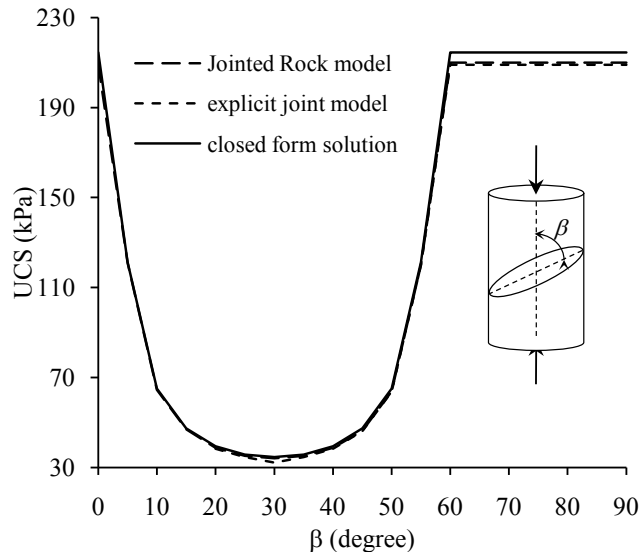


Figure 4.10: Uniaxial compressive strength of a rock sample with weakness plane

For both models, a cylindrical rock specimen of 2m in diameter and 4m in length is loaded to failure. The uniaxial compressive strengths of the rock obtained from the three methods are plotted versus weakness plane orientation in Figure 4.10. All three methods produce essentially identical results with the same typical U-shape graph. It should be noted that in the *JointedRock* model, the spacing of the joint set has no effect on the calculated strength as the model just checks the violation of the failure criterion along the joint orientation and does not take into account any length scale.

4.5 *JointedRock* Model Application

The *JointedRock* model was originally developed as a practical tool for analysis of complex deformational behavior observed during plate load tests on jointed rocks, i.e. deformation anisotropy and stress dependency, as described in the introduction. In this section, the *JointedRock* model is used for two different deformation analyses. The first case is for a semi-infinite body of an intensely jointed rock mass that resembles a plate load test. The second case is for non-linear deformation of a cylindrical rock specimen with a single joint with stress dependent normal stiffness.

4.5.1 Deformation and Stress Distribution in a Semi-infinite Body of Jointed Rock

A semi-infinite body of rock with one joint set is modeled to determine the surface deformation caused by a circular load applied on the top. The model consists of a block of rock with dimensions of $26 \times 26 \times 15$ m ($W \times L \times D$), intersected by a joint set with spacing of $S = 0.1$ m. A distributed normal stress of $P = 10$ MPa is applied on a circular area, of $d = 1$ m in diameter, on the top centre of the model (Figure 4.11).

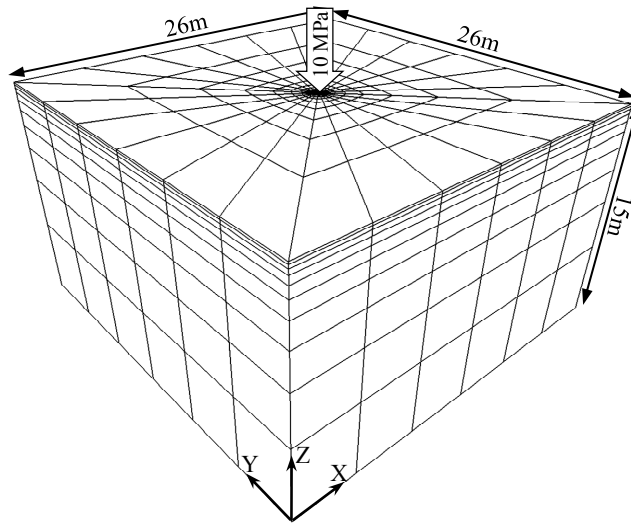


Figure 4.11: Semi-infinite body of rock loaded on the top in *FLAC^{3D}*

The induced vertical displacement at centre of the loaded area is measured by the model for various joint inclinations ranging from $\beta = 0^\circ$ to $\beta = 90^\circ$ (measured from loading direction). The rock and joint properties listed in Table 4.1 are assigned to the model. The analysis is repeated for a model of similar geometry and properties but in which the first joint set is intersected orthogonally by a second joint set with a spacing of $S = 0.2$ m. The measured vertical displacements at the top centre of the model are plotted against

joint orientation for both models in Figure 4.12. As observed, the induced deformation anisotropy due to the relative direction of loading to joint orientations is captured by the *JointedRock* model.

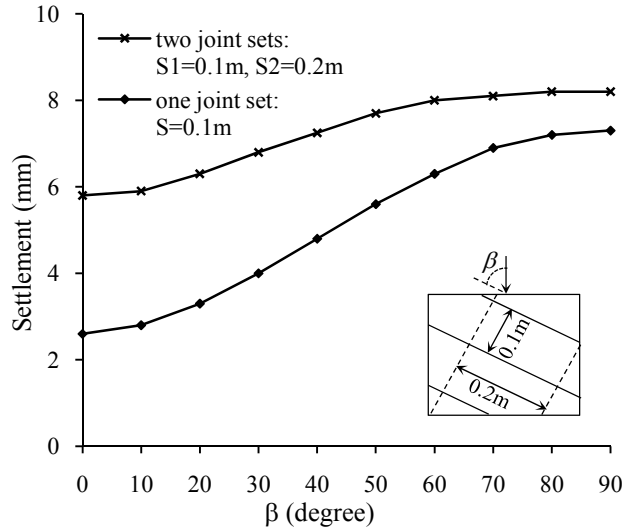


Figure 4.12: Vertical displacements versus joint set orientation for a semi-infinite body of rock intersected by one and two joint sets. A circular stress of 10 MPa is applied on the top centre of the model and displacements are measured at the centre of the loaded area.

The discontinuities also change the stress distribution pattern beneath the loaded area. For a given joint configuration, the stress distribution in the semi-infinite body depends on the relative stiffness of the joints and rock, and the ratio between joint normal and shear stiffness. But in general, joints give rise to deeper penetration of the stress and hence more deformation. Figure 4.13 shows the stress distribution beneath the loaded area in the model with one joint set. As observed, the *JointedRock* model captures the influence of the joints on the stress distribution despite no real discontinuities exist in the model. This differs from all other equivalent continuum models where equivalent deformation parameters, such as shear and Young moduli are used to represent the influence of the discontinuities (Yoshinaka and Yamabe 1986).

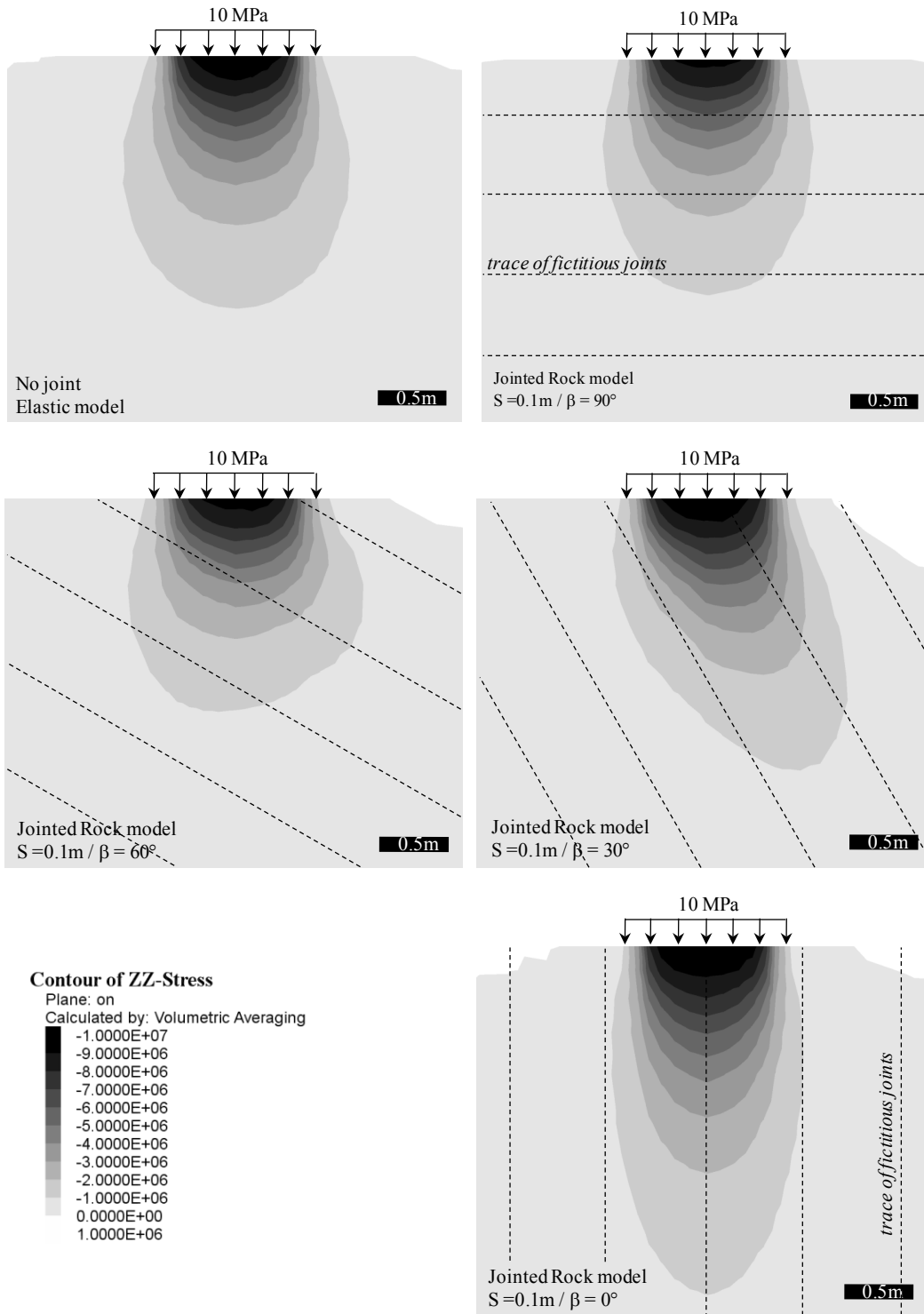


Figure 4.13: Stress distribution beneath the loaded area in the semi-infinite model with one joint set

4.5.2 Stress-Dependent Joint Stiffness and Non-Linear Deformation

A rock cylinder, cut by a single fictitious joint is loaded axially to $P = 10$ MPa. The intact rock is assumed to follow a linear elastic behavior while the joint closure is non-linear and stress-dependent. The hyperbolic relationship introduced by Bandis et al. (1983) is assumed for the joint closure (δ) as follows:

$$\delta = \frac{\delta_m \cdot \sigma_n}{k_{in} \cdot \delta_m + \sigma_n} \quad (17)$$

The tangent normal stiffness (k_n) of the joint can be calculated at each normal stress (σ_n) level from the derivative of equation (17) as follow:

$$k_n = k_{in} \cdot \left(1 - \frac{\sigma_n}{k_{in} \cdot \delta_m + \sigma_n}\right)^{-2} \quad (18)$$

where δ_m and k_{in} are the maximum joint closure and joint initial normal stiffness, respectively (Bandis et al. 1983). Assuming $\delta_m = 3.7$ mm and $k_{in} = 1$ MPa/mm the joint closure and normal stiffness curves of the model are plotted in Figure 4.14.

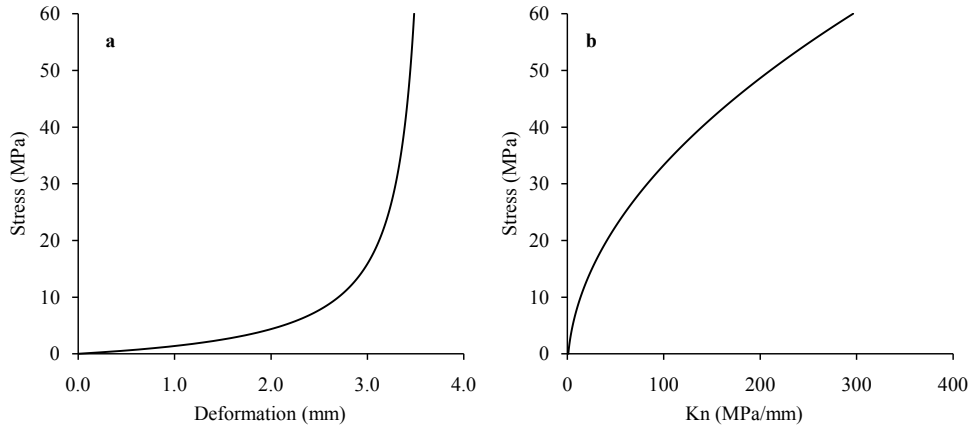


Figure 4.14: Assumed joint closure and tangent normal stiffness curves for the model ($\delta_m = 3.7$ mm and $k_{in} = 1$ MPa/mm)

The model is run for various orientations of the fictitious joint relative to specimen axis. The stress-deformation curve for the case when the applied load is perpendicular to the joint is shown in Figure 4.15. As observed, the total displacement is sum of the linear deformation of the intact rock and the non-linear closure of fictitious joint that produces a general non-linear response of the rock specimen. As the angle between the joint plane and the axis of the specimen reduces, the joint normal closure contribution to the total deformation decreases and response of the specimen converges to that of the intact rock.

At the limiting case of $\alpha = 0^\circ$ the total deformation of the rock specimen coincides with the deformation of the intact rock, which is totally linear (Figure 4.15).

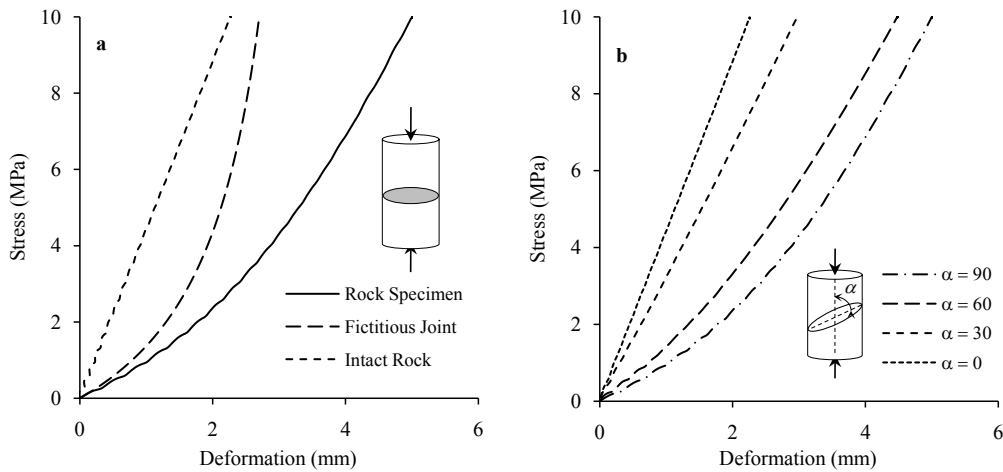


Figure 4.15: Axial deformation of a cylindrical rock specimen having a fictitious joint with stress-dependent normal stiffness. a) The total non-linear deformation is the sum of the linear deformation of the intact rock and non-linear closure of the fictitious joint. b) As the angle between fictitious joint and loading direction approaches zero, the deformation of the specimen converges to that of the intact rock

4.6 Discussion on Model Applicability and Limitations

An important factor that should be considered when comparing continua and discontinua modeling is the deformation kinematics. In continua the total deformation of a body is produced by shear deformation and compression or extension of the body elements. In contrast, in discontinua dislocation and detachment of the blocks are two potential mechanisms that can contribute to the total deformation of the body. Hence, application of the *JointedRock* model should be avoided when such mechanisms are likely, e.g., toppling detachment of rock layers.

As discussed before, in the uniaxial test model the *JointedRock* model tends to slightly overestimate the deformations, compared to the *3DEC* model. This issue arises from the different mechanisms that contribute to the deformation of the rock in the two models. In the *3DEC* model, when joints are inclined, the difference in the vertical displacement of two opposite ends of the layers results in bending of the intact rock layers. As a result, the total stiffness of the model builds up due to bending stiffness of these layers. But in the *JointedRock* model, no such mechanism develops, as the discontinuities are implicitly incorporated into the model, and total deformation of the body results from shear deformation and compaction of the body elements.

To evaluate the effect of bending stiffness on the *JointedRock* model, the bending of a simple cantilever plate under the action of a line load, F_z , (Figure 4.16) is modeled in *FLAC^{3D}*. The deflection of the plate tip is calculated for three different plate models. In the first model, the plate is assumed to be intact and free of any discontinuity. The properties of the intact rock are assigned to this model. In the second model, a horizontal discontinuity cuts the plate thickness in half. The Interface model is used for the discontinuity. In the third model the influence of the discontinuity plane is taken into account in an implicit way using the *JointedRock* model. The properties of the discontinuity and the intact rock are those listed in Table 4.1 for the joint set 1. Figure 4.17 shows the deflection of the plate tip plotted versus joint shear stiffness for two values of intact rock shear modulus.

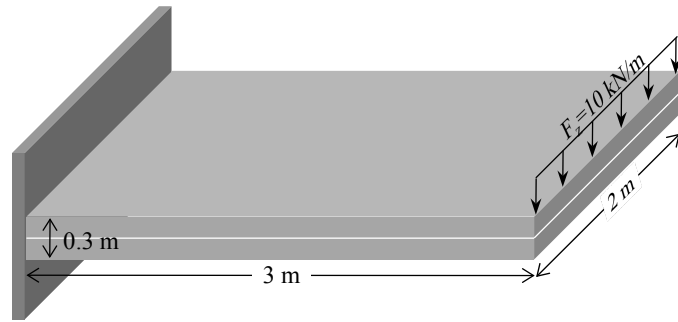


Figure 4.16: Cantilever plate loaded by a line load, F_z

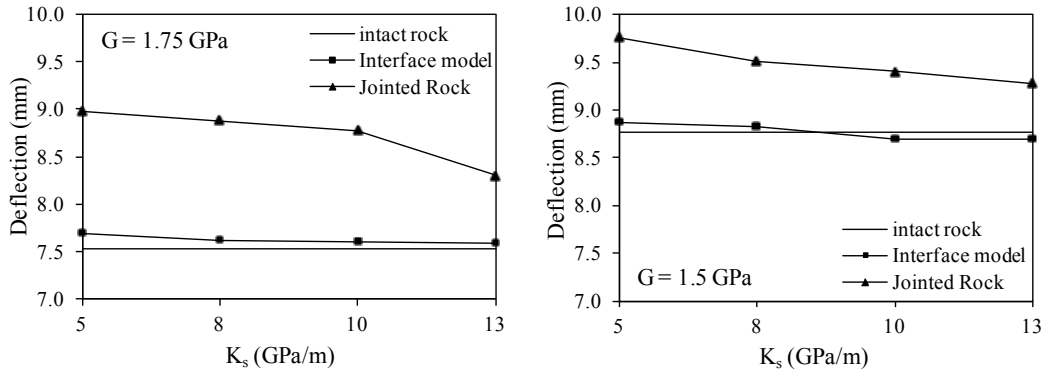


Figure 4.17: Deflection of cantilever plate tip versus discontinuity shear stiffness (k_s) for two intact rock shear moduli (G)

As observed, the deflection of the plate with the explicit joint is almost equal to that of the intact rock. The deflection of the plate in this model is controlled by bending of the two intact rock plates interacting along the joint. At higher values of joint shear stiffness the problem becomes similar to bending of an integrated plate. In the case of the *JointedRock* model, the deflection of the plate is calculated using the average mechanical

parameters for the equivalent continua. As the results show, at lower plate bending stiffness (lower intact rock shear modulus) the absolute deflection of the plate edge increases but the relative difference between the predicted values by two models decreases.

The *JointedRock* model, similar to other equivalent continuum models that have been developed based on the classical theory of elasticity, is inherently unable to take into account the bending moments of the material. The equivalent continuum model developed by Riahi (2008) based on the Cosserat theory is better suited for such problems in which bending of the layered rock is a potential deformation mechanism.

The relative size of the model and spacing of the joints is another factor that should be considered when the *JointedRock* model is used. Figure 4.18 shows two cases of the same geometry and boundary conditions but with different joint spacing. The *Jointed Rock* model can be applied efficiently to the first case with relatively high joint density. In the case of large joint spacing, compared to size of structure or loaded area, displacement along a single joint might govern the response of rock mass. Application of the *JointedRock* model for such cases might potentially produce poor results. On the other hand, for intensely jointed rock masses, where the spacing of the joints are small compared to the general size of the model, such as the semi-infinite model for plate test loading presented earlier, the *JointedRock* model is computationally efficient compared to discontinua numerical programs.

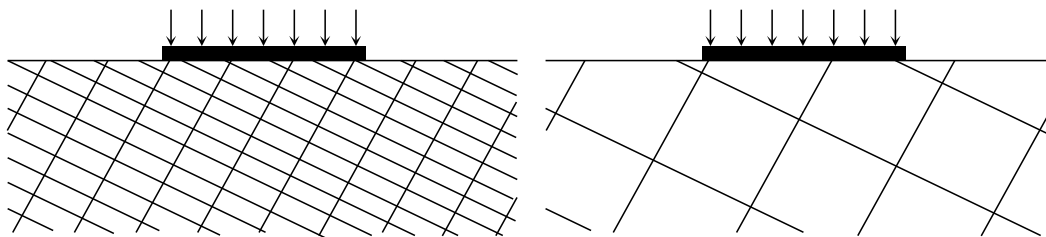


Figure 4.18: Impact of relative spacing of joints on applicability of *JointedRock* model.

Persistency of the joints is a basic assumption of the model. Plastic displacement along a joint set might change this condition as illustrated in Figure 4.19. This would only occur when the displacements are large and beyond the purpose of the model.

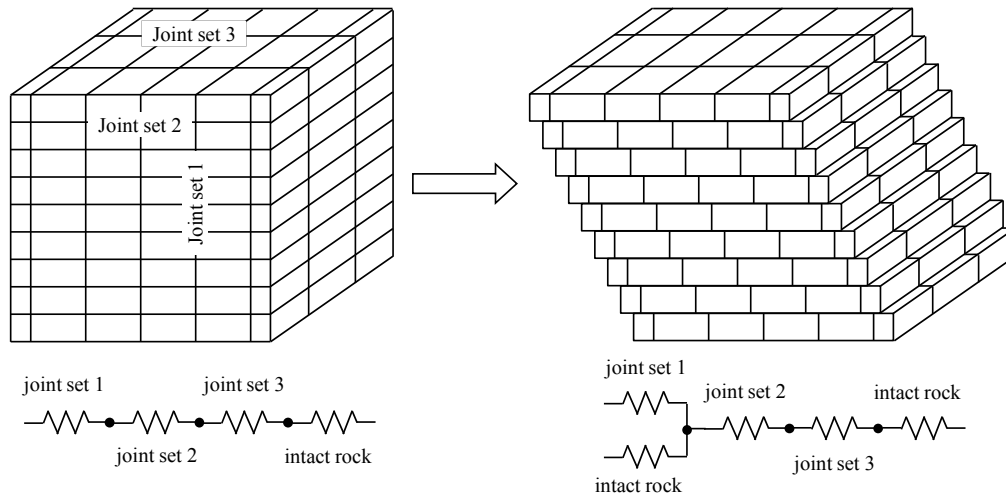


Figure 4.19: A persistent joint set becomes non-persistent as a result of large plastic displacement along another joint set

4.7 Conclusion

A three dimensional equivalent continuum constitutive model (*JointedRock*) was formulated for jointed rock masses containing up to three persistent joint sets. The model was developed to efficiently handle the deformation anisotropy and stress dependency in systematically jointed rocks. The model was implemented in $FLAC^{3D}$ and the results compared for typical example problems to the results from the discrete element method (*3DEC*), the Interface model in $FLAC^{3D}$ and analytical solutions. The results show that the *JointedRock* model provides an efficient tool for deformation analysis of systematically jointed rocks in which the general anisotropy of a rock mass is of importance to the analysis. Anisotropic behavior is frequently observed in plate load test results, and hence the *JointedRock* model may provide an efficient alternative for the interpretation of rock mass deformation test results. Because the model uses the stiffness of discontinuities as input parameters, deformation nonlinearity can also be incorporated into an analysis using appropriate stiffness models.

The relative size of the model and spacing of the joints should be considered before using the *JointedRock* model. The *JointedRock* model can be applied efficiently when the joint spacing is small relative to the loading structure such as a concrete gravity dam. However when the size of the loading structure is small compared to the joint spacing, displacement along a single joint may govern the response of rock mass. For this case, the use of the *JointedRock* model may not be appropriate. When modeling densely jointed rocks where the spacing of the joints is small compared to model dimensions the

JointedRock model also has considerable computing efficiency compared to the numerical demands for discrete element models.

4.8 Reference

- Amadei, B., Goodman, R. (1981). A 3-D constitutive relation for fractured rock masses. Proceedings of the international symposium on mechanical behaviour of structured media, Ottawa, Part B, pages 249-268 Balkema.
- Bandis, S. C., Lumsden, A. C., Barton, N. R. (1983). Fundamentals of Rock Joint Deformation. International Journal of Rock Mechanics and Mining Sciences & Geomechanics Abstracts, 20(6), 249-268.
- Cai, M., Horii, H. (1993). A constitutive model and FEM analysis of jointed rock masses. International Journal of Rock Mechanics and Mining Sciences & Geomechanics Abstracts, 30(4), 351-59.
- Hart, R., Cundall, P., & Lemos, J. (1988). Formulation of a three-dimensional distinct element model—Part II. Mechanical calculations for motion and interaction of a system composed of many polyhedral blocks. International Journal of Rock Mechanics and Mining Sciences & Geomechanics Abstracts, 25(3), 117-25.
- Huang, T., Chang, C., & Yang, Z. (1995). Elastic moduli for fractured rock mass. Rock Mechanics and Rock Engineering, 28(3), 135-44.
- Itasca Consulting Group, Inc. (2006). *FLAC^{3D}; Theory and Background*. Minneapolis: Itasca Consulting Group, Inc.
- Itasca Consulting Group, Inc. (2007). *3DEC 4.1, User's Guide*. Minneapolis: Itasca Consulting Group, Inc.
- Jaeger, J. C., Cook, N. G., Zimmerman, R. W. (2007). *Fundamentals of Rock Mechanics*. Blackwell Publishing Ltd.
- Kawamoto, T., Ichikawa, Y., & Kyoya, T. (1988). Deformation and fracturing behaviour of discontinuous rock mass and damage mechanics theory. International Journal for Numerical and Analytical Methods in Geomechanics, 12, 1-30.
- Min, K., & Jing, L. (2003). Numerical determination of the equivalent elastic compliance tensor for fractured rock masses using the distinct element method. International Journal of Rock Mechanics and Mining Sciences, 40, 795-816.
- Oda, M., Yamabe, T., Ishizuka, Y., Kumasaka, H., Tada, H., & Kimura, K. (1993). Elastic stress and strain in jointed rock masses by means of crack tensor analysis. Rock Mechanics and Rock Engineering, 26(2), 89-112.

- Riahi, A. (2008). 3D Finite element Cosserat continuum simulation of layered geomaterials. PhD Thesis. University of Toronto.
- Samadhiya, N., Viladkar, M., & Al-Obaydi, M. (2008). Numerical implementation of anisotropic continuum model for rock masses. *International Journal of Geomechanics ASCE*, 8(2), 157-61.
- Singh, B. (1973). Continuum characterization of jointed rock masses. *International Journal of Rock Mechanics and Mining Sciences & Geomechanics Abstracts*, 37, 311-49.
- Wang, T., & Huang, T. (2009). A constitutive model for the deformation of a rock mass containing sets of ubiquitous joints. *International Journal of Rock Mechanics and Mining Sciences*, 46, 521-530.
- Yoshinaka, R., & Yamabe, T. (1986). Joint stiffness and the deformation behaviour of discontinuous rock. *International Journal of Rock Mechanics and Mining Sciences & Geomechanics Abstracts*, 23(1), 19-28.

Chapter 5

Numerical analysis of plate loading test results using an equivalent continuum model “*JointedRock*” – Case study: Bakhtiary dam site³

5.1. Introduction

Plate loading tests (PLT) are commonly used to determine the rock mass deformability at the large scale. The test is often conducted in small exploratory galleries and involves loading two opposing rock surfaces and measuring the induced displacements beneath the loading plates. Depending on the loading method, two PLT types are distinguished: flexible loading by flat jacks and rigid loading by hydraulic jacks through a stiff plate. The closed form equation for loading of a semi-infinite medium is frequently used to interpret the PLT results, as suggested by ASTM (2008) and ISRM (1979). In this method, the rock mass is assumed to behave as a continuous homogeneous isotropic linear elastic material. But due to existence of discontinuities, jointed rock masses are often characterised as discontinuous media with anisotropic and non-linear behaviour. This inconsistency between the theoretical assumptions and the real rock mass behaviour is a main source of error in the interpretation of the PLT results (Agharazi et al. 2012a).

Agharazi et al. (2012a) divided the factors influencing PLT results into “operational factors” and “theoretical factors”. The operational factors are associated with the quality of the site preparation and test execution such as rock disturbance around the test gallery (Palmstrom and Singh 2001) and quality of the measurement instruments. The theoretical factors result from inconsistency of the theoretical assumptions with the real rock mass conditions and depend on the selected method for the interpretation of test results. The geometry of the test gallery is an important factor that affects the test result interpretation when using the analytical equation suggested by ISRM (1979) and ASTM (2008). For the tests in which the deformations are measured through depth beneath the loading plates, the confining effect of the test gallery results in deviation of the calculated moduli through depth versus that for an ideal elastic half space (Agharazi et al 2012a; Boyle 1992).

³ A version of this chapter has been submitted as a paper to International Journal of Geomechanics; ASCE

Numerical methods can also be used to interpret PLT results. In this method, the rock mass is usually assumed as a linear elastic material and an equivalent deformation modulus is sought through back calculation of the measured deformations during the test. By applying proper boundary conditions, the confining influence of the test gallery can be taken into account in this method.

Given that both the analytical and numerical methods provide an equivalent deformation modulus based on the measured deformations, the anisotropic deformability of a transversely isotropic or orthotropic rock mass can be determined by these methods provided enough data are available from tests conducted at appropriate directions. However, for a general case of anisotropic rock, such as a rock mass with arbitrarily oriented joint sets, a large number of PLTs conducted at various directions are required to provide enough data to determine the general deformability of the rock mass by these methods.

A detailed study by Agharazi et al. (2012a) on the results of a series of PLTs carried out at the Bakhtiary dam site in southwestern Iran showed that the deformation of the rock mass is highly anisotropic and depends not only on the mechanical properties of the intact rock and the discontinuities but also on the direction of loading relative to the discontinuities. It was shown that in a given rock mass different deformation mechanisms can be mobilized depending on the test configuration.

In this study, an equivalent continuum model for the jointed rocks, *JointedRock* (Agharazi et al. 2012b), was used to interpret the PLT results at the Bakhtiary dam site. The anisotropic deformability of the dam foundation rock mass was determined using the *JointedRock* model and the estimated stiffness of the discontinuities. The rock mass deformation modulus was also estimated using different methods, i.e. empirical relations, analytical method, and numerical method. By comparison of these moduli with the moduli predicted by the *JointedRock* model, it is shown that the observed scatter in the estimated moduli, to a large extent, relates to the anisotropy of the rock mass.

The *JointedRock* model is briefly introduced in the next section. The capability of the model in stress-deformation analysis of the jointed rocks is assessed by a test model of a jointed rock cylinder loaded axially and comparing the results with the results of a model in which the joints were defined explicitly.

5.2. *JointedRock* Model

The *JointedRock* model is a three dimensional equivalent continuum model developed for stress-deformation analysis of jointed rock masses with anisotropic and non-linear deformational characteristics. In this model, up to three joint sets can be implicitly added to an intact rock to construct an equivalent continuum model of a systematically jointed rock mass. Joints can be of any arbitrary spatial orientation that is defined by their dip, dip direction, and spacing in the model. The deformational characteristics of the joints are directly defined in the model by their normal and shear stiffness.

The elastic compliance of the equivalent continua is established by the definition of a so-called Representative Elementary Volume (REV) and superpositioning of strains of the REV elements, i.e. the joint sets and the intact rock based on the principles of the conservation of energy for the work done on elastic bodies. The model adopts an elastic-perfect plastic mechanical behavior for both the intact rock blocks and the joint sets, using the Mohr-Coulomb failure criterion. The model was implemented in *FLAC^{3D}* and can be used for numerical analysis of the jointed rock masses. Agharazi et al. (2012b) provide further details on the *JointedRock* model.

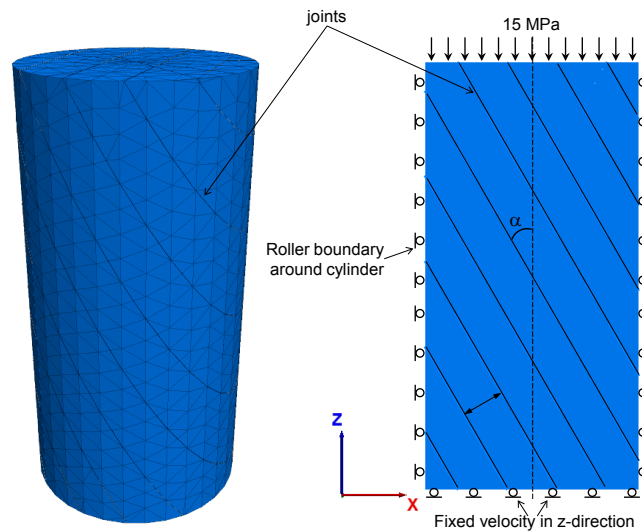


Figure 5.1: Jointed rock cylinder of the 3D uniaxial test model (left), cross section of the cylinder and boundary condition (right).

The *JointedRock* model was used to carry out a three dimensional numerical analysis of a uniaxial test on a hypothetical jointed rock cylinder of 1 m in length and 0.5 m in diameter. The lateral displacement of the cylinder was confined by applying roller

boundaries around the cylinder. This boundary condition is necessary to prevent the dislocation and rotation of the rock blocks. The axial load was provided by applying a fixed velocity to the top of the model until the test load of $P = 15$ MPa was reached (rigid loading).

Two cases were studied: a rock cylinder with one joint set, and a rock cylinder with two perpendicular joint sets. A $FLAC^{3D}$ model was constructed and the joint sets were added to the model implicitly. A $3DEC$ model of the same test was also made with the joint sets being added to the model explicitly. The mechanical properties of the joints and the intact rock are listed in Table 5.1.

Table 5.1: Mechanical properties of joints and intact rock for the uniaxial test model.

parameter	intact rock	joint set 1	joint set 2
bulk modulus (GPa)	44	--	--
shear modulus (GPa)	26.4	--	--
normal stiffness (GPa/m)	--	13.9	13.9
shear stiffness (GPa/m)	--	6.95	6.95
spacing (m)	--	0.1	0.1

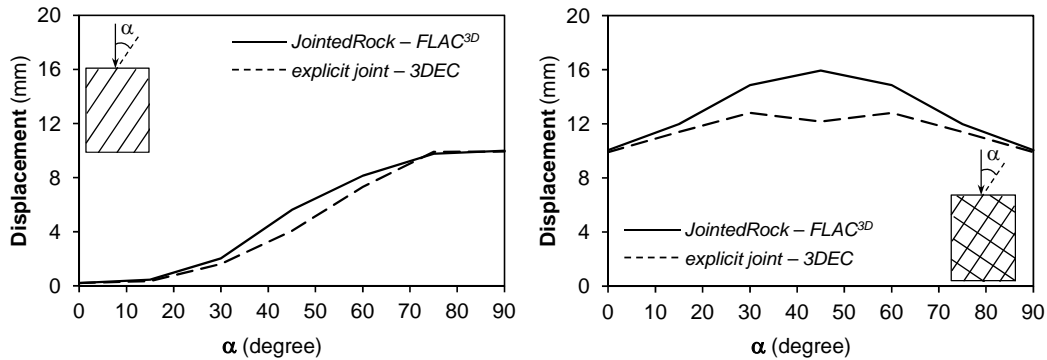


Figure 5.2: Deformation versus joint angle plots for uniaxial test with one joint set (left) and two joint sets (right).

The models were run for different joint angles ranging from $\alpha = 0$ to 90° . The axial deformation of the cylinder is plotted versus the joint angle in Figure 5.2 for models with one joint set and models with two joint sets. The deformations from the *JointedRock* model show a good agreement with the results from the *3DEC* model, for the simulations with one joint set. The minor differences observed at the mid-range joint dip angles arise mainly from the bending stiffness of the rock layers in the *3DEC* model (Agharazi et al. 2012b). The anomaly observed in the predicted deformation pattern by the *3DEC* model

for the test with two joint sets at $\alpha \approx 45^\circ$ is a boundary condition effect caused by rotation and dislocation of the boundary blocks on top of the model under the applied fixed velocity boundary condition.

Figure 5.3 shows the maximum stress and the axial displacement contours for the test with one joint set and joint angles of $\alpha = 30^\circ$ and $\alpha = 60^\circ$. Despite there being no explicit discontinuities in the *JointedRock* model, the influence of the discontinuities is properly reflected in the stress and displacement distributions defined by the model. The results also show a close match with the results from the *3DEC* model with explicit joints.

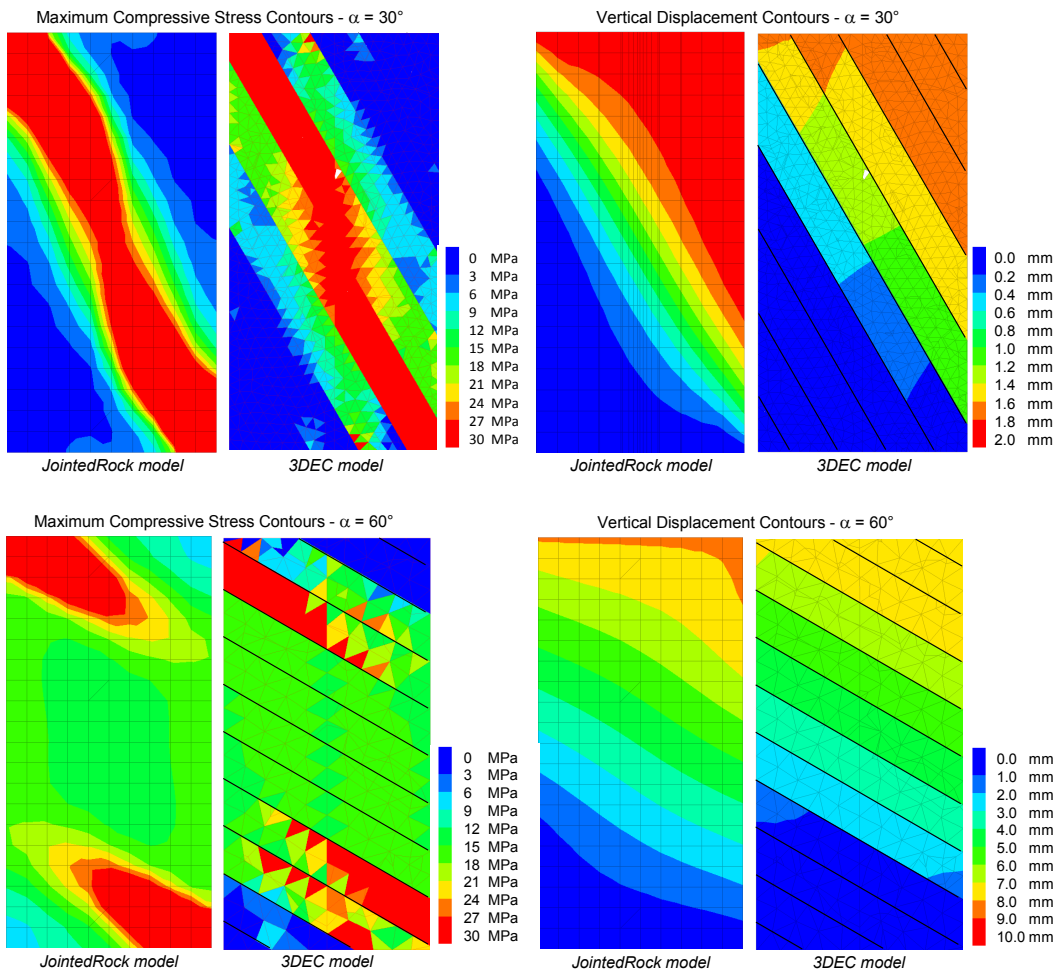


Figure 5.3: Maximum principal stress and axial displacement contours for the uniaxial test with one joint set at $\alpha = 30^\circ$ (upper) and $\alpha = 60^\circ$ (lower).

The numerical simulation of large uniaxial tests shows the capability of the *JointedRock* model for stress-deformation analysis of the jointed rocks in which the deformations

result from the deformation of rock blocks and the normal and shear displacements of joints.

5.3. Case Study: Bakhtiary Dam and Hydroelectric Project

5.3.1. Site Geology

The Bakhtiary dam and hydroelectric project consists of a 315 m high arch dam and an underground powerhouse with a nominal power generation capacity of 1500 MW after construction. The dam site is located in the Zagros Mountains in southwest Iran (IWPCO 2009).

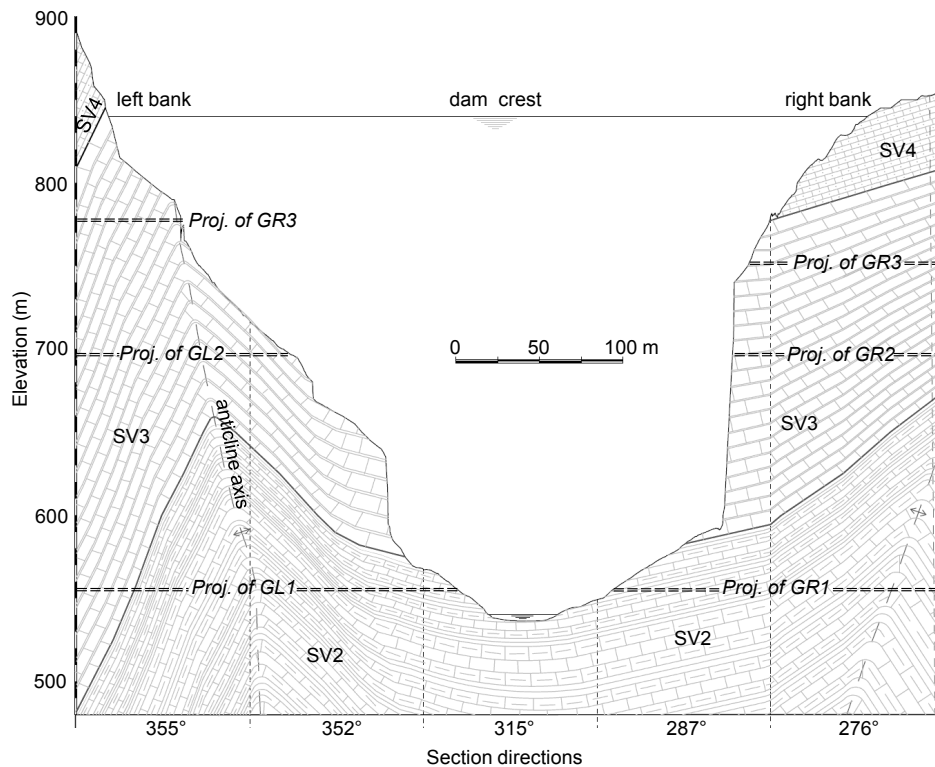


Figure 5.4: Geological section at the dam axis with projection of the test galleries, GL1, GL2 and GL3 on the left abutment and GR1, GR2 and GR2 on the right abutment.

The limestone layers of the Sarvak formation form the main rock at the dam site. The Sarvak formation is composed of seven geological units, namely SV1 to SV7, at the Bakhtiary site. Three of these units, i.e., SV2, SV3 and SV4 outcrop at the dam axis. These units are described as thinly (SV2), medium (SV3) and thickly (SV4) bedded grey limestone. Bedding surfaces and a major joint set J1 are the main discontinuities. The joints intersect the bedding at right angles at most locations. Intense folding of the rock

layers within the core of the Siah Kuh anticline has formed kink band zones that have weaker geomechanical characteristics (Stucky Pars Engineering Co. (SPEC) 2008).

Field assessment of the rock mass quality resulted *RMR* ratings of 48 to 66 and *GSI* of 45 to 66 for the SV2, SV3 and SV4 units. These values reduce to $RMR = 30$ to 55 and $GSI = 35$ to 55 for the intensely folded zones. Results from petite seismic tests yielded average deformation values of $E = 14$ GPa, $E = 7.3$ GPa and $E = 2.7$ GPa for slightly folded layers of SV2, slightly folded layers of SV3 and intensely folded thin layers of SV3, respectively (SPEC 2008).

Figure 5.4 shows the geological section of the dam axis along with projections of the exploratory galleries where PLTs were performed.

5.3.2. Plate Loading Test Results

Thirty-five plate loading tests were performed in six exploratory galleries at the dam axis (Figure 5.4) as a part of a comprehensive site investigation program completed during the study phase of the project. From these tests, 15 successful and well-documented tests were selected for a detailed study of the anisotropic deformability of the rock mass at the dam axis. The details of these tests are included in Appendix 4. Tests with unreliable results and missing discontinuity data and repeated tests were excluded from this study. The tests were performed using a rigid plate test apparatus, in test galleries of nominal dimensions of 2 m wide and high. Three loading plates with diameters of 925 mm, 971 mm and 650 mm were used for the tests. In each test, the maximum load was reached after four consecutive loading-unloading cycles with the peak load being increased at each loading cycle. A further loading-unloading cycle was also run after the fourth loading cycle to assess the stiffening of the rock mass under cyclic loading. At each loading cycle, time-dependent deformability of the rock mass was investigated by maintaining the peak load for a given time interval and measuring the corresponding deformations. The induced deformations in the rock mass were measured with multi-point borehole extensometers, installed in a 76 mm diameter central borehole drilled beneath the plates (Agharazi et al. 2012a).

Agharazi et al. (2012a) categorized the PLTs of the Bakhtiary dam site into five groups based on the direction of loading relative to the orientation of the bedding and a dominant joint set, J1, in each test. The response of the rock mass to loading was investigated through analysis of the stress-deformation curves of the tests in each group. By studying

characteristics of the deformations, i.e. total deformation, irrecoverable deformation, time-dependent deformation, and deformation hysteresis, four main deformation mechanisms namely *JND*, *JSD*, *JSDP*, and *CD* were identified and described. These mechanisms are associated with the dominant deformation component in each test: joint normal displacement (*JND*), joint shear displacement (*JSD*), joint shear displacement with plastic deformation (*JSDP*), and compaction of discrete rock fragments (*CD*) (Agharazi et al. 2012a).

The stress-deformation curves for measured surface displacements showed that the slope of the loading segment of the curves increases over the first three loading cycles and then reach a plateau over the next two loading cycles (Agharazi et al. 2012a). The lower stiffness observed in the first two loading cycles are associated with the rock damages due to blasting and stress relaxation around the test gallery. The deformation moduli calculated based on the first two loading cycles can be considered as the disturbed rock mass deformation modulus. The deformation modulus of the undisturbed rock mass can be determined from the deformations of the 3rd or 4th loading cycles. In this analysis, the surface displacements measured during the 3rd loading cycles (Figure 5.5) were used to determine the rock mass modulus and estimate the joint stiffness.

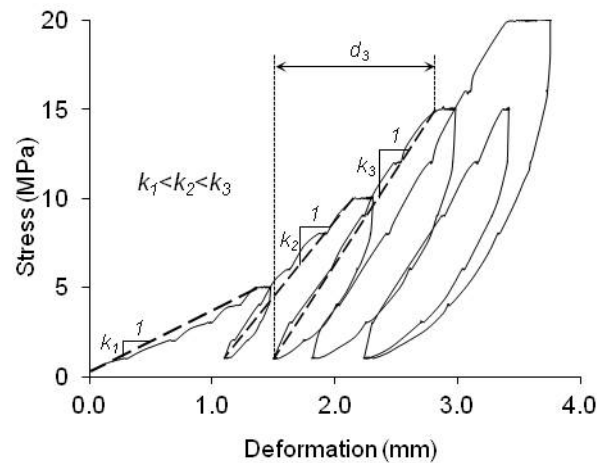


Figure 5.5: Stress-deformation plot of a PLT at the Bakhtiary dam site. The slope of the loading segment of the curves increases over the first three loading cycles.

For each test the deformation modulus of the rock mass was calculated using three methods: the empirical equations, the analytical relation suggested by ISRM (1979) and ASTM (2008) test standards, and the numerical simulation of the tests by *FLAC*^{3D}.

Determination of Deformation Modulus - Empirical Methods

The empirical relationships have been established by the correlation of in-situ test results with the rock mass classification ratings and can be used for the preliminary estimation of the rock mass deformation modulus. In these methods the rock mass is assumed as an isotropic material (Hoek and Diederichs 2006).

The empirical relationships developed by Hoek and Diederichs (2006) and Bieniawski (1978) were used to estimate the rock mass deformation modulus for each test site as follows:

$$E \text{ (GPa)} = 2RMR - 100 \text{ (for } RMR > 50) \quad \text{(Bieniawski 1978)} \quad (5.1)$$

$$E \text{ (GPa)} = 100 \left[\frac{1 - D/2}{1 + e^{\left(\frac{75 + 25D - GSI}{11}\right)}} \right] \quad \text{(Hoek and Diederich 2006)} \quad (5.2)$$

where, RMR is the Rock Mass Rating, GSI is the Geological Strength Index and D is the disturbance factor as defined by Hoek et al. (2002).

For each test, the RMR rating was determined using the joint survey data collected at the test site, the RQD values reported in the extensometer borehole logs, and the results of the uniaxial compressive strength tests on intact rock samples. For the tests with no detailed joint mapping, the test gallery joint mapping was used as a reference. The RQD values were determined from the extensometer borehole logs. The RMR values were calculated using the 1989 version of the Bieniawski rock mass rating method (Hoek 2007) with no adjustment for the orientation of discontinuities. The GSI values were calculated from RMR values as $GSI = RMR_{89} - 5$ (Hoek and Diederichs 2006). The disturbance factor D was assumed zero for all tests. This is consistent with the deformation moduli calculated based on the 3rd loading cycle of the PLTs. The estimated GSI and RMR values along with the corresponding deformation modulus for each test are listed in Table 5.2.

Determination of Deformation Modulus - Analytical Relation

The Boussinesq's equation for the loading of an isotropic, homogeneous, elastic half space medium (Timoshenko 1970) is frequently used for the calculation of the deformation modulus from PLT results, as suggested by the ISRM (1979) and ASTM (ASTM Standard D4394-08, 2008) test standards. For surface displacements under a

theoretically rigid circular loading plate of radius a , this relationship can be written as follows (Agharazi et al. 2012; ASTM 2008):

$$E = \frac{\pi a(1-\nu^2)}{2w} q \quad (5.3)$$

where w is displacement beneath the loading plate, q is average stress beneath the plate, E is deformation modulus and ν is the Poisson's ratio. In this equation, the influence of the central borehole is ignored. The Poisson's ratio was taken as $\nu = 0.2$ determined from the uniaxial test results on the core samples taken at the site (SPEC 2008). The influence of Poisson's ratio on the moduli calculated by Equation (5.3) is very limited and for a possible range of $\nu = 0.1$ to 0.3 the maximum variation of modulus is 8%. The secant deformation moduli calculated based on the deformations of the 3rd loading cycle of the tests are listed in Table 5.2.

Determination of Deformation Modulus –FLAC^{3D}- Elastic Model

Three *FLAC^{3D}* models corresponding to the three loading plate diameters were constructed as shown in Figure 5.6. The models include one side of a plate loading test in a test gallery of 2×2 m. The extensometer borehole with a diameter of 76 mm was also included in the model. The confining effect of the test gallery was taken into account by fixing the z-displacements at the top of the model. In all models, the built-in *Elastic* constitutive model was assigned to the rock mass. This provides an isotropic elastic behaviour for the rock mass which is consistent with the fundamental assumptions taken in the analytical relationship of Boussinesq.

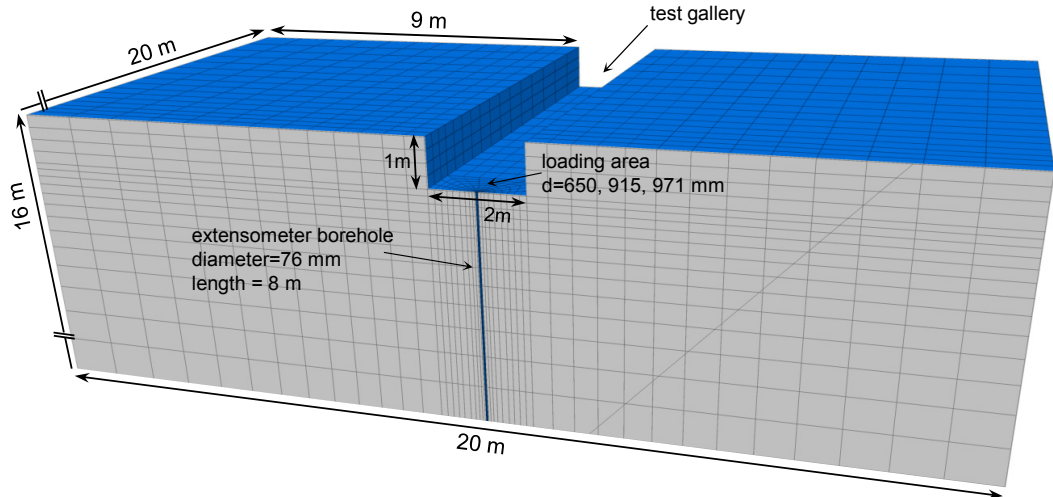


Figure 5.6: Numerical model of PLT ($FLAC^{3D}$). The model was cut in half by a vertical plane crossing the centre of the loading plate. Just upper part of the model is shown. Vertical displacements were fixed at the top of the model (excluding the inside of the gallery) to simulate the confining effect of the gallery.

Table 5.2: RMR and GSI and modulus of deformation for PLTs.

Test	Rock Unit	RMR	GSI	Modulus of Deformation (GPa)					
				Empirical Methods		Analytical Solution		$FLAC^{3D}$ - Elastic	
				B*	H-D**	Left/Up***	Right/Down	Left/Up	Right/Down
PLV1L1	SV3	68	63	36	25	17.6	26.4	13.9	20.9
PLH1L1	SV3	68	63	36	25	9.9	9.2	7.7	7.3
PLV2L1	SV3	55	50	10	9	21.5	--	16.8	--
PLH2L1	SV3	55	50	10	9	12.6	10.7	9.9	8.4
PLV3L1	SV3	65	60	30	20	13.7	21.6	10.8	17.0
PLH3L1	SV3-Kink Band Zone	67	62	34	23	--	7.2	--	5.5
PLV1R1	SV2-Kink Band zone	69	64	38	27	10.6	18.1	8.4	14.4
PLH1R1	SV2-Kink Band Zone	62	57	24	16	18.7	--	14.9	--
PLV2R1	SV2 Kink Band Zone	69	64	38	27	14.9	14.2	11.7	11.1
PLH2R1	SV2-Kink Band zone	65	60	30	20	28.1	25.9	21.9	20.4
PLV1R2	SV3	65	60	30	20	10.1	9.6	7.9	7.5
PLH1R2	SV3	66	61	32	22	8.6	--	6.8	--
PLV3R2	SV3 Kink Band zone	66	61	20	14	6.7	7.4	5.3	5.8
PLH2L2	SV4	58	53	16	12	--	9.3	--	6.9
PLV2L2	SV4	58	53	16	12	16.2	17.5	12.9	13.7

* Bieniawski Relationship $E=2RMR-100$

** Simplified Hoek and Diederichs Relationship $E = 100[(1-D)/2]/(1+e^{(75+25D-GSI)/11})$ ($D = 0$)

*** Left/Right and Up/Down refer to loading plate direction for horizontal and vertical tests, respectively

An average stiff circular stress of $q = 14$ MPa, corresponding to the applied pressure interval over the 3rd loading cycle of the tests (1-15 MPa), was applied to the models. The loading was provided by applying a fixed velocity boundary condition over a circular area corresponding to the loading plates in each model. The fixed velocity boundary condition was kept for a given number of calculation steps until the average test load was

reached. A Poisson's ratio of $\nu = 0.2$ was assigned to the rock mass. By running the models for a range of deformation moduli, deformation versus modulus plots were constructed for the three loading plate diameters used for the tests (Figure 5.7). A deformation modulus range of $E = 2$ to 25 GPa was selected so the calculated deformations by the models cover the full range of deformations measured during the plate loading tests. Using these plots, a first estimation of the equivalent deformation moduli were obtained for each test, based on the measured deformations at the site. The determined moduli were then refined by back calculation of the exact deformations for each test. Similar to the analytical method, the surface deformations measured during the 3rd loading cycles were used for the calculation of moduli. The results are listed in Table 5.2.

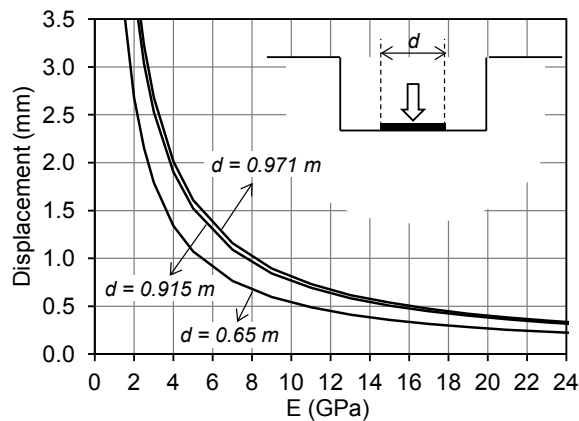


Figure 5.7: Displacement versus deformation moduli plots calculated by the numerical models of the tests.

Comparison of the Results

The maximum, minimum and average deformation modulus values calculated using different methods are listed in Table 5.3. As observed from Table 5.2 and Table 5.3, the range of variation of the calculated moduli is relatively high for all methods with the maximum modulus being almost as high as four times of the minimum modulus. The moduli estimated by the empirical methods fall in a range of $E = 9$ to 38 GPa. The range of variation for the moduli calculated using the analytical method is $E = 6.8$ to 28.6 GPa and for the moduli calculated from the $FLAC^{3D}$ model is $E = 5.2$ to 22 GPa. A considerable scatter also exists in the calculated moduli. Given the main variable in these tests is the direction of loading relative to the orientation of discontinuities, the high range

of variation and the scatter in the results can be attributed to the influence of discontinuities on the test results.

Table 5.3: Maximum, minimum and average deformation moduli calculated using different methods.

	Deformation Modulus (GPa)			
	Empirical Methods		Analytical Solution	<i>FLAC^{3D}</i> Model
	B	H-D		
Minimum	10.0	9.0	6.7	5.1
Average	26.7	18.7	14.7	11.5
Maximum	38.0	27.0	28.1	21.9
Standard Deviation	9.9	6.3	6.3	5.0

As shown in Figure 5.8, the moduli calculated using the analytical method and the *FLAC^{3D}* models show a poor correlation with the empirical relations. The anisotropy of the rock mass deformability is a major factor contributing to this inconsistency.

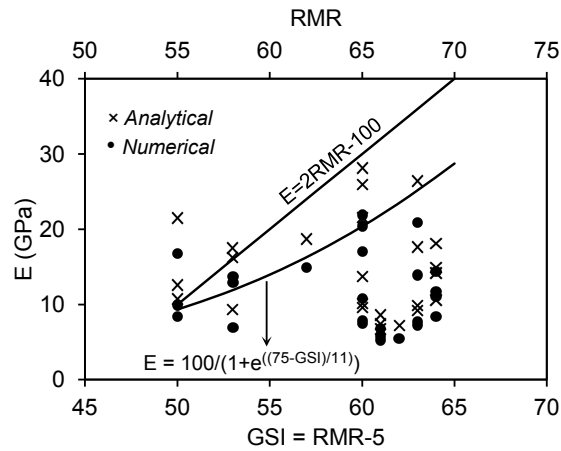


Figure 5.8: Comparison of moduli calculated using the analytical and numerical methods with the empirical relationships.

The calculated moduli using the analytical method show a linear correlation with the moduli determined from the *FLAC^{3D}*- *Elastic* models as shown in Figure 5.9. The confining effect of the test gallery on the test results causes a systematic error in the moduli calculated using the analytical relation (5.3) (Agharazi et al. 2008). This problem is addressed in the *FLAC^{3D}*- *Elastic* models by incorporating the real geometry of the test gallery and applying appropriate boundary conditions. The comparison of the results show that a correction factor of 0.79 is required to compensate for the effect of the test gallery geometry on the moduli calculated using Equation (5.3).

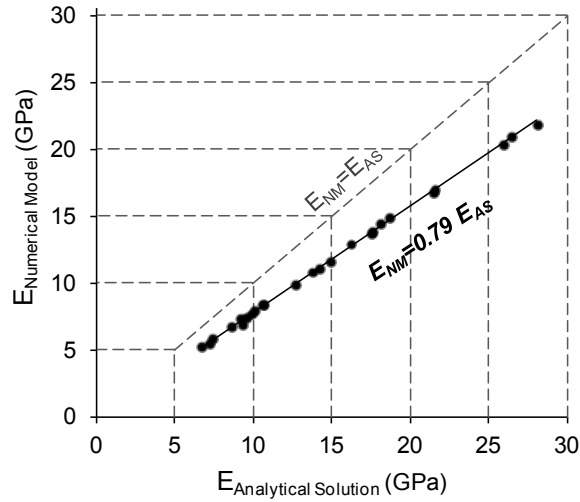


Figure 5.9: Correlation of the moduli calculated using the numerical method with those by the analytical relation.

While the joint parameters, such as spacing, stiffness and orientation, have a dominant influence on the deformability of the rock mass, and thus on the calculated moduli, none of the applied methods can directly take them into account for the interpretation of the test results. The equivalent moduli calculated using the *FLAC^{3D} - Elastic* models are only valid for joint configurations that are similar to those tested rocks and cannot be extrapolated to rock masses with different joint spacing or joint orientation.

In the next section, the *JointedRock* model is used as the constitutive model of the rock mass in *FLAC^{3D}* simulations of the tests. By using this model, the spacing, stiffness, and orientation of the discontinuities are directly incorporated into the test result interpretation.

5.4. Numerical Interpretation of the Plate Loading Test Results Using the *JointedRock* Model

5.4.1. Rock Mass Deformation Parameters

The deformability of the rock mass is defined as a function of:

- deformability of the rock blocks defined by Young modulus and Poisson's ratio,
- deformability of the bedding and J1, defined by their normal and shear stiffness,
- spatial configuration of the bedding and J1, defined by their spacing, dip, and dip direction in the model.

Rock block deformability: The rock blocks are formed by intersection of the bedding surfaces and J1. The blocks are assumed to contain some minor random joints. The block deformability was assumed isotropic and was estimated using Hoek and Diederichs empirical equation (Hoek and Diederichs 2006). After ignoring the influence of the bedding and J1, the rock block deformation modulus, E_m , is taken as:

$$E_m = E_i \left[0.02 + \frac{1-D/2}{1+e^{((60+15D-GSI)/11)}} \right] \quad (5.4)$$

where E_i is intact rock deformation modulus. Since the analyses were done using the deformations measured during the 3rd loading cycle of the tests, the disturbance factor, D , was taken as zero. The average intact rock deformation modulus was estimated as $E_i = 65$ GPa from the unconfined compressive tests on intact rock samples (Agharazi et al. 2012a). By ignoring the bedding and J1 in the rock mass, a GSI value of 65 was selected that represents a massive rock with widely spaced non-persistent random joints (Hoek 2007). The deformation modulus of the rock blocks was calculated as $E_m = 43.5$ GPa using Equation (5.4).

Deformability of Discontinuities: Since no test results were available on the mechanical properties of the joints, the normal stiffness of J1, k_{nj} , was assumed to be proportional to the normal stiffness of the bedding, k_{nb} . Based on a joint survey conducted in the exploratory galleries (SPEC 2008), the bedding and J1 have an aperture of 0.1 to 1 mm (90% of surveyed cases) with the infilling being clay (43% of cases) or calcite (46% cases) for the bedding, and calcite (68% of cases) or no infilling (22% of cases) for J1 (Agharazi et al. 2012a). On this basis, the normal stiffness of J1 was taken to be 1.25 times stiffer than that of the bedding ($k_{nj} = 1.25 k_{nb}$).

The bedding is described as mainly planar with rough (17% of cases), smooth (23% of cases) and slickenside (60% of cases) surfaces. J1 is described as planar with smooth (48% of cases) and rough (48% of cases) surfaces (Agharazi et al. 2012a). Given the small aperture of the bedding and J1, a shear stiffness of 75% the normal stiffness was assumed for both discontinuities. This assumption results in a 25% higher shear stiffness for J1 which is consistent with the high proportion of rough and unfilled surfaces reported for J1 as opposed to the high population of slickenside and clay-filled surfaces for the bedding ($k_{sj} = 1.25 k_{sb}$).

Spatial configuration of discontinuities: The selected plate loading tests were divided into two groups based on the direction of loading relative to the orientation of the bedding and J1. The first group includes eight tests with loading direction parallel to the bedding but with an angle of β with respect to J1. The second group includes seven tests with the loading direction intersecting both the bedding and J1 at an angle of α and $90-\alpha$, respectively as depicted in Figure 5.10.

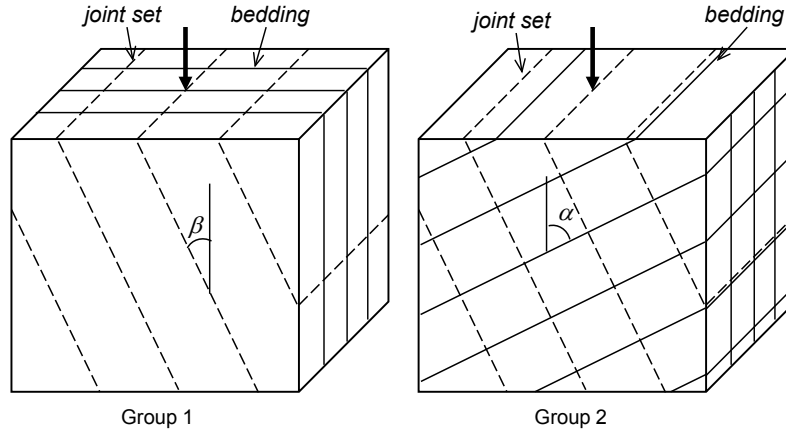


Figure 5.10: Loading direction and the orientation of discontinuities in two test groups

For each test, the detailed joint data, i.e. the orientation and spacing of the bedding and J1 were extracted from the extensometer borehole logs and the joint mapping of the test surfaces. These data were used for the construction of the numerical model of each test. For the tests in the first group, the average spacing of the bedding and J1 was determined as $S_{b1} = 0.27$ m and $S_{j1} = 0.37$ m, respectively. For the tests in the second group, the average spacing of bedding and J1 was determined as $S_{b2} = 0.24$ m and $S_{j2} = 0.4$ m, respectively. For both groups, the range of spacing for the bedding was 0.15 to 0.35 m and for the joints it was 0.3 to 0.45 m.

5.4.2. Back Calculation of Joint Stiffness from the Test Results

Similar *FLAC^{3D}* models, as in the previous section, were used for this analysis with the *Elastic* model being replaced with the *JointedRock* model. This allows the joint-dependent anisotropy of the rock mass to be incorporated into the analysis. The bedding and J1 were added implicitly to the model using dip, dip direction and spacing values determined for each test. The deformation modulus of $E_m = 43.5$ GPa, as calculated by Equation 4, was assigned to the rock blocks. The Poisson's ratio was taken to be $\nu = 0.2$, similar to the previous analyses. An average stiff load of $q = 14$ MPa, corresponding to

the load interval of the 3rd loading cycle of the tests (1-15 MPa), was applied to the models as the test load. Using this model the normal stiffness of the bedding was back calculated based on the surface displacements measured during the 3rd loading cycle, for each test. Plastic deformations were prevented in the models by setting the built-in plasticity switch off for both the discontinuities and the intact rock (Agharazi et al. 2012b). Table 5.4 shows the estimated average shear and normal stiffness values from the PLT results.

Table 5.4: Average normal and shear stiffness values back-calculated from PLT results using *FLAC^{3D}-JointedRock* model

	Stiffness (GPa/mm)			
	k_{nb}	k_{sb}	k_{nj}	k_{sj}
Minimum	14	-	-	-
Average	37.5	28.1	46.9	35.2
Maximum	59	-	-	-
Standard Deviation	16	-	-	-

5.4.3. Determination of the Anisotropic Deformation Modulus of the Rock Mass

A hypothetical model of the plate loading test was constructed using *FLAC^{3D}* with the *JointedRock* model being the constitutive model of the rock mass. The same geometry, boundary conditions and test load ($q = 14$ MPa) were applied to the model as in the previous analyses (Figure 5.6). The rock blocks were assigned a deformation modulus of $E_m = 43.5$ GPa and a Poisson's ratio of $\nu = 0.2$. The bedding and J1 were implicitly added to the model using the measured average spacing values of $S_{b1} = 0.27$ m and $S_{j1} = 0.37$ m for the first group and $S_{b2} = 0.24$ m and $S_{j2} = 0.4$ m for the second group.

The estimated normal and shear stiffness of the discontinuities were used as input in the hypothetical *FLAC^{3D}-JointedRock* model to calculate the rock deformations for a full range of loading direction (α and $\beta = 0 - 90^\circ$) for both groups. Figure 5.11 shows the deformation versus joint angle plots calculated with the hypothetical *FLAC^{3D}-JointedRock* model. The deformations from the PLTs are also depicted on the figure.

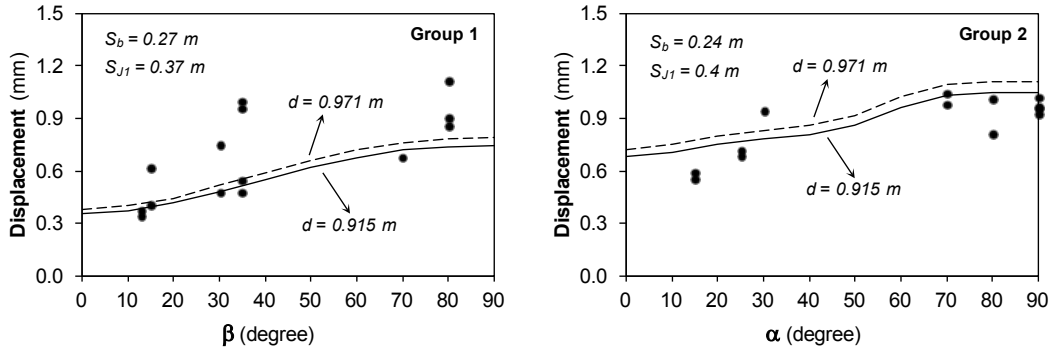


Figure 5.11: Deformation versus joint angle determined by the hypothetical PLT models, for plate diameters of $d = 915$ mm and $d = 971$ mm. The *JointedRock* model was used as the constitutive model. The estimated average normal and shear stiffness from PLT results were used in the model. The measured PLT deformations are depicted by solid circles.

The deformations calculated with the hypothetical *FLAC^{3D}-JointedRock* models were then used to determine the equivalent anisotropic deformation modulus of the rock mass using the deformation versus modulus plots shown in Figure 5.7. Plots of deformation modulus versus joint angle are shown in Figure 5.12. The back-calculated moduli from the PLT results are also shown on the figure.

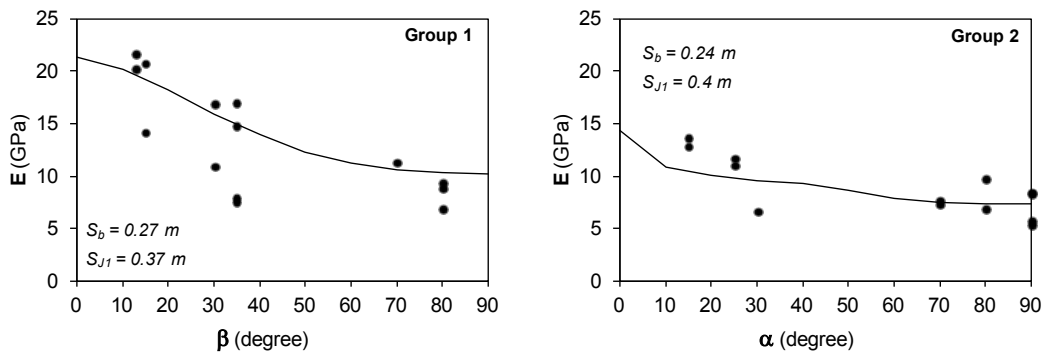


Figure 5.12: Anisotropic equivalent deformation modulus for the rock mass based on the calculated deformations using the hypothetical *FLAC^{3D}-JointedRock* models. The back-calculated moduli from the PLT results are depicted by solid circles.

The plot of calculated anisotropic deformation modulus matches well the back-calculated moduli from the plate loading tests. It should be noted that the anisotropic deformation moduli were calculated for the average bedding and joint spacing. Figure 5.12 shows that the observed trend in the calculated moduli from the PLT results can be related to the anisotropy of the rock deformation. Based on this analysis, the maximum to minimum moduli ratios of $E_{max}/E_{min} = 2.09$ and $E_{max}/E_{min} = 1.97$ were calculated for the first and second test groups, respectively. The overall ratio was estimated as $E_{max}/E_{min} = 2.92$ for the rock mass.

5.5. Conclusion

The results from fifteen plate loading tests carried out at the Bakhtiary dam site were analyzed. The deformation moduli were calculated using three different methods: the empirical equations by Bieniawski (1978) and Hoek & Diederichs (2006), the analytical relation suggested by ASTM and ISRM, and the back calculation of the test results by numerical simulation of the tests (*FLAC^{3D}-Elastic*). The moduli estimated from the empirical methods did not show a good agreement with the moduli determined by the two other methods. It was shown that the suggested analytical relationship by ISRM and ASTM test standards tend to overestimate the deformation moduli due to the confining effect of test gallery. A correction factor of $k = 0.79$ was determined for the moduli calculated using the analytical relationship.

The scatter in the calculated moduli was attributed to the influence of discontinuities on the test results. An equivalent continuum model, *JointedRock*, was used to incorporate the influence of discontinuities in the interpretation of the test results. By applying the *JointedRock* model as the constitutive model in the numerical simulations, the normal and shear stiffness of the bedding and the major joint set J1 were back calculated from the plate loading test results. The estimated average joint stiffness values were then used in hypothetical numerical models of the plate loading tests in which the *JointedRock* model was applied as the constitutive model of rock mass. The hypothetical test model was run for a full range of loading directions relative to the orientation of discontinuities and the corresponding deformations were calculated. From these deformations, the anisotropic deformation modulus of the rock mass was back calculated. The anisotropic deformation modulus showed a good agreement with the back calculated moduli from the plate loading test results. It was shown that the scatter in the test results can be addressed by taking into account the anisotropy of rock mass deformability using an appropriate interpretation method. A general anisotropy ratio of $E_{max}/E_{min} = 2.9$ was calculated for the rock mass deformation modulus.

5.6. References

- Agharazi, A., Martin, C. D., Tannant, D. D. (2012). A three-dimensional equivalent continuum constitutive model for jointed rock masses containing up to three random joint sets. *Geomechanics and Geoengineering: An International Journal*, 7(4), 227-238.
- Agharazi, A., Tannant, D. D., Martin, C. D. (2012). Characterizing rock mass deformation mechanisms during plate loading tests at the Bakhtiary dam project. *International Journal of Rock Mechanics and Mining Sciences*, 49, 1-11.
- Agharazi, A., Tannant, D., Jafari, A. (2008). Stress and tunnel geometry effects on deformation modulus derived from plate load tests. *Proceedings of 61st Canadian Geotechnical Conference & 9th Joint CGS/IAH-CNC Groundwater*, Edmonton, volume 1, pages 601-608. Bi-Tech Publishers Ltd., Richmond.
- ASTM Standard D4394-08. (2008 August). Standard test method for determining in situ modulus of deformation of rock mass using rigid plate loading method. West Conshohocken, PA, USA: ASTM International. doi:10.1520/D4394-08
- Bieniawski, Z. (1978). Determining rock mass deformability: Experience from case histories. *International Journal of Rock Mechanics and Mining Sciences & Geomechanics Abstracts*, 15, 237-247.
- Boyle, W. (1992). Interpretation of plate loading test data. *International Journal of Rock Mechanics and Mining Sciences*, 29, 133-141.
- Hoek, E. (2007). *Practical Rock Engineering*. Retrieved May 31, 2013, from http://www.rocksience.com/education/hoek_corner
- Hoek, E., Diederichs, M. (2006). Empirical estimation of rock mass modulus. *International Journal of Rock Mechanics and Mining Sciences*, 43, 203-215.
- Hoek, E., Carranza-Torres, C., Corkum, B. (2002). Hoek - Brown failure criterion: 2002 edition. *Proceedings of the 5th North American Rock Mechanics Symposium and 17 The Tunnelling Association of Canada Conference: NARMS-TAC*, Toronto, volume 1, pp. 267-273.
- Iran Water and Power Resources Company (IWPCO). (n.d.). Bakhtiary Project: IWPCO web site. Retrieved 11 01, 2009, from IWPCO web site: <http://en.iwpcoco.ir/Bakhtiari>
- ISRM. (1979). Suggested method for determination of insitu deformability of rock. *International Journal of Rock Mechanics and Mining Sciences* (16), 143-146.
- Palmstrom, A., Singh, R. (2001). The deformation modulus of rock masses - comparisons

between in situ tests and indirect estimates. *Tunnelling and Underground Space Technology*, 16, 115-131.

Stucky Pars Engineering Co. (2008). *Engineering Geology and Rock Mechanics Report - Site investigation Phase I & II*. Tehran.

Timoshenko, S., Goodier, J. (1970). *Theory of Elasticity* (3rd ed.). McGraw-Hill.

Chapter 6

Conclusion

This research was focused on the characterization of the mechanisms of deformation in systematically jointed rock masses and the development of an equivalent continuum model to simulate such deformations. The results of a series of plate loading tests, conducted at the Bakhtiary dam site on a jointed rock mass, were thoroughly analyzed to determine the main deformation mechanisms mobilized during the tests. An equivalent continuum model, the *JointedRock* model, was formulated for deformation analysis of a rock mass containing up to three randomly oriented persistent joint sets. The *JointedRock* model was used for interpretation of the Bakhtiary dam plate loading test results and determination of the anisotropic deformation modulus of the rock mass.

The research was structured into three main sections: a) study of the dominant deformation mechanisms in a jointed rock mass by analysis of the Bakhtiary dam site plate loading test results, b) development of the constitutive relations for the *JointedRock* model and implementation of the model in *FLAC^{3D}*, and c) interpretation of the Bakhtiary plate loading test results using the *JointedRock* model.

The detailed analysis of the stress-deformation behaviour of the rock mass during the plate loading tests showed that the rock mass deformability depends primarily on the rock structure. In a fractured rock mass formed by the intersection of randomly oriented joints, the main deformation mechanism is compaction of rock blocks. Deformability of the rock mass under this mechanism is potentially isotropic and can be linear or non-linear depending on the properties of both the intact rock and fractures. For a systematically jointed rock mass, however, rock mass deformation is mainly governed by the deformation of primary joints. For such rock masses, deformability is highly anisotropic and depends on the direction of loading relative to the orientation of discontinuities. Deformation can be linear or non-linear depending on mechanical properties of the primary joints. Four main deformation mechanisms were identified, corresponding to two different joint structures and two loading configurations. For a systematically jointed rock mass, depending on the loading configuration, the mobilized deformation mechanism is prevailed upon by either normal displacement or shear

displacement along the primary joints. Total deformation during a full loading-unloading cycle, deformations under constant load, and the shape of the stress-deformation curves depend on the mobilized deformation mechanism during a given test. This forms the main source of scatter in plate loading test results for a given rock mass.

The explicit definition of discontinuities using discontinuum models is associated with two major problems: the dependency of numerical discretization on the spacing and orientation of discontinuities, and the necessity of detailed data on the geometry of discontinuities to be modeled. This restricts the applicability of the discontinuum models to problems with the limited number of widely spaced discontinuities with well-defined geometry parameters. The *JointedRock* model was introduced as an alternative to the discontinuum models to analyze the deformation and strength of jointed rock masses with tightly spaced persistent joint sets. The main advantages of the model are:

- It relies on a solid theoretical basis, i.e., the principles of classical continuum mechanics. No empirical factor was incorporated in the formulations of the model.
- The numerical discretization is independent of the geometry of discontinuities. As a result, large problems with small spacing joint sets can be efficiently modeled.
- No restriction applies to the orientation and spacing of joint sets to be modeled. Joint sets can take any arbitrary orientation and spacing.
- The model addresses both deformability and strength anisotropy.

The model was implemented in *FLAC^{3D}* as a constitutive model. Several example simulations were run using the *JointedRock* model and the discrete element method (*3DEC*). The comparison of the results showed that the model performs well as long as the applied boundary conditions are consistent with theoretical assumptions embedded in the model. A fundamental assumption in the model is the continuity of deformation. This limits the application of the model to problems in which the rigid body motion of rock blocks is not a component of total deformations. The *JointedRock* model results were also compared with some closed form solutions where available. Further verification of the model can be done by comparison of the model results with the results obtained from experimental studies on the deformation of jointed materials.

The model adopts an elastic-perfect plastic behaviour for both intact rock blocks and discontinuities. Upon a stress increment, the model checks for the possibility of failure through intact rock and one discontinuity surface. Compared to other equivalent continuum plasticity models, such as the Ubiquitous joint model, the *JointedRock* model is advantageous in that it considers both elastic and plastic anisotropy, so the true elastic stress distribution is calculated before the violation of failure criterion is checked.

The model takes no account of the bending stiffness of rock layers. This theoretically gives rise to the underestimation of the equivalent continuum stiffness for a layered rock mass. However, it should be noted that geomaterials, such as sedimentary rock layers, rarely carry significant bending moment mainly due to the existence of micro or macro scale discontinuities. The model also does not account for the rotation of anisotropy orientation during large deformations. Extra care should be considered when applying the model to problems in which rock mass undergoes large deformations, particularly plastic deformations.

The analysis of the results of the plate loading tests conducted at the Bakhtiary dam project showed that the ISRM suggested relationship overestimates the rock mass deformation modulus, because it disregards the constraining effect of the test gallery geometry on the test results. The method is also unable to address directly the effect of joint parameters on the rock mass deformability. Some of the observed scatter in the test results was attributed to anisotropy of the rock mass deformability and the variation of discontinuity geometrical parameters, i.e., spacing and orientation. A new method, based on the numerical simulation of the tests, was introduced to address these issues in the interpretation of the plate loading test results. The *JointedRock* model was used to back calculate the stiffness of the bedding planes from the test results. The rock mass deformation moduli were then determined for all directions relative to the orientation of the bedding planes and the joint set J1. There are several advantages to the proposed interpretation methodology:

- The rock mass deformability is determined as a function of the discontinuities mechanical and geometrical parameters.
- Rock mass deformability can be determined for any direction from the available test results for some given directions. This significantly reduces the number of required tests for a jointed rock mass.

- The results of other tests, such as large scale in-situ direct shear test and dilatometer test, can be used in combination with plate loading test results to improve the accuracy of the deformation parameters determined for a jointed rock mass.
- The constraining effect of the test gallery on the test results is taken into account.

The empirical relationships used to estimate the deformation modulus of the rock mass at the Bakhtiary dam site were shown to result in non-representative values. Further works can be done on this subject to establish a new empirical relationship that incorporates the spatial and mechanical parameters of discontinuities in the formulation. Numerical simulations using the *JointedRock* model as the constitutive model can be used for this purpose.

The *JointedRock* model is also of particular interest for the settlement and bearing capacity analysis of dam foundations on jointed sedimentary deposits. In these cases, rock mass deformability and strength are potentially anisotropic and depend on the characteristics and orientation of discontinuities. However, the spacing of joints is usually too small, compared to the size of a dam foundation, so the explicit definition of the joints is impractical. Using the *JointedRock* model, the deformability and strength of the foundation rock mass can be directly related to the rock joint properties.

The model can also be used in hybrid models for implicit modelling of far field joints, while the joints close to the study area are defined explicitly using discrete element methods. This results in a significant reduction in model size when the influence of far-field joints needs to be taken into account.

Appendix 1

***JointedRock* model: $FLAC^{3D}$ keywords**

The “*JointedRock*” model can be loaded in $FLAC^{3D}$ using the following commands:

config *cppudm*

load *model* *modeljointed005_64* (for $FLAC^{3D}$ version 5.0)

model *jointedrock*

Further instructions on loading of a user defined constitutive model in $FLAC^{3D}$ can be found in the code user's guide (Itasca 2012). A list of model specific keywords follows:

Model general keywords:

Nj: Defines the number of joint sets in a model - can vary from 0 to 3. By default *Nj*= 0.

rPlas: Disables/enables the failure check and plastic stress correction algorithm for intact rock (*rPlas*=0 disables failure check and *rPlas*=1 enables it). By default *rPlas*=0 or disabled

jPlas: Disables/enables the failure check and plastic stress correction algorithm for joint set (*jPlas*=0 disables failure check and *jPlas*=1 enables it). By default *jPlas*=0 or disabled.

Intact Rock

Bulk: bulk modulus of deformation (Pa)

Shear: shear modulus of deformation (Pa)

Cohesion: cohesion (Pa)

Friction: friction angle (degree)

Tension: tensile strength (Pa)

Dilation: dilation angle (degree)

Joint Set 1:

<i>Dip1:</i>	<i>dip angle of joint set 1 measured from horizontal (degree)</i>
<i>DD1:</i>	<i>dip direction of joint set 1 measured from north clockwise (degree)</i>
<i>Spac1:</i>	<i>spacing of joint set 1 (m)</i>
<i>Kss1:</i>	<i>shear stiffness of joint set 1 in dip direction (Pa/m)</i>
<i>Ktt1:</i>	<i>shear stiffness of joint set 1 in strike direction (Pa/m)</i>
<i>Knn1:</i>	<i>normal stiffness of joint set 1 (Pa/m)</i>
<i>jCohesion:</i>	<i>cohesion of joint set 1 (Pa)</i>
<i>jFriction:</i>	<i>friction angle of joint set 1 (degree)</i>
<i>jTension:</i>	<i>tensile strength of joint set 1 (Pa)</i>
<i>jDialation:</i>	<i>dilation angle of joint set 1 (degree)</i>

Join set 2:

<i>Dip2:</i>	<i>dip angle of joint set 2 measured from horizontal (degree)</i>
<i>DD2:</i>	<i>dip direction of joint set 2 measured from north clockwise (degree)</i>
<i>Spac2:</i>	<i>spacing of joint set 2 (m)</i>
<i>Kss2:</i>	<i>shear stiffness of joint set 2 in dip direction (Pa/m)</i>
<i>Ktt2:</i>	<i>shear stiffness of joint set 2 in strike direction (Pa/m)</i>
<i>Knn2:</i>	<i>normal stiffness of joint set 2 (Pa/m)</i>

Join set 3:

<i>Dip3:</i>	<i>dip angle of joint set 3 measured from horizontal (degree)</i>
<i>DD3:</i>	<i>dip direction of joint set 3 measured from north clockwise (degree)</i>
<i>Spac3:</i>	<i>spacing of joint set 3 (m)</i>
<i>Kss3:</i>	<i>shear stiffness of joint set 3 in dip direction (Pa/m)</i>
<i>Ktt3:</i>	<i>shear stiffness of joint set 3 in strike direction (Pa/m)</i>
<i>Knn3:</i>	<i>normal stiffness of joint set 3 (Pa/m)</i>

Reference

Itasca Consulting Group, Inc. (2012). FLAC^{3D}; User's Guide. Minneapolis: Itasca Consulting Group, Inc.

Appendix 2

Effect of boundary conditions and the bending stiffness of intact rock layers on simulations using the *JointedRock* model

The influence of boundary conditions on the *JointedRock* model is investigated by simulating a uni-axial loading test on a jointed rock cylinder that is $l = 1$ m in length and $d = 0.5$ m in diameter (Figure 1). A stiff load of $p = 15$ MPa is applied to the top of the cylinder, while the bottom is fixed. Each test is simulated by two methods: the continuum method using *FLAC^{3D}* and the discontinuum model using *3DEC*. The simulations are repeated for various discontinuity orientations relative to the axis of the cylinder. In the *FLAC^{3D}* models, the *JointedRock* model is used to simulate the joints implicitly. To investigate the influence of boundary conditions on the simulations, all tests are run for two boundary conditions: confined and unconfined.

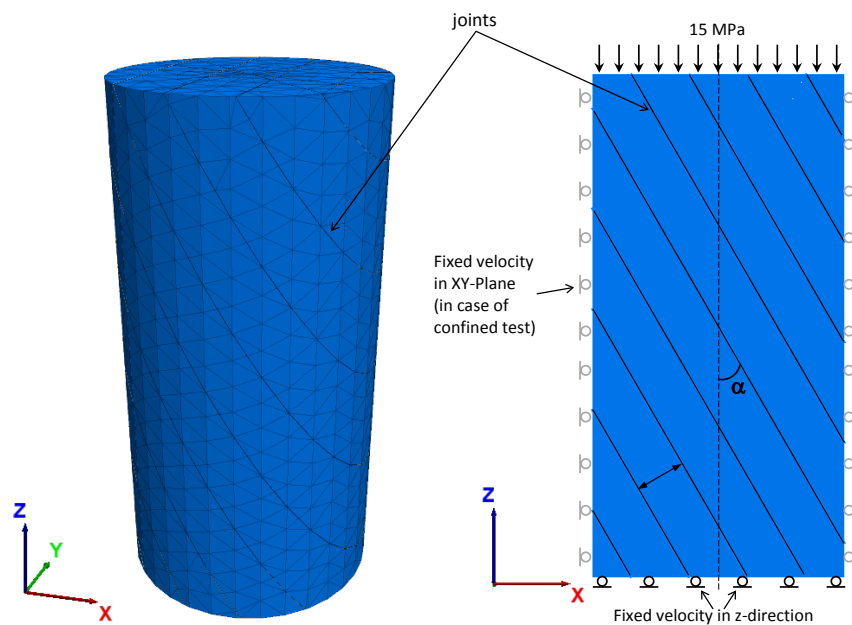


Figure 1: Geometry and boundary conditions for the uni-axial test on a jointed rock cylinder

In this study, just the elastic stresses and deformations are considered. The yielding of the rock is prevented in all simulations. This is done by setting the plasticity switches off in the *FLAC^{3D}* models and by applying an elastic model in the *3DEC* models. One can refer to Appendix 1 for a list of the *JointedModel* specific keywords in *FLAC^{3D}*.

Two series of simulations are run: one includes a single joint set and the other includes two perpendicular joint sets. For the sake of simplicity, the spacing and mechanical properties of the joint sets are kept identical in all simulations. Table 1 shows the mechanical and physical properties of the intact rock and the rock joints. The simulations are run for various joint angles ranging from $\alpha = 0^\circ$ to $\alpha = 90^\circ$, with respect to the cylinder axis. Figure 2 and Figure 3 show the axial deformation versus joint angle plots for the simulations.

Table 1: Mechanical parameters of intact rock and rock joints in simulations

parameter	intact rock	joint set 1	joint set 2
bulk modulus (GPa)	44	--	--
shear modulus (GPa)	26.4	--	--
normal stiffness (GPa/m)	--	13.9	13.9
shear stiffness (GPa/m)	--	6.95	6.95
spacing (m)	--	0.1	0.1

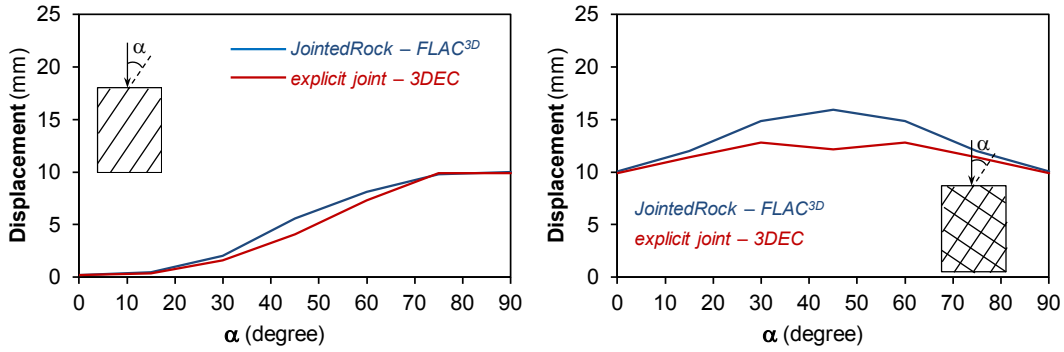


Figure 2: Axial deformation versus joint angle plots for confined uni-axial loading of the rock cylinder. Left: one joint set; right: two perpendicular joint sets.

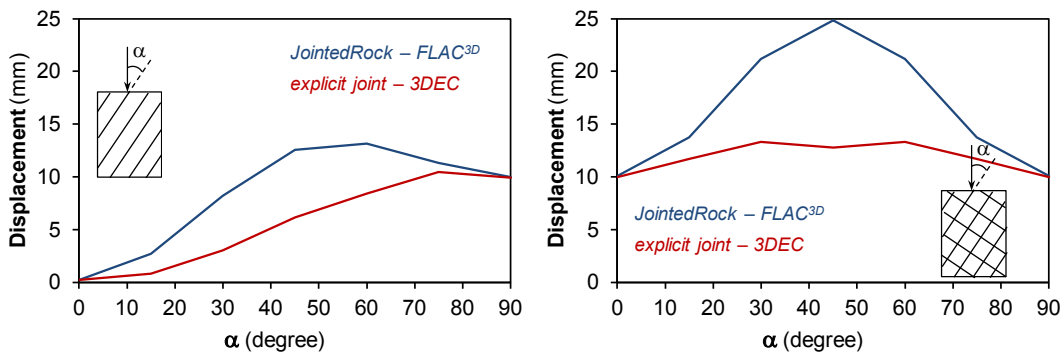


Figure 3: Axial deformation versus joint angle plots for unconfined uni-axial loading of the rock cylinder. Left: one joint set; right: two perpendicular joint sets.

The factors contributing to the observed difference in the simulation results are:

- The bending stiffness of the intact rock layers in the 3DEC models
- The boundary condition effect

Bending stiffness of intact rock layers

In the discontinuum models, the deformation of the cylinder is accompanied by the rotation of rock layers/blocks. In the case of the unconfined cylinder with one joint set, the free rotation of intact rock layers is restricted by the fixed z-velocity boundary condition applied to the top and bottom of the cylinder. This configuration leads to the bending of intact rock layers, as depicted in Figure 4. The bending of rock layers is resisted by their bending stiffness (k_b), which is a function of the elastic modulus (E) of intact rock and the second moment of area of the layers' cross section (I):

$$k_b = EI$$

The second moment of area is a function of the spacing of the rock layers (s) to the power of three, through the following relationship:

$$I = \frac{bs^3}{12}$$

where b is the length of the layers' cross section.

The decrease of the joint spacing reduces the bending stiffness of rock layers, so the results from both models merge together (Figure 5). In the confined tests, the applied lateral fixity restricts the bending of the rock layers, thereby significantly reducing the influence of bending stiffness on the model results. Figure 6 and Figure 7 show the maximum principal stress distribution and the axial displacement contours for confined tests with one and two joint sets, respectively. The results from the *JointedRock* models and *3DEC* models show a good agreement.

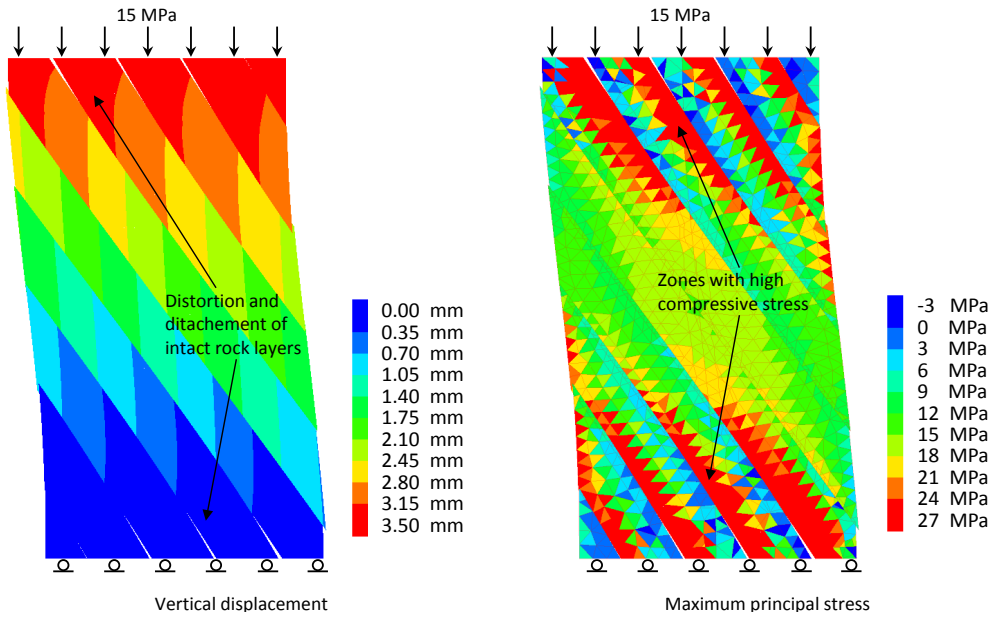


Figure 4: Bending of intact rock layers during an unconfined uni-axial loading test with joint set angle $\alpha = 30^\circ$. (Grid deformation has been magnified by a factor of 20.) Maximum principal stress distribution in the rock layers (right) follows the typical stress distribution for a bending beam.

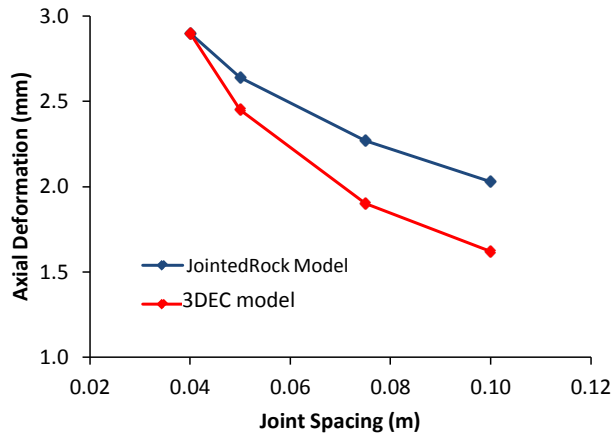


Figure 5: Variation of axial deformation versus joint spacing for a confined uni-axial test with one joint set ($\alpha = 30^\circ$).

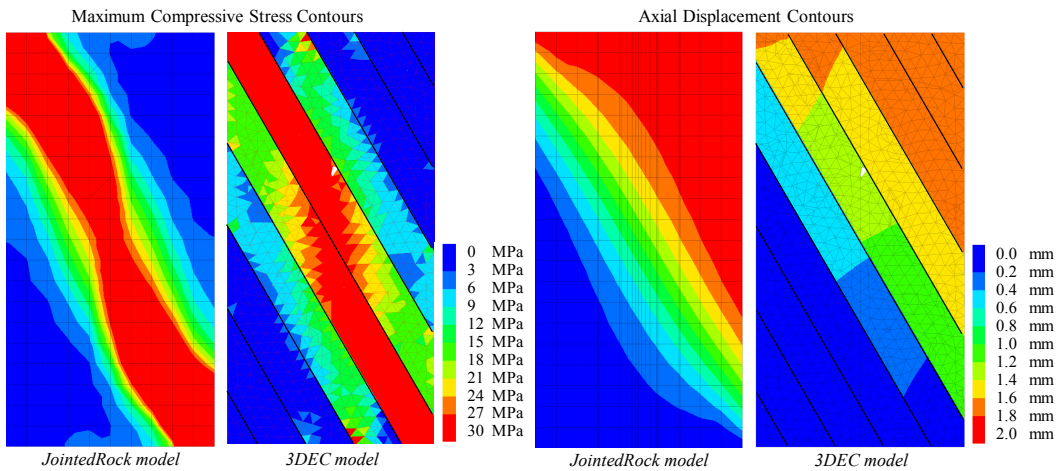


Figure 6: Distribution of the vertical displacement and maximum principal stress in a confined test with one joint set ($\alpha = 30^\circ$).

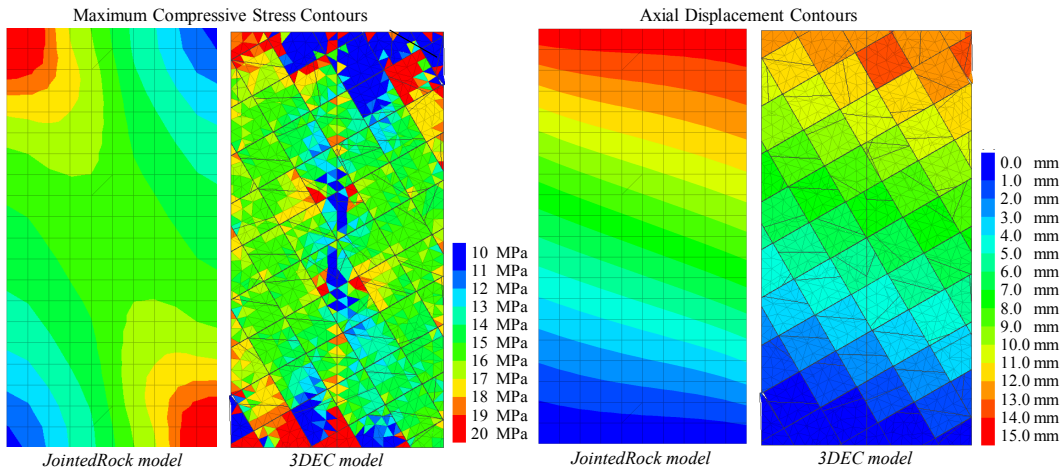


Figure 7: Distribution of the vertical displacement and maximum principal stress in a confined test with two joint sets ($\alpha = 30^\circ$).

Boundary Condition Effect

The deformation of the rock cylinder in the *3DEC* models includes the dislocation and rotation of intact rock blocks formed by the intersection of the joint sets. In the unconfined tests, these mechanisms form the principal components of deformations. The interaction of the rock blocks with each other and with the fixed z-velocity boundary conditions applied to the top and bottom of the model lead to a non-uniform stress distribution within the model (Figure 8). The fixed z-velocity boundary condition applied to the top of the model (stiff loading) prevents free rotation of the boundary rock blocks, producing high tensile stresses at the boundary. This effect is more pronounced in the unconfined tests and causes the results from two models to diverge considerably.

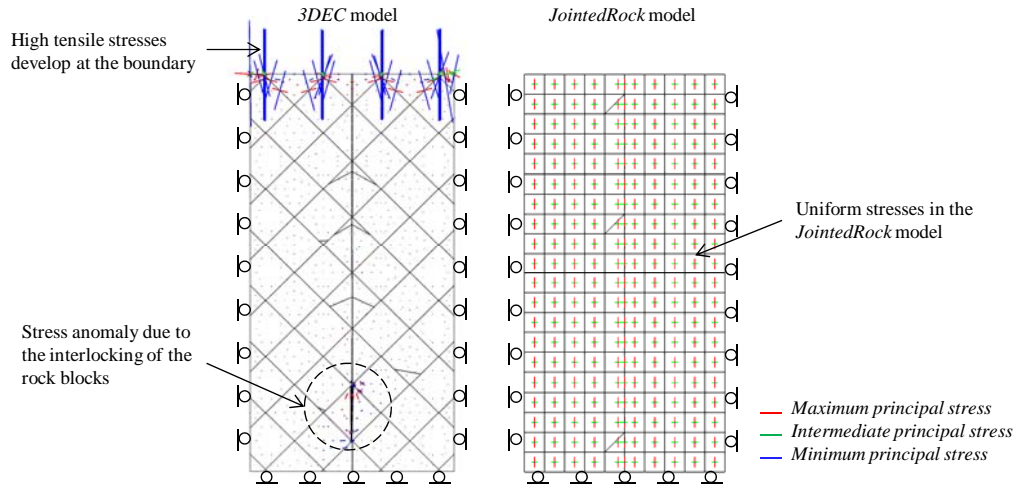


Figure 8: Stress tensors for a confined test with two joint sets ($\alpha = 45^\circ$). (Stress indicator bars for the two models are not on the same scale. Positive compressive stress convention applies.)

Conclusion

These analyses show that:

- When free rotation/dislocation of intact rock blocks/layers is confined by proper boundary conditions, the *JointedRock* model provides an acceptable approximation of the deformation of jointed rock masses.
- Discontinuum simulations are sensitive to the applied boundary conditions.
- The bending stiffness of intact rock layers increases the overall stiffness of a discontinuum model, compared to its equivalent continuum model. Decreasing the joint spacing reduces the bending stiffness of intact rock layers.

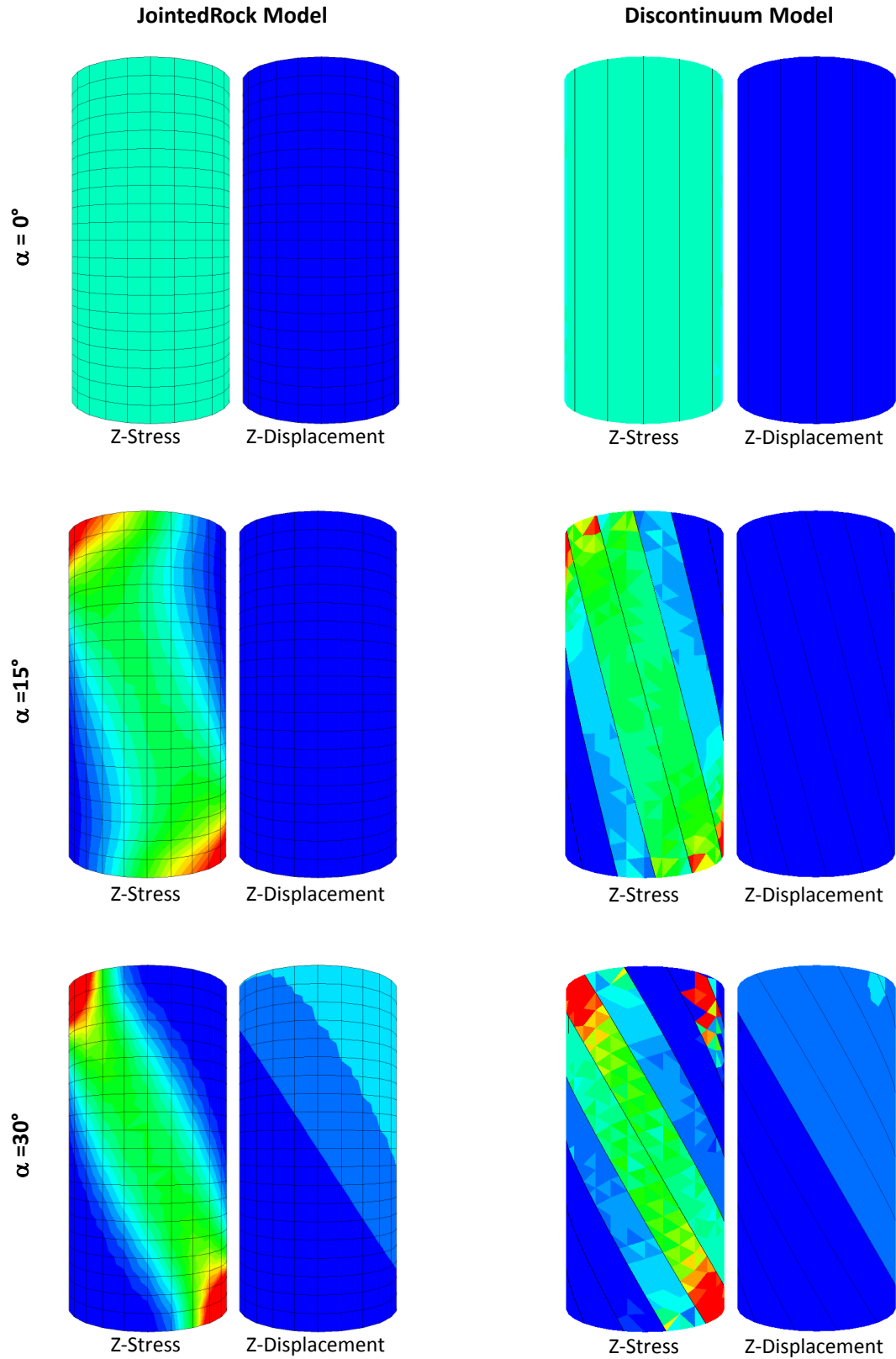


Figure 9: Vertical stress and vertical displacement contours for the confined tests with a single joint set ($s = 0.1$ m); left: *JointedRock* model, right: discontinuum (*3DEC*) model

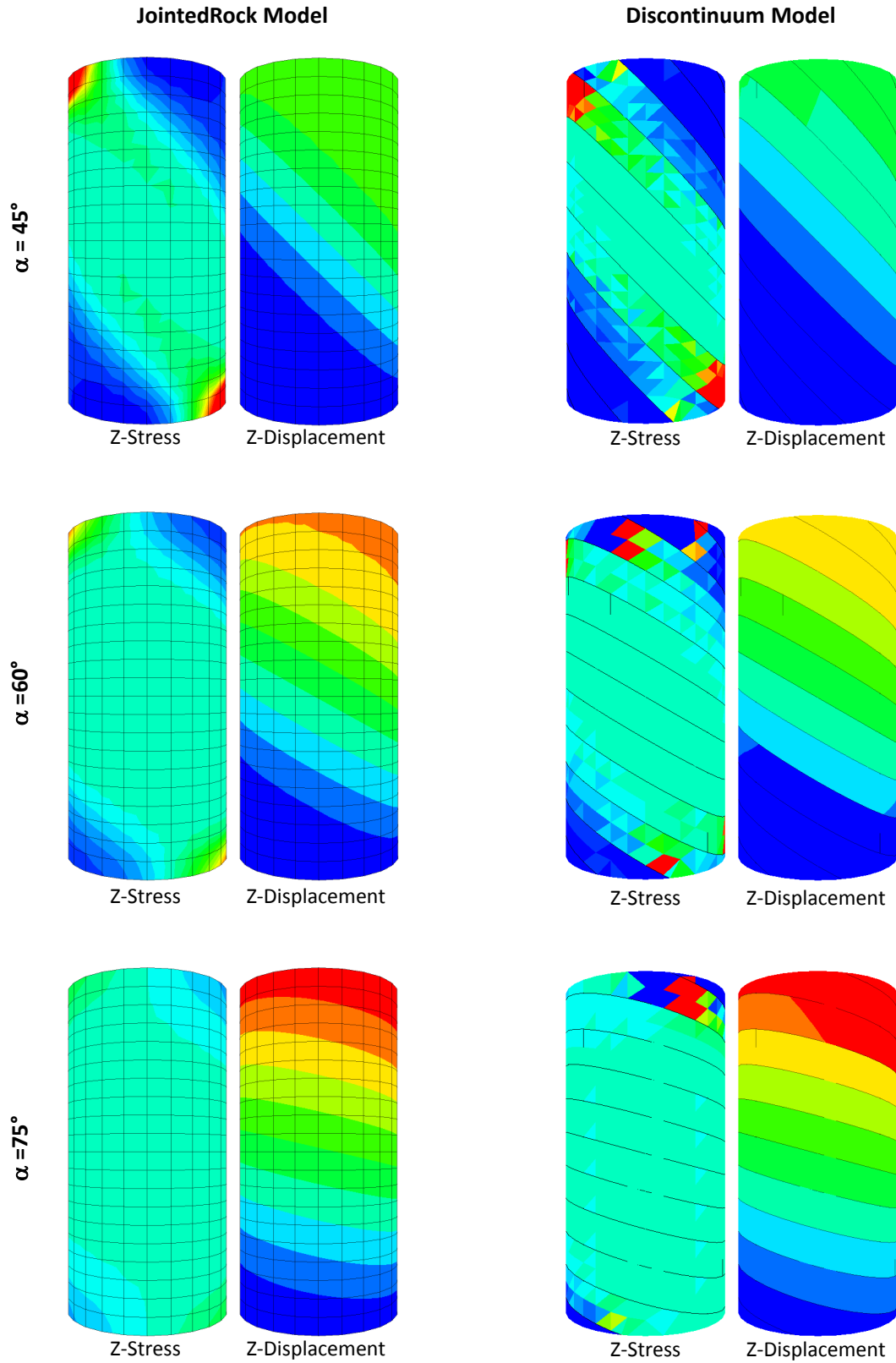


Figure 9: Vertical stress and vertical displacement contours for the confined tests with a single joint set ($s = 0.1$ m); left: *JointedRock* model, right: discontinuum (*3DEC*) model (*continued*)

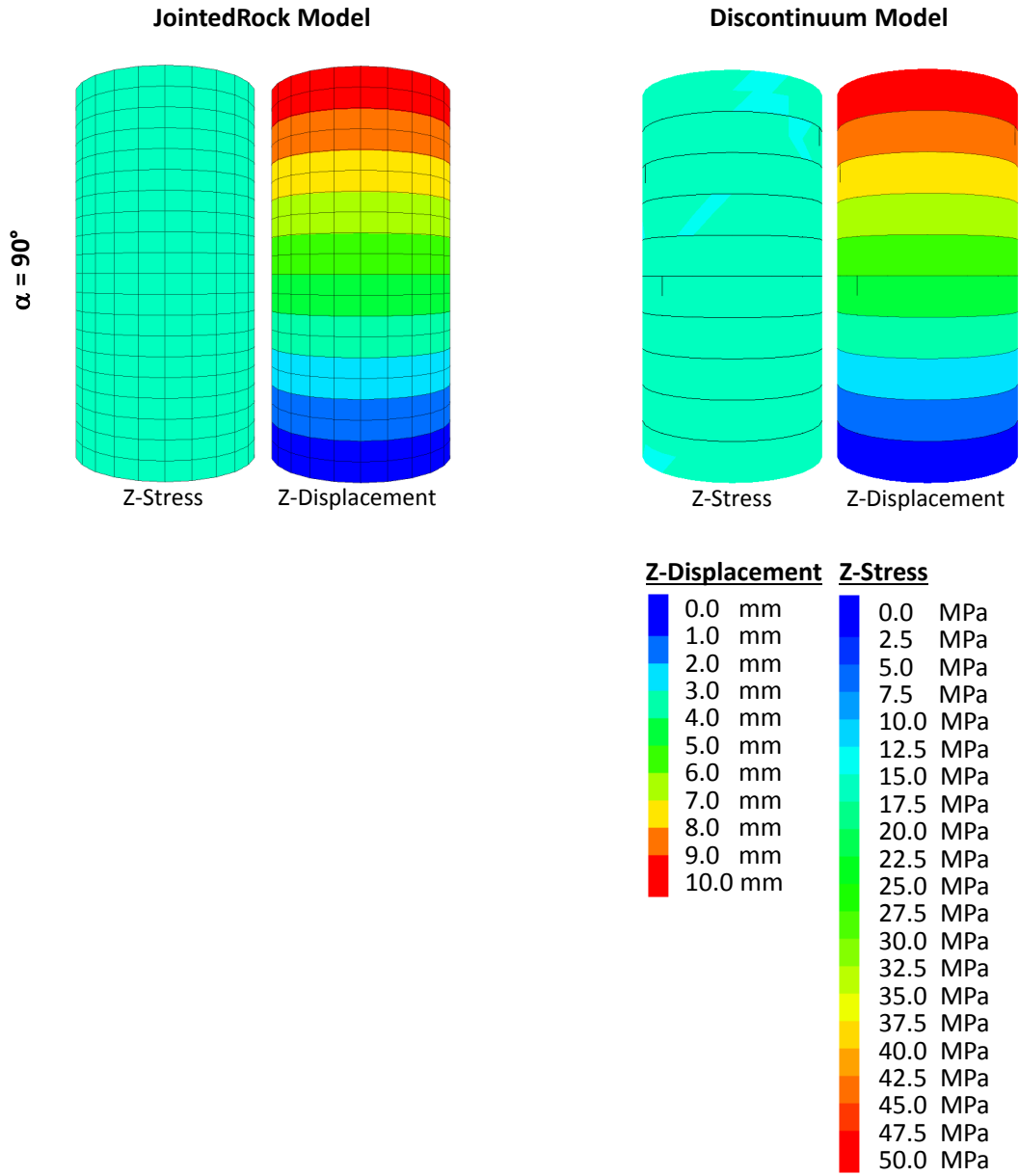


Figure 9: Vertical stress and vertical displacement contours for the confined tests with a single joint set ($s = 0.1$ m); left: *JointedRock* model, right: discontinuum (*3DEC*) model (*continued*)

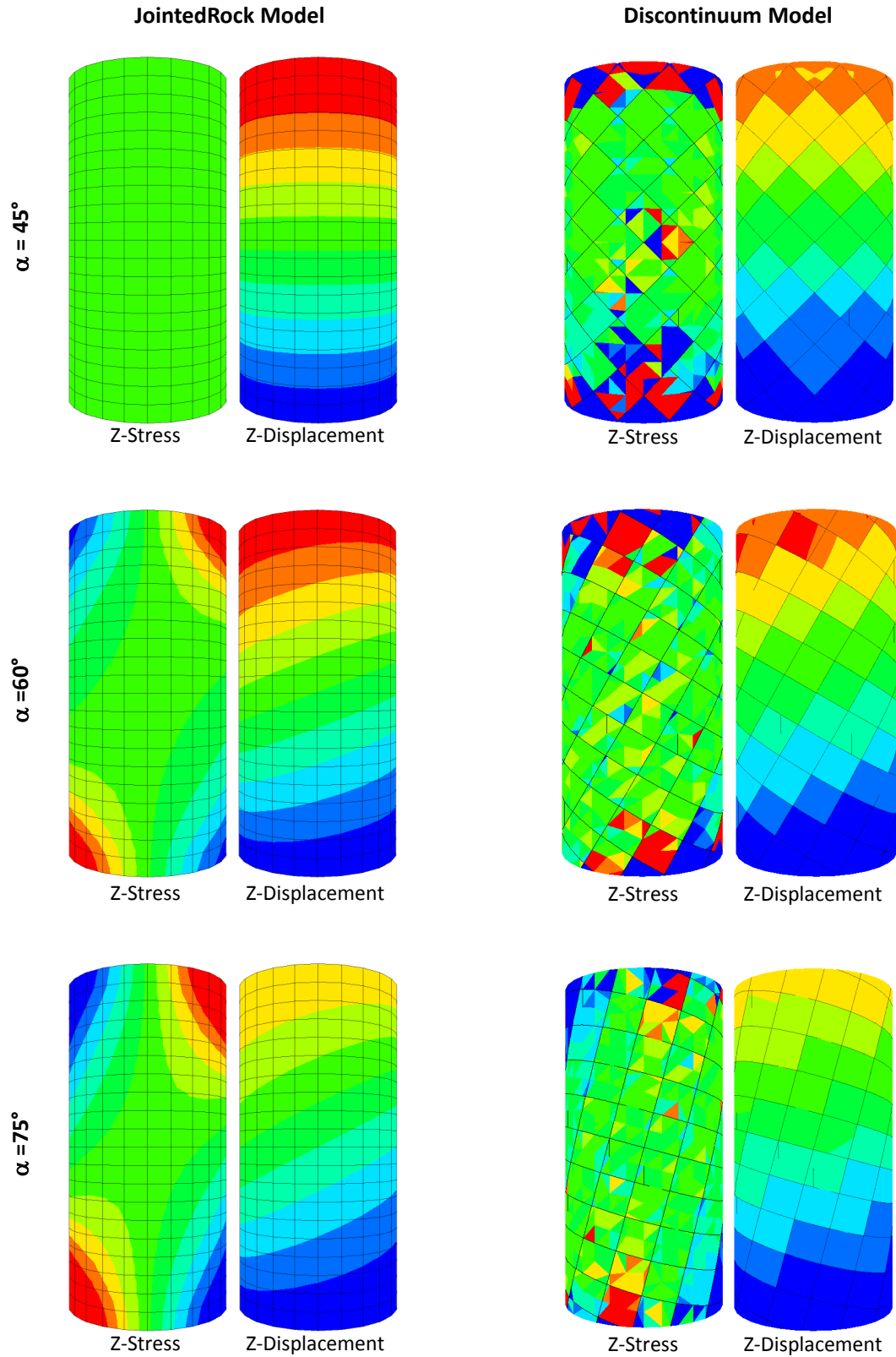


Figure 10: Vertical stress and vertical displacement contours for the confined tests with double joint sets ($s = 0.1$ m); left: *JointedRock* model, right: discontinuum (*3DEC*) model.

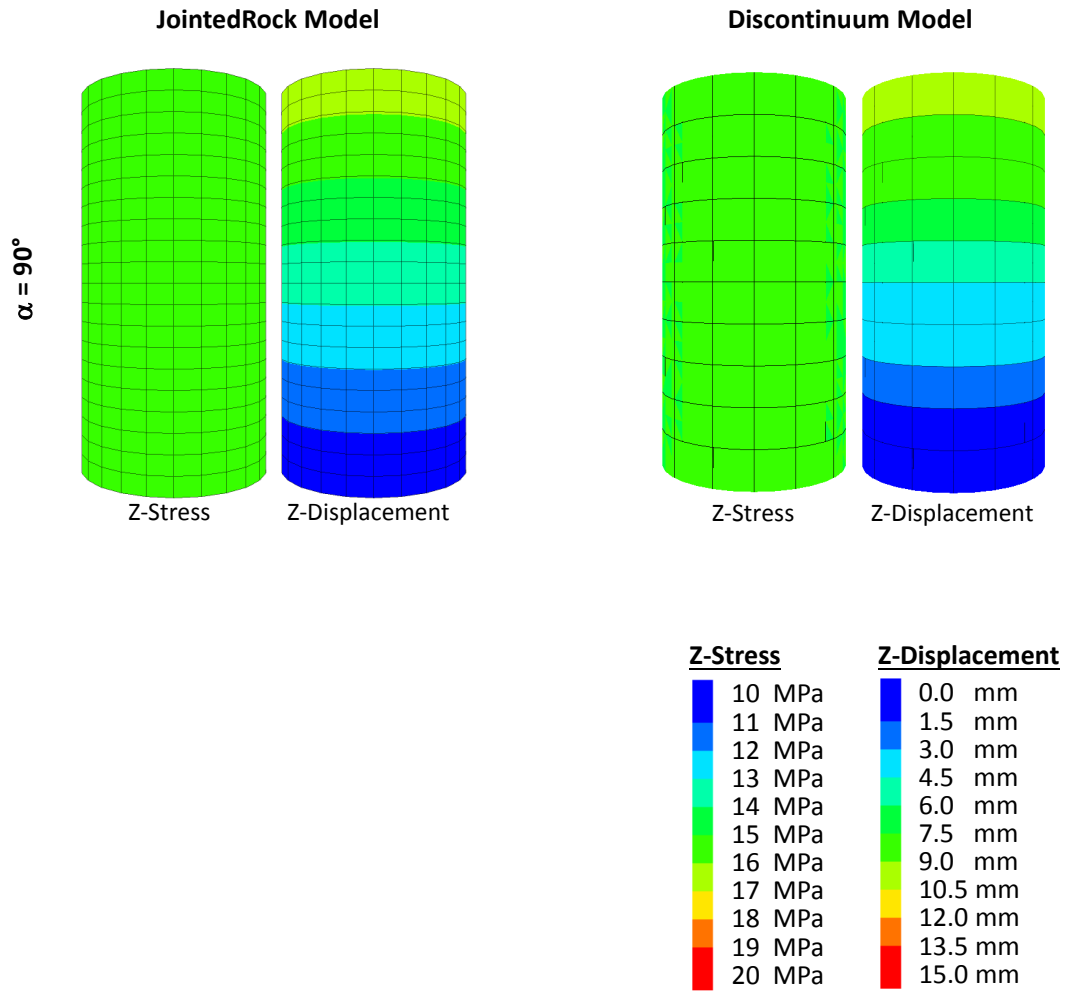


Figure 10: Vertical stress and vertical displacement contours for the confined tests with double joint sets ($s = 0.1$ m); left: *JointedRock* model, right: discontinuum (*3DEC*) model (*continued*).

Appendix 3

Closed Form Relationships for Loading of a Semi-Infinite Body

Circular Load

When a point load, p , is applied at the origin of a semi-infinite body of an elastic material (Figure 1) the elastic vertical displacement of each point within the body can be calculated using Equation (1) (Timoshenko and Goodier 1970):

$$w = \frac{P}{2\pi E} \left[z^2(1 + \nu)(r^2 + z^2)^{-3/2} + 2(1 - \nu^2)(r^2 + z^2)^{-1/2} \right] \quad (1)$$

where:

w : vertical displacement,

p : force,

E : Modulus of Elasticity,

ν : Poisson's ratio

z : vertical distance from applied force

r : horizontal distance from z-axis

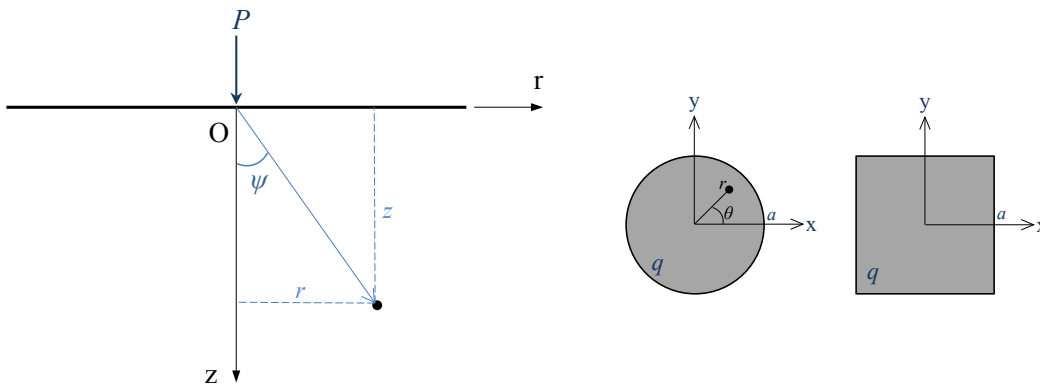


Figure 1: Point load on a semi-infinite body (right). Circular and square distributed loads (left)

For a uniformly distributed circular load q with radius of a the vertical displacement of each point within the body is the sum of the vertical displacements caused by each individual finite element of the load (dw), and can be calculated as follows:

$$dw = \frac{q r dr d\theta}{2\pi E} \left[z^2(1 + \nu)(r^2 + z^2)^{-3/2} + 2(1 - \nu^2)(r^2 + z^2)^{-1/2} \right] \quad (2)$$

$$w = \frac{q}{2\pi E} \int_0^{2\pi} \int_0^a \left[z^2(1+\nu)(r^2+z^2)^{-3/2}r + 2(1-\nu^2)(r^2+z^2)^{-1/2}r \right] drd\theta \quad (3)$$

For the points on z-axis ($r = 0$) equation (3) can be written as follows:

$$w = \frac{zq(1+\nu)}{E} \left[1 - z(a^2+z^2)^{-1/2} \right] + \frac{2q(1-\nu^2)}{E} \left[(a^2+z^2)^{1/2} - z \right] \quad (4)$$

Equation (4) is the ISRM suggested relationship for the calculation of the rock mass deformation modulus from plate loading test results. The influence of the extensometer borehole can be taken into account by modifying the lower limit of the integration in equation (3). The vertical component of the induced stresses in the semi-infinite body can be calculated using equation (5):

$$\sigma_z = q \left[-1 + \frac{z^3}{(a^2+z^2)^{3/2}} \right] \quad (5)$$

Square Load

For a uniformly distributed load of q with dimensions $2a$, the horizontal distance from origin (r) can be calculated as:

$$r^2 = x^2 + y^2 \quad (6)$$

where x and y are the coordinates of the points. By substituting equation (6) in (3) we will have:

$$w = \frac{2q}{\pi E} \int_0^a \int_0^a \left[(1+\nu)z^2(x^2+y^2+z^2)^{-3/2} + 2(1-\nu^2)(x^2+y^2+z^2)^{-1/2} \right] dx dy \quad (7)$$

After integration for x and y we will have:

$$w = \frac{2q(1+\nu)}{\pi E} [4a(1-\nu)A + 2z(1-\nu)B + zC] \quad (8)$$

where:

$$A = Ln \left(\frac{\sqrt{a^2+k^2} + a}{k} \right)$$

$$B = 2 \tan^{-1} \left(\frac{az}{(k+a)(k+\sqrt{a^2+k^2})} \right) - \tan^{-1} \left(\frac{a}{z} \right)$$

$$C = \tan^{-1} \left(\frac{a^2}{z\sqrt{k^2+a^2}} \right)$$

$$k^2 = z^2 + a^2$$

The maximum vertical displacement at the semi-infinite body surface occurs at the centre of the loaded area and can be calculated as:

$$w_o = 2.24 \frac{qa(1-\nu^2)}{E} \quad (9)$$

The vertical displacements at the corners of the loaded area are half the displacement at surface:

$$w_o = 1.12 \frac{qa(1-\nu^2)}{E} \quad (10)$$

Reference

Timoshenko, S., Goodier, J. (1970). Theory of Elasticity (3rd ed.). McGraw-Hill.

Appendix 4

Bakhtiary Dam Site Plate Loading Test Data

Supplementary Data on Fifteen PLTs Analyzed in Chapter 5

PLH1L1

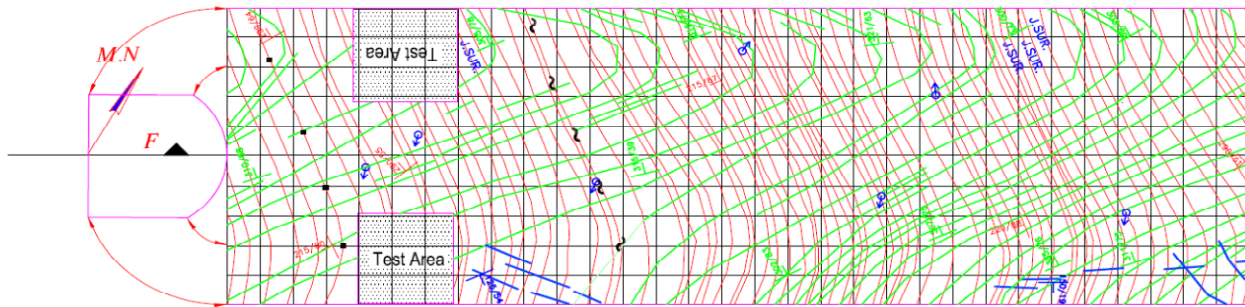
Test Gallery:	GL1	Pressure (3rd cycle):	14 MPa
Test Orientation:	Horizontal - N150°	Displacement (left/up):	0.979 mm
Test Gallery Azimut:	N060°	Displacement (right/down):	1.045 mm
Overburden:	124 m	Beddings dip/dd:	215/85
Plate Diameter:	915 mm	Beddings average spacing:	0.15 m
Rock Unit:	SV3	α^*	23°
Poisson's ratio:	0.2	J1 dip/dd:	305/75
		J1 average spacing:	0.4 m
RMR (89)**	68	β^*	60°
GSI (RMR-5)	63	<small>* beddings and J1 intersection angle with extensometer borehole</small>	

** (UCS 115MPa, RQD 50-75%, Spac 60-200mm, slightly rough<1mm, damp, no adjustment for orientation)

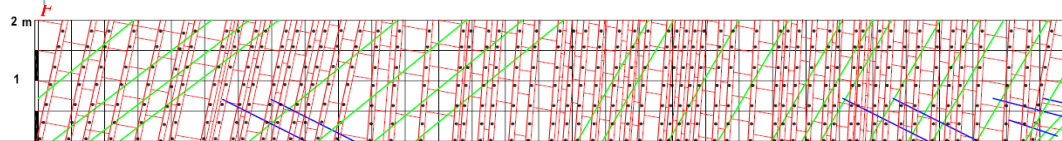
Deformation Modulus (GPa)	ISRM (1979)	Numerical Simulation	Bieniawski (1978)	Hoek and Diederich (2006)
left/up plate	9.9	7.7	36	25
right/down plate	9.2	7.3		

Normal stiffness (k_n) of beddings back calculated using the <i>JointedRock</i> model (GPa/mm)	
left/up plate	58
right/down plate	56

Test Group: 2



CHAINAGE(m)	30	31	32	33	34	35	36	37	38	39	40	41	42	43	44	45
ROCK TYPE	Sarak Formation, Unit SV3, Limestone and Inter															
DIP DIRECTION/ DIP (BEDDING)	215/80			215/87			220/88			215/85						
STRENGTH	Strong															
R.Q.D	25-50															
INFILLING	Calcite - Tight															
ROUGHNESS	Rough															
SPACING OF DISCONTINUITIES (cm)	20 - 60															
WEATHERING	Slightly Weathered															
GROUND WATER	Damp															



CHAINAGE(m)	30	31	32	33	34	35	36	37	38	39	40	41	42	43	44	45
Direction of Section	N060															
Dip Direction/Dip/Apparent Dip (Bedding)	215/80/79			215/87/86			220/88/87			215/85						
Discontinuity Systems	Bedding	217/81/80			Spacing: 6-20 cm			Opening: 0-1 mm								
	J1	305/72/52			Spacing: 20-60 cm			Opening: 0-1 mm								
	J2	119/43/42			Spacing: 20-60 cm			Opening: <1 mm								

PLV1L1

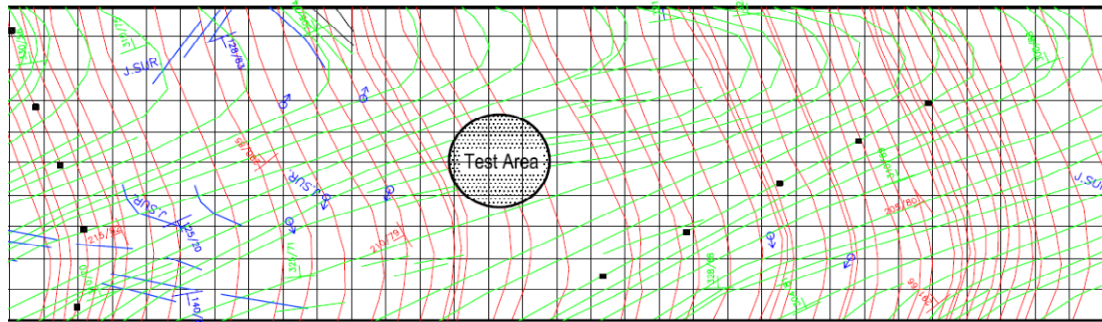
Test Gallery:	GL1	Pressure (3rd cycle):	15.7 MPa
Test Orientation:	Vertical	Displacement (left/up):	0.615 mm
Test Gallery Azimut:	N060°	Displacement (right/down):	0.41 mm
Overburden:	124 m	Beddings dip/dd:	215/80
Plate Diameter:	915 mm	Beddings average spacing:	0.15 m
Rock Unit:	SV3	α^*	5°
Poisson's ratio:	0.2	J1 dip/dd:	305/75
		J1 average spacing:	0.4 m
RMR (89)**	68	β^*	15°
GSI (RMR-5)	63	<small>* beddings and J1 intersection angle with extensometer borehole</small>	

** (UCS 115MPa, RQD 50-75%, Spac 60-200mm, slightly rough<1mm, damp, no adjustment for orientation)

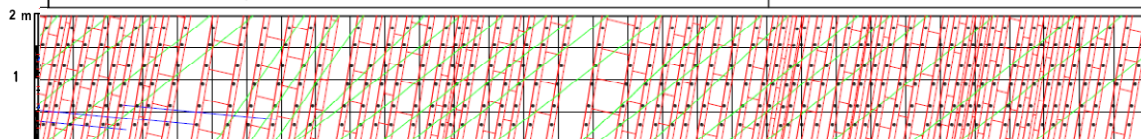
Deformation Modulus (GPa)	ISRM (1979)	Numerical Simulation	Bieniawski (1978)	Hoek and Diederich (2006)
left/up plate	17.6	13.9	36	25
right/down plate	26.4	20.9		

Normal stiffness (k_n) of beddings back calculated using the <i>JointedRock</i> model (GPa/mm)	
left/up plate	20
right/down plate	50

Test Group: 2



CHAINAGE(m)	3 14 15 16 17 18 19 20 21 22 23 24 25 26 27 28 29			
ROCK TYPE	Sarvak Formation, Unit SV3, Limestone and Interbeds of Siliceous Limestone , Dark Grey to Black			
DIP DIRECTION/ DIP (BEDDING)	215/82		210/79 205/80	
STRENGTH	Strong		Strong	
R.Q.D	75 – 90		50–75	
INFILLING	Tight–Calcite		Clay–Calcite	
ROUGHNESS	Rough		Smooth – Rough	
SPACING OF DISCONTINUITIES(cm)	20 – 60		20 – 60	
WEATHERING	Fresh		Fresh–Slightly Weathered	
GROUND WATER	Damp		Damp	



CHAINAGE(m)	3 14 15 16 17 18 19 20 21 22 23 24 25 26 27 28 29			
Direction of Section				
Dip Direction/Dip/Apparent Dip (Bedding)	215/82/81		210/79/78 205/80/79 210	
Discontinuity Systems	Bedding	Thickness: 0–2 mm	Infilling: Tight–Calcite	Roughness: Rough
	J1	Thickness: 0–2 mm	Infilling: Tight–Calcite	Roughness: Rough–Smooth
	J2	Thickness: <1 mm	Infilling: Tight	Roughness: Rough

PLH2L1

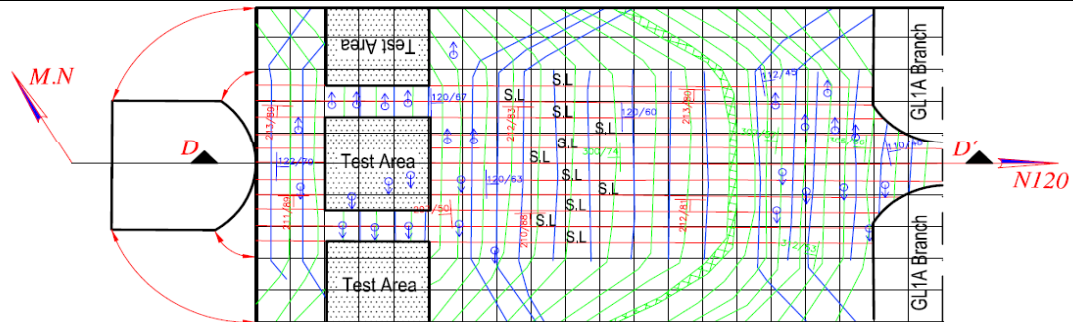
Test Gallery:	GL1	Pressure (3rd cycle):	14 MPa
Test Orientation:	Horizontal - N030°	Displacement (left/up):	0.814 mm
Test Gallery Azimut:	N120°	Displacement (right/down):	0.958 mm
Overburden:	84 m	Beddings dip/dd:	210/85
Plate Diameter:	971 mm	Beddings average spacing:	0.225 m
Rock Unit:	SV3	α^*	90°
Poisson's ratio:	0.2	J1 dip/dd:	305/52
		J1 average spacing:	0.35 m
RMR (89)**	55	β^*	0°
GSI (RMR-5)	50	<small>* beddings and J1 intersection angle with extensometer borehole</small>	

** (UCS 115MPa, RQD 50-75%, Spac 200-600mm, slickensided<5mm, damp, no adjustment for orientation)

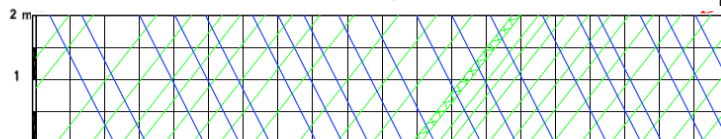
Deformation Modulus (GPa)	ISRM (1979)	Numerical Simulation	Bieniawski (1978)	Hoek and Diederich (2006)
left/up plate	12.6	9.9	10	9
right/down plate	10.7	8.4		

Normal stiffness (k_n) of beddings back calculated using the <i>JointedRock</i> model (GPa/mm)	
left/up plate	59
right/down plate	50

Test Group: 2



CHAINAGE(m)	0 1 2 3 4 5 6 7 8 9 10
ROCK TYPE	Sarvak Formation, Unit SV3, Limestone and Interbeds of Siliceous Limestone , Dark Grey to Black
DIP DIRECTION/ DIP (BEDDING)	211/85 212/80
STRENGTH	Medium Strong
R.Q.D	25-50
INFILLING	Calcite - Clay
ROUGHNESS	Smooth - Slickenside
SPACING OF DISCONTINUITIES(cm)	6 - 60
WEATHERING	Slightly Weathered
GROUND WATER	Damp



CHAINAGE(m)	0 1 2 3 4 5 6 7 8 9 10	
Direction of Section	N120	
Dip Direction/Dip/Apparent Dip (Bedding)	211/85/11 212/80/11	
Discontinuity Systems	Bedding	211/83/08 Spacing: 20-60 cm
	J1	305/52/51 Spacing: 6-20 cm
	J2	119/65/65 Spacing: 6-20 cm

PLV2L1

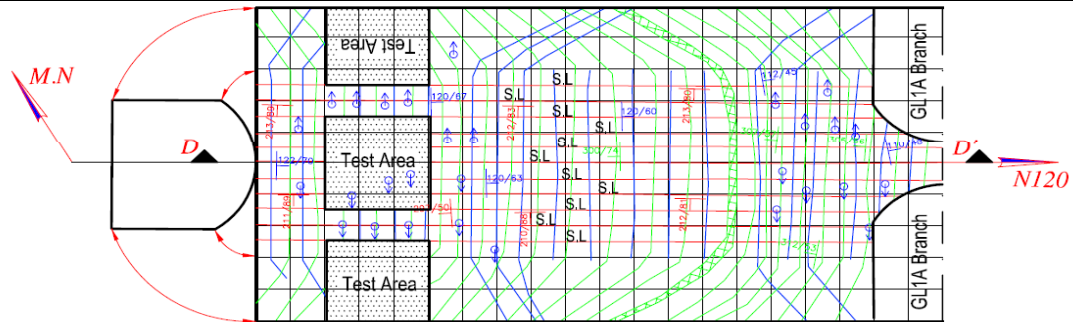
Test Gallery:	GL1	Pressure (3rd cycle):	14 MPa
Test Orientation:	Vertical	Displacement (left/up):	0.476 mm
Test Gallery Azimut:	N120°	Displacement (right/down):	--
Overburden:	84 m	Beddings dip/dd:	210/85
Plate Diameter:	971 mm	Beddings average spacing:	0.225 m
Rock Unit:	SV3	α^*	0°
Poisson's ratio:	0.2	J1 dip/dd:	305/52
		J1 average spacing:	0.35 m
RMR (89)**	55	β^*	35°
GSI (RMR-5)	50	<small>* beddings and J1 intersection angle with extensometer borehole</small>	

** (UCS 115MPa, RQD 50-75%, Spac 200-600mm, slickensided<5mm, damp, no adjustment for orientation)

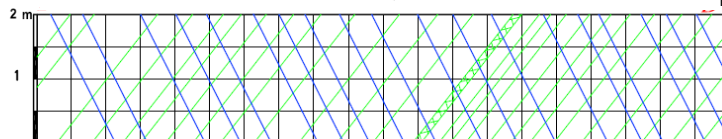
Deformation Modulus (GPa)	ISRM (1979)	Numerical Simulation	Bieniawski (1978)	Hoek and Diederich (2006)
left/up plate	21.5	16.8	10	9
right/down plate	--	--		

Normal stiffness (k_n) of beddings back calculated using the <i>JointedRock</i> model (GPa/mm)	
left/up plate	51
right/down plate	--

Test Group: 1



CHAINAGE(m)	0 1 2 3 4 5 6 7 8 9 10
ROCK TYPE	Sarvak Formation, Unit SV3, Limestone and Interbeds of Siliceous Limestone , Dark Grey to Black
DIP DIRECTION/ DIP (BEDDING)	211/85 212/80
STRENGTH	Medium Strong
R.Q.D	25-50
INFILLING	Calcite - Clay
ROUGHNESS	Smooth - Slickenside
SPACING OF DISCONTINUITIES(cm)	6 - 60
WEATHERING	Slightly Weathered
GROUND WATER	Damp



CHAINAGE(m)	0 1 2 3 4 5 6 7 8 9 10		
Direction of Section	N120		
Dip Direction/Dip/Apparent Dip (Bedding)	211/85/11 212/80/11		
Discontinuity Systems	Bedding	211/83/08	Spacing: 20-60 cm
	J1	305/52/51	Spacing: 6-20 cm
	J2	119/65/65	Spacing: 6-20 cm

PLV3L1

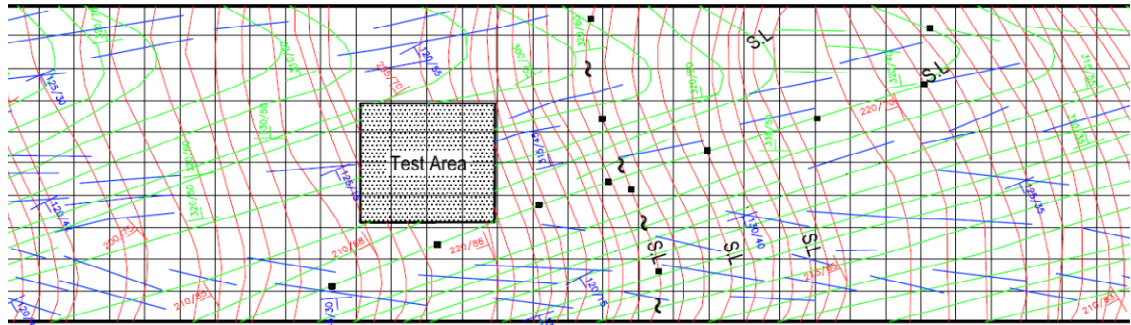
Test Gallery:	GL1	Pressure (3rd cycle):	14 MPa
Test Orientation:	Vertical	Displacement (left/up):	0.749 mm
Test Gallery Azimut:	N60°	Displacement (right/down):	0.475 mm
Overburden:	84 m	Beddings dip/dd:	210/85
Plate Diameter:	971 mm	Beddings average spacing:	0.225 m
Rock Unit:	SV3	α^*	0°
Poisson's ratio:	0.2	J1 dip/dd:	305/58
		J1 average spacing:	0.45 m
RMR (89)**	65	β^*	30°
GSI (RMR-5)	60	<i>* beddings and J1 intersection angle with extensometer borehole</i>	

** (UCS 115MPa, RQD 50-75%, Spac 200-600mm, slightly rough weathered<1mm, dry, no adjustment for orientation)

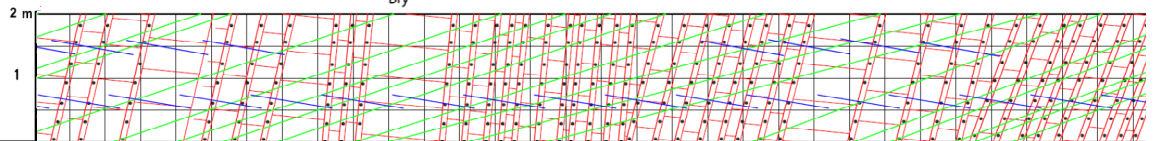
Deformation Modulus (GPa)	ISRM (1979)	Numerical Simulation	Bieniawski (1978)	Hoek and Diederich (2006)
left/up plate	13.7	10.8	30	20
right/down plate	21.6	17		

Normal stiffness (k_n) of beddings back calculated using the <i>JointedRock</i> model (GPa/mm)	
left/up plate	16
right/down plate	36

Test Group: 1



CHAINAGE(m)	97 98 99 100 101 102 103 104 105 106 107 108 109 110 111 1
ROCK TYPE	arvak Formation, Unit SV3, Limestone and Interbeds of Siliceous Limestone , Dark Grey to Black
DIP DIRECTION/ DIP (BEDDING)	80 210/86 217/78 210/73
STRENGTH	Strong
R.Q.D	75-90
INFILLING	Calcite-Clay
ROUGHNESS	Rough-Smooth
SPACING OF DISCONTINUITIES(cm)	6 - 200
WEATHERING	Fresh/Faintly Weathered
GROUND WATER	Dry



CHAINAGE(m)	97 98 99 100 101 102 103 104 105 106 107 108 109 110 111 112
Direction of Section N060	
Dip Direction/Dip/Apparent Dip (Bedding)	8 210/86/85 217/78/77 210/73/71
Discontinuity Systems	Bedding: ing: 20-60 cm Opening: 1-3 mm Infilling: Clay-Calcite
	J1 ng: 60-200 cm Opening: 1-3 mm Infilling: Calcite-Clay
	J2 ing: 6-20 cm Opening: <1 mm Infilling: Tight

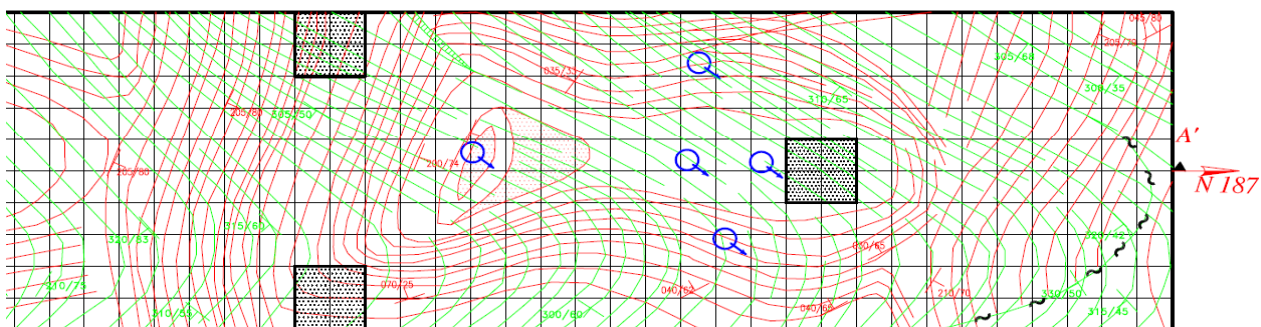
PLH3L1

Test Gallery:	GL1	Pressure (3rd cycle):	13.9 MPa
Test Orientation:	Horizontal - N097°	Displacement (left/up):	--
Test Gallery Azimut:	N187°	Displacement (right/down):	0.941 m
Overburden:	24 m	Beddings dip/dd:	060 / 33
Plate Diameter:	65 mm	Beddings average spacing:	0.27 m
Rock Unit:	SV3 KINK band zone	α^*	30°
Poisson's ratio:	0.2	J1 dip/dd:	315 / 75
		J1 average spacing:	0.30 m
RMR (89)	67	β^*	40°
GSI (RMR-5)	62	<i>* beddings and J1 intersection angle with extensometer borehole</i>	

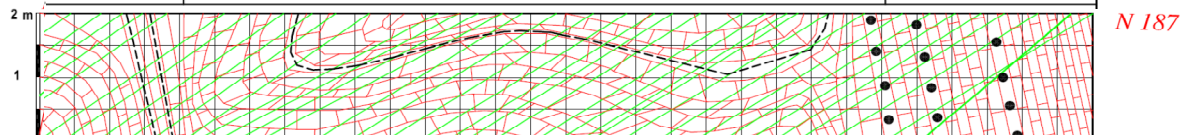
Deformation Modulus (GPa)	ISRM (1979)	Numerical Simulation	Bieniawski (1978)	Hoek and Diederich (2006)
left/up plate	--	--	34	23
right/down plate	7.2	5.5		

Normal stiffness (k_n) of beddings back calculated using the <i>JointedRock</i> model (GPa/mm)	
left/up plate	--
right/down plate	17

Test Group: 2



CHAINAGE(m)	2 13 14 15 16 17 18 19 20 21 22 23 24 25 26 27	
ROCK TYPE	thin laminated Black Shale , Dark Grey to Black0 (KINK BAND ZONE)	Unit SV3, Limestone
DIP DIRECTION/ DIP (BEDDING)		205/79
STRENGTH	Strong	Strong
R.Q.D	0 - 25	50 - 75
INFILLING	Clay and Calcite	Clay and Calcite
ROUGHNESS	Slickenside - Rough	Slickenside - Rough
SPACING OF DISCONTINUITIES (cm)	-60 (>2 m in Anticline)	6 - 20 cm
WEATHERING	Moderately Weathered	Faintly Weathered
GROUND WATER	Wet	Dry



CHAINAGE(m)	2 13 14 15 16 17 18 19 20 21 22 23 24 25 26 27	
Direction of Section	17	
Dip Direction/Dip/Apparent Dip (Bedding)	Kink Band Zone	205/79/78
Discontinuity Systems	Bedding	Opening: 1-5 mm Infilling: Calcite Clay Roughness: Slickenside+Rough
	J1	Opening: 1-5 mm Infilling: Calcite Roughness: Rough

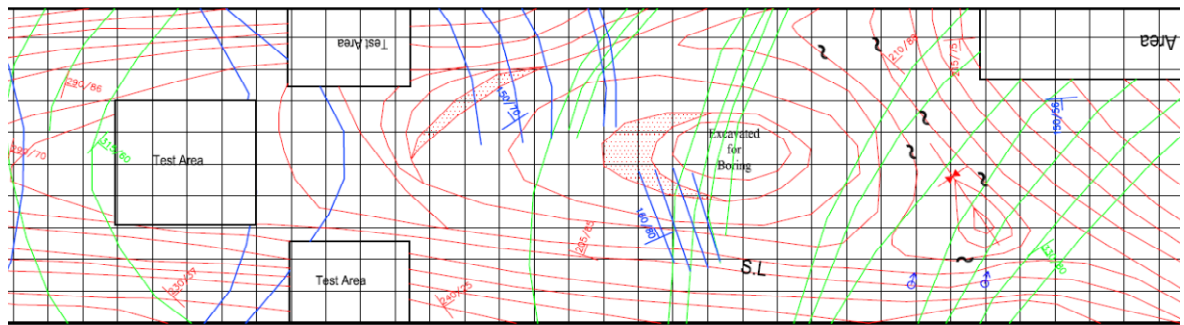
PLV1R1

Test Gallery:	GR1	Pressure (3rd cycle):	14 MPa
Test Orientation:	Sub-Vertical 055/70	Displacement (left/up):	0.967 mm
Test Gallery Azimut:	N275°	Displacement (right/down):	--
Overburden:	101 m	Beddings dip/dd:	235 / 20
Plate Diameter:	971 mm	Beddings average spacing:	0.35 m
Rock Unit:	SV2 - KINK band zone	α^*	90°
Poisson's ratio:	0.2	J1 dip/dd:	304 / 73
		J1 average spacing:	0.5 m
		β^*	15°
		* beddings and J1 intersection angle with extensometer borehole	
RMR (89)	69		
GSI (RMR-5)	64		

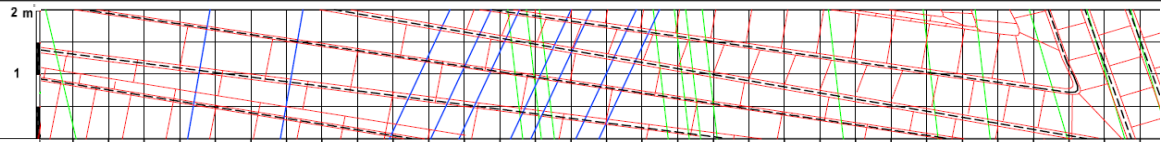
Deformation Modulus (GPa)	ISRM (1979)	Numerical Simulation	Bieniawski (1978)	Hoek and Diederich (2006)
left/up plate	10.6	8.4	38	27
right/down plate	--	--		

Normal stiffness (k_n) of beddings back calculated using the <i>JointedRock</i> model (GPa/mm)	
left/up plate	56
right/down plate	--

Test Group: 2



CHAINAGE(m)	11	12	13	14	15	16	17	18	19	20	21	22	23	24	25	26	27
ROCK TYPE	Formation, Unit SV2, Limestone With thin laminated Black Shale , Dark Grey to Black (KINK BAND ZONE)																
DIP DIRECTION/ DIP (BEDDING)	30/37			240/25				210/80				215/76					
STRENGTH	Strong																
R.Q.D	0-25																
INFILLING	Calcite and Clay																
ROUGHNESS	Rough-Smooth																
SPACING OF DISCONTINUITIES (c)	20-60																
WEATHERING	Faintly Weathered																
GROUND WATER	Dry																



CHAINAGE(m)	12	13	14	15	16	17	18	19	20	21	22	23	24	25	26	27
Direction of Section	N275															
Dip Direction/Dip/Apparent Dip (Bedding)				240/25/21				205/25/09				215/76/63				
Discontinuity Systems	Bedding	Opening: 0.1-1 mm				Infilling: Calcite-Clay				Roughness: Smooth						
	J1	Opening: 1-5 mm				Infilling: Calcite				Roughness: Rough-						

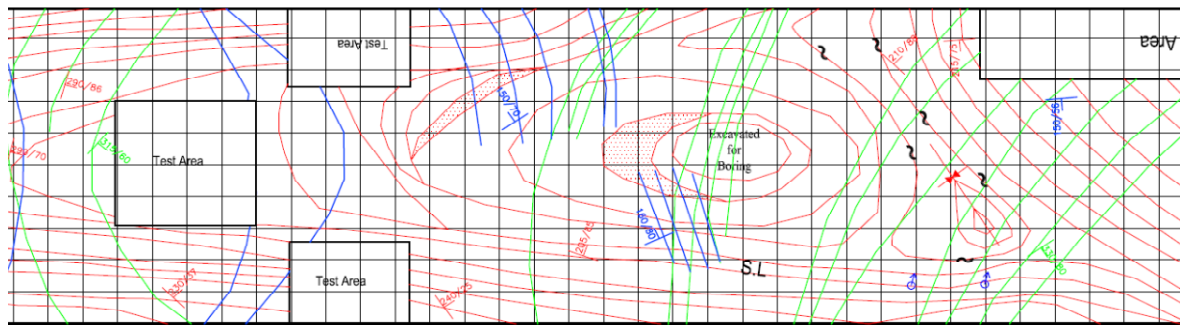
PLH1R1

Test Gallery:	GR1	Pressure (3rd cycle):	14 MPa
Test Orientation:	Horizontal - N185°	Displacement (left/up):	0.549 mm
Test Gallery Azimut:	N275°	Displacement (right/down):	--
Overburden:	116 m	Beddings dip/dd:	220 / 34
Plate Diameter:	971 mm	Beddings average spacing:	0.4 m
Rock Unit:	SV2 - KINK band zone	α^*	5°
Poisson's ratio:	0.2	J1 dip/dd:	312 / 58
		J1 average spacing:	0.35 m
RMR (89)	62	β^*	35°
GSI (RMR-5)	57	<i>* beddings and J1 intersection angle with extensometer borehole</i>	

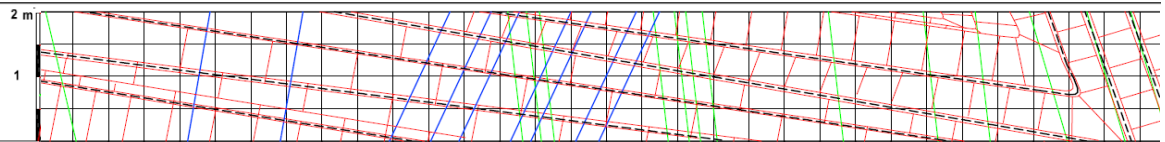
Deformation Modulus (GPa)	ISRM (1979)	Numerical Simulation	Bieniawski (1978)	Hoek and Diederich (2006)
left/up plate	18.7	14.9	24	16
right/down plate	--	--		

Normal stiffness (k_n) of beddings back calculated using the <i>JointedRock</i> model (GPa/mm)	
left/up plate	33
right/down plate	--

Test Group: 1



CHAINAGE(m)	11	12	13	14	15	16	17	18	19	20	21	22	23	24	25	26	27
ROCK TYPE	Formation, Unit SV2, Limestone With thin laminated Black Shale , Dark Grey to Black (KINK BAND ZONE)																
DIP DIRECTION/ DIP (BEDDING)	30/37			240/25				210/80				215/76					
STRENGTH	Strong																
R.Q.D	0-25																
INFILLING	Calcite and Clay																
ROUGHNESS	Rough-Smooth																
SPACING OF DISCONTINUITIES (c)	20-60																
WEATHERING	Faintly Weathered																
GROUND WATER	Dry																



CHAINAGE(m)	12	13	14	15	16	17	18	19	20	21	22	23	24	25	26	27
Direction of Section	N275															
Dip Direction/Dip/Apparent Dip (Bedding)	30/37			240/25/21				205/25/09				215/76/63				
Discontinuity Systems	Bedding	Opening: 0.1-1 mm			Infilling: Calcite-Clay				Roughness: Smooth							
	J1	Opening: 1-5 mm			Infilling: Calcite				Roughness: Rough							

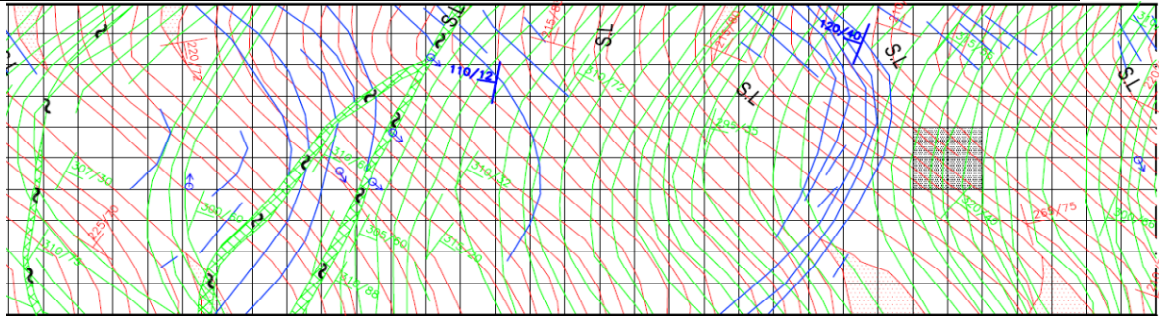
PLV1R2

Test Gallery:	GR2	Pressure (3rd cycle):	14 MPa
Test Orientation:	Vertical	Displacement (left/up):	0.956 mm
Test Gallery Azimut:	N280°	Displacement (right/down):	1.001 mm
Overburden:	65 m	Beddings dip/dd:	215 / 80
Plate Diameter:	915 mm	Beddings average spacing:	0.3 m
Rock Unit:	SV3	α^*	10°
Poisson's ratio:	0.2	J1 dip/dd:	315 / 55
		J1 average spacing:	0.3 m
RMR (89)	65	β^*	35°
GSI (RMR-5)	60	<i>* beddings and J1 intersection angle with extensometer borehole</i>	

Deformation Modulus (GPa)	ISRM (1979)	Numerical Simulation	Bieniawski (1978)	Hoek and Diederich (2006)
left/up plate	10.1	7.9	30	20
right/down plate	9.6	7.5		

Normal stiffness (k_n) of beddings back calculated using the <i>JointedRock</i> model (GPa/mm)	
left/up plate	16
right/down plate	15

Test Group: 1



CHAINAGE(m)	14	15	16	17	18	19	20	21	22	23	24	25	26	27	28	29	30
ROCK TYPE	ne and Interbeds of Siliceous Limestone , Dark Grey to Black																
DIP DIRECTION/ DIP (BEDDING)	220/72					215/82					215/78						
STRENGTH	Strong																
R.Q.D	75-90																
INFILLING	Calcite-Tight																
ROUGHNESS	Rough-Slickenside																
SPACING OF DISCONTINUITIES(cm)	20-60																
WEATHERING	Fresh-Slightly Weathered																
GROUND WATER	Damp-Wet																

	2 m																				
	1																				
CHAINAGE(m)	14	15	16	17	18	19	20	21	22	23	24	25	26	27	28	29	30				
Direction of Section																					
Dip Direction/Dip/Apparent Dip (Bedding)		220/72/57					215/82/72					215/78/63									
Discontinuity Systems	Bedding	: 1-5 mm	Infilling: Clay-Calcite	Roughness: Slickenside																	
	J1	: 0.1-1 mm	Infilling: Tight-Calcite	Roughness: Rough																	
	J2	: 0.1-1 mm	Infilling: Tight-Calcite	Roughness: Rough																	

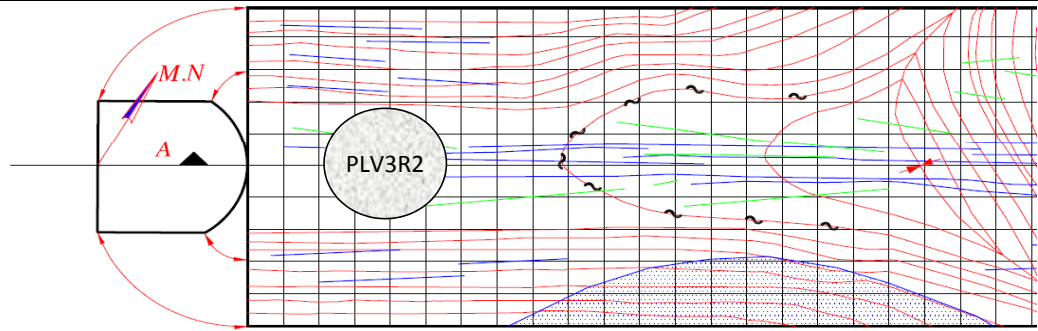
PLV3R2

Test Gallery:	GR2	Pressure (3rd cycle):	14 MPa
Test Orientation:	Vertical	Displacement (left/up):	1.02 mm
Test Gallery Azimut:	N060°	Displacement (right/down):	0.924 mm
Overburden:	115 m	Beddings dip/dd:	000 / 00
Plate Diameter:	65 mm	Beddings average spacing:	0.17 m
Rock Unit:	SV3 - KINK band zone	α^*	0°
Poisson's ratio:	0.2	J1 dip/dd:	--
		J1 average spacing:	0.8 m
RMR (89)	60	β^*	10°
GSI (RMR-5)	55	<small>* beddings and J1 intersection angle with extensometer borehole</small>	

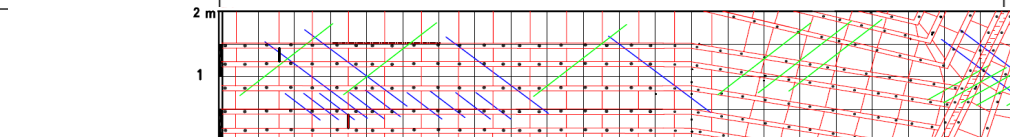
Deformation Modulus (GPa)	ISRM (1979)	Numerical Simulation	Bieniawski (1978)	Hoek and Diederich (2006)
left/up plate	6.7	5.3	20	14
right/down plate	7.4	5.8		

Normal stiffness (k_n) of beddings back calculated using the <i>JointedRock</i> model (GPa/mm)	
left/up plate	34
right/down plate	36

Test Group: 2



CHAINAGE(m)	0	1	2	3	4	5	6	7	8	9	10	11
ROCK TYPE	Sarvak Formation, Unit SV3, Limestone, Shaley Limestone											
DIP DIRECTION/ DIP (BEDDING)	000/00					030/50						
STRENGTH	Strong											
R.Q.D	0-25											
INFILLING	Thight-Calcit-Clay											
ROUGHNESS	Smooth-Slickenside											
SPACING OF DISCONTINUITIES(cm)	6-60											
WEATHERING	Slightly weatherd											
GROUND WATER	Dry											



CHAINAGE(m)	0	1	2	3	4	5	6	7	8	9	10	11	
Direction of Section	N060												
Direction/Dip/Apparent Dip (Bedding)	000/00/00					030/50/46							
scontinuity Systems	Bedding	212/80/78 & 354/17/07 & 023/49/45					Spacing: 20-60 cm						
	J1	305/83/73					Spacing: 6-20 cm						
	J2	135/72/38 & 132/44/16					Spacing: 6-20 cm						

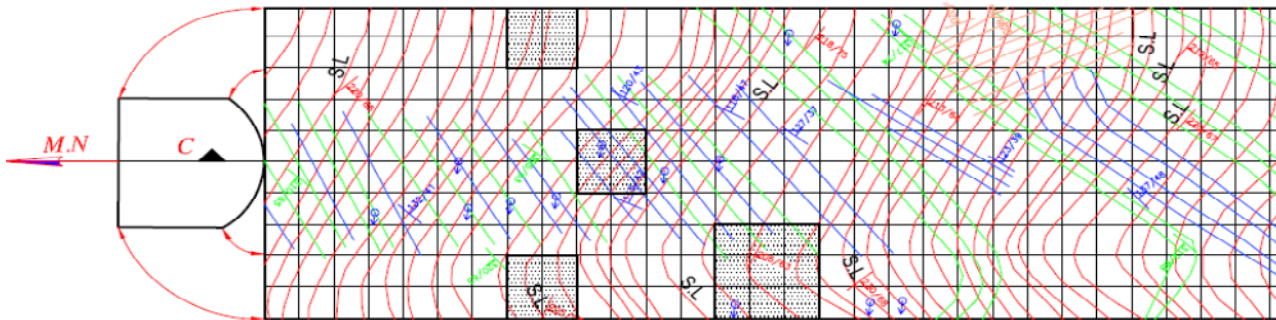
PLV2L2

Test Gallery:	GL2	Pressure (3rd cycle):	14 MPa
Test Orientation:	Vertical	Displacement (left/up):	0.596 mm
Test Gallery Azimut:	N180°	Displacement (right/down):	0.551 mm
Overburden:	165 m	Beddings dip/dd:	215 / 75
Plate Diameter:	915 mm	Beddings average spacing:	0.15 m
Rock Unit:	SV4	α^*	15°
Poisson's ratio:	0.2	J1 dip/dd:	305 / 60
		J1 average spacing:	0.25 m
RMR (89)	58	β^*	30°
GSI (RMR-5)	53	<i>* beddings and J1 intersection angle with extensometer borehole</i>	

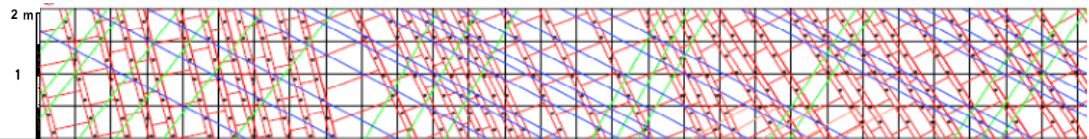
Deformation Modulus (GPa)	ISRM (1979)	Numerical Simulation	Bieniawski (1978)	Hoek and Diederich (2006)
left/up plate	16.2	12.9	16	12
right/down plate	17.5	13.7		

Normal stiffness (k_n) of beddings back calculated using the <i>JointedRock</i> model (GPa/mm)	
left/up plate	35
right/down plate	23

Test Group: 2



CHAINAGE(m)	46	47	48	49	50	51	52	53	54	55	56	57	58	59	60
ROCK TYPE	Sarvak Formation, Unit SV4, Limestone with Small Siliceous Nodule														
DIP DIRECTION/ DIP (BEDDING)	220/80			212/70			213/64			225					
STRENGTH	Strong														
R.Q.D	25-50														
INFILLING	Tight-Calcite														
ROUGHNESS	Slickenside-Smooth														
SPACING OF DISCONTINUITIES(cm)	20-60														
WEATHERING	Slightly Weathered														
GROUND WATER	Wet														



CHAINAGE(m)	46	47	48	49	50	51	52	53	54	55	56	57	58	59	60	
Direction of Section	N180															
Dip Direction/Dip/Apparent Dip (Bedding)	220/80/77			212/70/67			213/64/60									
Discontinuity Systems	Bedding	220/64/51			Spacing: 20-60 cm			Opening: 1-5 mm								
	J1	310/71/67			Spacing: 20-60 cm			Opening: 0.1-1 mm								
	J2	121/42/39			Spacing: 20-60 cm			Opening: >0.1 mm								

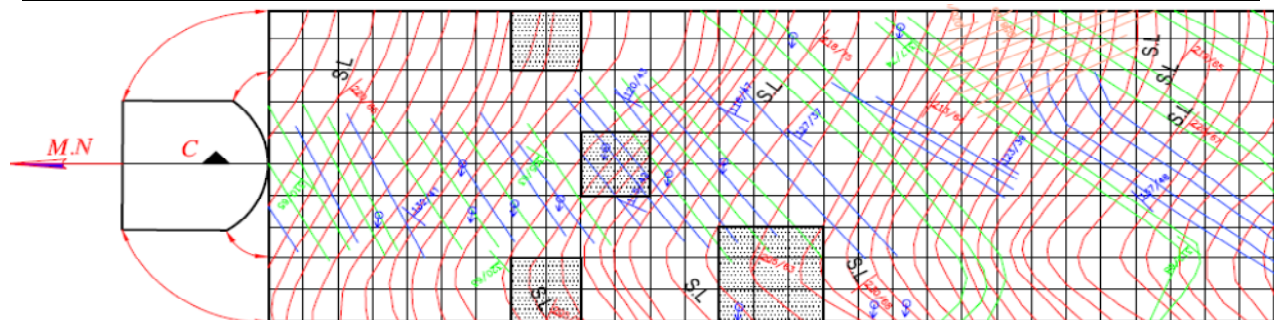
PLH2L2

Test Gallery:	GL2	Pressure (3rd cycle):	14 MPa
Test Orientation:	Horizontal - N090°	Displacement (left/up):	--
Test Gallery Azimut:	N180°	Displacement (right/down):	1.035 mm
Overburden:	165 m	Beddings dip/dd:	220 / 80
Plate Diameter:	915 mm	Beddings average spacing:	0.15 m
Rock Unit:	SV4	α^*	40°
Poisson's ratio:	0.2	J1 dip/dd:	310 / 71
		J1 average spacing:	0.25 m
RMR (89)	58	β^*	10°
GSI (RMR-5)	53	<small>* beddings and J1 intersection angle with extensometer borehole</small>	

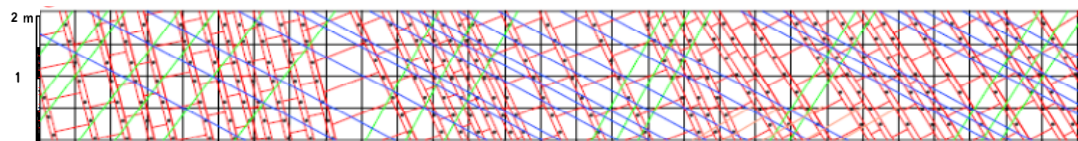
Deformation Modulus (GPa)	ISRM (1979)	Numerical Simulation	Bieniawski (1978)	Hoek and Diederich (2006)
left/up plate	--	--	16	12
right/down plate	9.3	6.9		

Normal stiffness (k_n) of beddings back calculated using the <i>JointedRock</i> model (GPa/mm)	
left/up plate	--
right/down plate	--

Test Group: 2



CHAINAGE(m)	46	47	48	49	50	51	52	53	54	55	56	57	58	59	60
ROCK TYPE	Sarvak Formation, Unit SV4, Limestone with Small Siliceous Nodule														
DIP DIRECTION/ DIP (BEDDING)	220/80			212/70			213/64			225					
STRENGTH															Strong
R.Q.D															25-50
INFILLING															Tight-Calcite
ROUGHNESS															Slickenside-Smooth
SPACING OF DISCONTINUITIES(cm)															20-60
WEATHERING															Slightly Weathered
GROUND WATER															Wet



CHAINAGE(m)	46	47	48	49	50	51	52	53	54	55	56	57	58	59	60	
Direction of Section	N180															
Dip Direction/Dip/Apparent Dip (Bedding)	220/80/77			212/70/67			213/64/60									
Discontinuity Systems	Bedding	220/64/51			Spacing: 20-60 cm			Opening: 1-5 mm								
	J1	310/71/67			Spacing: 20-60 cm			Opening: 0.1-1 mm								
	J2	121/42/39			Spacing: 20-60 cm			Opening: >0.1 mm								